Eindhoven University of Technology

MASTER

An unsupervised learning approach for detecting and labeling landmarks in the VFR waveform

Catani, V.M.

Award date:
2021

Link to publication

EINDHOVEN UNIVERSITY OF TECHNOLOGY

Department of Mathematics and Computer Science

An unsupervised learning approach for detecting and labeling landmarks in the VFR waveform

Master Thesis

V.M.Catani 0923540

Supervisors:

dr. N. Sidorova (Tu/e)

dr. R. Joshi (Philips Research, Patient Care and Monitoring)

PHILIPS

Acknowledgments

Abstract

This master thesis has been realized in collaboration with Philips Research. The main objective was to develop an unsupervised machine learning model for detecting and labeling characteristics, or as referred to in this work, landmarks, of the volumetric flow rate (VFR) waveform measured in an animal study. Machine learning has mainly been applied to predicting and classifying pathological states, using parameters derived from these landmarks of signal segments or the whole signal segments as input. In addition, previous work investigating the VFR waveform has commonly been scoped to characterizing only one cardiac cycle, where the landmarks were either manually marked or by using a customized algorithm. Therefore, we have identified a gap in using machine learning for the actual detection and labeling of the landmarks in the VFR waveform. This work proposed a model which combined components of unsupervised learning, namely hierarchical clustering, and derivative analysis to automatically detect and label successive landmarks in VFR signal segments of one minute. In this work there were four landmark groups of interest which were defined based on available literature. We used hierarchical clustering for first finding the global peaks of each cardiac cycle, after which we used the first- and second order derivative of the VFR waveform to define windows were the remaining landmarks were expected to occur. The model was evaluated by analysis of the periodicities which were computed as the number of timestamps between successive landmarks belonging to the same group. The differences in periodicities between landmark groups were then used to evaluate if the model managed to detect and label some landmarks better than others. The differences were expected to be around 0 since the periodicity between successive landmarks within each landmark group should be separated by approximately the same period. The results of the model evaluation showed that the differences of periodicities between the global peaks and one specific landmark group yielded more variability compared to the two other landmark groups. In addition, the proposed model was validated by a domain expert, who concluded that the model performed satisfactory for detecting selected landmarks in a subset of the results. The model validation also confirmed the results obtained in the model evaluation, namely, that the model had difficulties detecting and labeling landmarks of one specific landmark group. Based on the results of the model validation, we believe that our model is a step towards automating the process of detecting and labeling landmarks, which could aid in development of a method used to perform non-invasive hemodynamic monitoring in a clinical setting in the future.

Table of Contents

1 Introduction

In this first chapter, we introduce this work with respect to context, state-of-the-art and research questions. In addition, we present the outline of this master thesis, which gives an overview of what can be expected from the remainder of the report.

1.1 Context

The cardiovascular system is one of the main building blocks of the human body. It is a network of arteries and veins through which blood is transported from the heart to tissues, enabling cellular function. Cardiovascular diseases account for 31 % of deaths globally, where 85% are due to strokes and cardiac arrest [1]. Even though many factors contribute to the development of cardiovascular diseases, the outcomes are eventually linked to the failure of the cardiovascular system to provide oxygenated blood to the tissues [2]. If the cardiovascular system fails to provide the required quantity of oxygenated blood to meet the body's metabolic demands, the body reaches a clinical state of shock [3], [4]. Depending on the duration of oxygen deficiency, inadequate perfusion and oxygenation of the tissues can result in organ failure or worst-case death [3], [4].

Patients with severe cardiovascular diseases are often subjected to hemodynamic monitoring [4], [5]. Hemodynamic monitoring is used to measure various hemodynamic parameters, where two key parameters commonly associated with blood flow are cardiac output (CO) and stroke volume (SV) [3]. CO represents the volume of blood flowing from the heart to the circulatory system per minute whereas SV measures the volume of blood flowing from the heart to the circulatory system per heartbeat. To measure such parameters, various commercial hemodynamic monitoring methods have become available in the last decades, where the main issue of many methods is their invasive nature which inherently introduces risks to the patient [6], [7]. Therefore, the trend has shifted towards usage and development of noninvasive hemodynamic monitoring methods [5]–[7].

Two arterial pulse wave signals reflecting on blood flow are blood volumetric flow rate (VFR) waveforms and Pulse Wave Doppler velocity (PWD) waveforms [2]. The gold standard hemodynamic measurement method for the VFR waveform is the invasive perivascular flow sensor, whereas a common method for measuring the velocity waveform is Pulse Wave Doppler (PWD) ultrasound which is a noninvasive measurement method [2]. These waves are often studied through arterial wave analysis. Arterial wave analysis is a method used to analyze and unravel patterns of the waves and gain insights about progression of cardiovascular diseases and therapies [2]. A 'wave' in the context of hemodynamics is based on a definition by Hughes et al. [8]. Hughes states that a wave is a simultaneous alternation of both pressure and flow while moving through a blood vessel. On the other hand, the 'waveform' of both the VFR or PWD signals indicates the flow pulse signal measured at a specific arterial location [2].

In this work, we wish to automate the process of detecting key features of the VFR waveform measured by perivascular flow sensor. We hope that this model can be used in the future for development of a noninvasive hemodynamic monitoring method.

1.2 State of the art

The ability to **characterize** these pulse waveforms over the cardiac cycle is considered important for establishment of baselines against which pathological changes can be assessed [9], [10]. In previous studies, the temporal VFR and PWD waveforms have been characterized by the detection of key features in the waveform associated with the cardiac cycle measured at the common carotid artery (CCA) [9]–[12]. The term cardiac cycle refers to all events taking place in the cardiovascular system from the start of one heartbeat to the start of the next [13], whereas the CCA is one of the most important arteries supplying oxygenated blood to the brain [14]. The CCA is currently of interest when performing point-of-care ultrasound (POCUS) in the ICUs due to that this artery is often easily accessible [6]. The characteristics, or as referred to in this master thesis, **landmarks**, are often (1) labelled through customized algorithms or manual notation and (2) used for characterizing the waveform of only one cardiac cycle.

Applying machine learning on different physiological signals is an active field of research and open for exploration. Physiological signals can be defined as signals describing a physiological phenomenon [15]. With respect to this master thesis, we identified that machine learning is not commonly used for **detecting** landmarks in physiological signals, however, machine learning and neural networks have been applied for predicting physiological states using physiological signals and hemodynamic parameters derived from landmarks as input [16]–[18]. In other words, the landmarks are computed beforehand for creating features which are then used as input for prediction or classification tasks. However, it was noted that in many of the approaches, clustering was commonly used as an unsupervised learning approach on biological data. Therefore, in this work, the idea is to use clustering to perform the pre-work by detecting and labeling landmarks which then could be used for further analysis.

1.3 Research questions and research goal

In this section, the research goal and research questions are defined. The goal in this work is to explore the VFR waveform to (1) detect and label landmarks of the VFR waveforms and (2) determine if the obtained landmarks can be used to describe the waveform in terms of state-of-the-art descriptors in accordance with a consensus article [19].

We formulate one research goal which we have used to develop two research questions. The research goal of this work is the following:

Research Goal: *Develop a model for automatically detecting and labeling landmarks of the volumetric flow rate (VFR) waveform.*

Based on this goal we formulate the first research question (RQ1), which we attempt to answer by developing a model and iteratively improving it.

Research Question 1: *How can we apply machine learning techniques for automating the detection and labeling of landmarks in signal segments measuring the volumetric flow rate (VFR) waveform?*

In addition to detecting and labeling landmarks, we are also interested in exploring if these landmarks can be used to describe the waveform of interest based on key descriptors defined in a consensus article [19]. These descriptors were actually defined for another waveform, namely, the pulse wave doppler (PWD) waveform. However, we believe that the same descriptors can be used for describing the VFR waveform, which could be useful for better understanding the blood flow in the CCA. Therefore, the second research question (RQ2) was formulated.

Research Question 2: *Can we use the landmarks obtained by the model for describing the volumetric flow rate (VFR) waveform in terms of state-of-the-art descriptors?*

1.4 Approach

In this section, an overview is given of how the research goal can be achieved and how the research questions can be answered in accordance with the process of the chosen methodology CRISP-DM (Cross Industry Standard Process for Data Mining) [20]. This methodology was chosen because (i) it is not restricted to a specific industry, and (ii) the process model is clear and simple as it follows a specific number of steps, where the model can be iteratively improved.

The main foundation for the understanding the data was to first get two types of domain knowledge. Firstly, the study from which the data was collected had to be researched. This required (1) having sessions with experts who were present during the study for discussing the process and (2) exploring all available documents. In addition, it was important to reflect on the sources contributing to errors associated with the study. Secondly, it was essential to understand the underlying physiology of the heart and circulatory system.

After acquiring the necessary domain knowledge of the physiology and study, the next step was to prepare the available data for modeling. This implied verifying the correct data and identifying missing values, where sometimes sessions with experts had to be scheduled for clarification. After exploring the data, we incorporated domain knowledge for defining the expected waveform and the desired landmarks, which were important factors when choosing the modeling approach.

Since the data of interest was a physiological signal measured by a sensor, the possible sources of error had to be identified. Many sources of error were identified, which gave us an understanding what deviations could be expected in the signal. Finally, by reflecting on the possible errors in the data, a data cleaning method was developed for excluding interrupted waveforms. This was the final step before the modeling approach.

After the correct data had been verified and data preparation had been performed, modeling techniques were chosen. In the first iteration of the model, the chosen modeling techniques were applied, and the respective model evaluation was performed. By following the chosen methodology CRISP-DM, the model was then improved by incorporating additional components of the first-and second order derivatives of the waveform for detecting and labeling landmarks, after which the model was evaluated.

Finally, the model was validated by a domain expert and scientists from Philips Research. In this model validation session, five cardiac cycles in five randomly chosen signal segments containing the labeled landmarks were shown to the domain expert who then determined if the landmarks were detected and labelled correctly. In addition, the domain expert gave thoughts about if these landmarks could be used for describing the waveform in terms of key descriptors. In the end, the conclusions were that the model was able to detect and label some of the landmarks better than others. Consequently, some descriptors could be used based on the values of the landmarks.

1.5 Outline

The outline of the remainder of this master thesis is as follows:

Chapter 2 provides selected articles in the related work with respect to the link between machine learning and physiological signals which is the foundation of the gap in research which we aim to address. In addition, we present preliminaries with respect to all phases of the chosen methodology CRISP-DM, the underlying physiology of the heart, and performing measurements in a study. These preliminaries will give the reader the preliminary knowledge we believe is required to better understand the work presented in the remainder of the thesis.

Chapter 3 presents the business understanding by describing the objectives of this work, the study, the different sources of error in the study, the goals with respect to data mining, and finally, the technical tools that were used.

Chapter 4 begins with providing an overview of the consensus article and presenting the key descriptors used to describe the waveform. In addition, more related work regarding finding landmarks is given by reviewing selected articles. The remainder of the chapter gives an extensive explanation of data exploration, data understanding, data preparation, sources of error in the signal itself, and data cleaning.

Chapter 5 presents the initial model and the revised model in this work. The first model represents a naïve approach which is then improved based on the limitations from the first model evaluation. The second model iteration is then explained and evaluated.

Chapter 6 describes the model validation. In this chapter five cardiac cycles in randomly chosen signal segments containing the landmarks detected by the model are shown to the domain expert who validates the results.

Chapter 7 provides a summary of this work and explains the limitations of the proposed model with respect to which possibilities of future work are discussed. Finally, we conclude this master thesis by giving some final words with respect to the project.

2 Related work and preliminaries

The objective of this chapter is to present related work and discuss any topic that we believe is required to follow the remainder of this thesis. We start by giving an overview of the chosen methodology. Then we present selected articles for introducing the related work with respect to the current situation regarding machine learning using physiological signals. In this related work, we do not discuss the methods for detecting and labeling landmarks since this requires understanding the VFR signal. Therefore, a more specified related work section addressing the state-of-the-art with respect to characterizing the VFR waveform will be given in Section 4.2. After the related work section, we provide background information with respect to criteria when performing measurements in research. This is important to discuss since this work uses measurement data collected in a study. Finally, the physiology of the heart is explained, which we believe is essential for understanding the waveform of the VFR signal discussed later in this master thesis.

2.1 CRISP-DM methodology

In this master thesis, the **cross-industry standard process for data mining (CRISP-DM)** methodology is applied. CRISP-DM is an industry-independent process model that is considered a standard methodology for data mining projects [20]. In this section, the CRISP-DM methodology together with its various phases are presented.

The CRISP-DM is divided into six *iterative* phases. These six phases are (1) Business Understanding, (2) Data Understanding, (3) Data Preparation, (4) Modeling, (5) Evaluation, and (6) Deployment. The idea is that the chosen model is iteratively improved and developed until the best model has been achieved. The iterative nature of the approach can be depicted in Figure 1 [21]. In the following sub sections, these different phases will be described in detail.
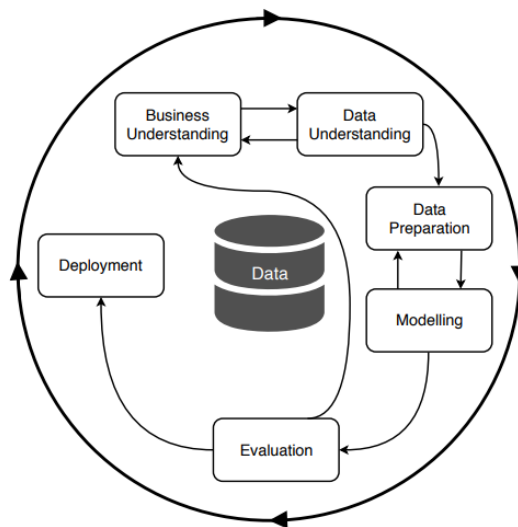
Figure 1. CRISP-DM process model [21]

2.1.1 Business understanding

The objective of the business understanding phase is to define the objectives of the research, together with available resources, requirements and limitations [22]. In other words, the current business situation should be evaluated. In addition, the goal of the project should be defined in terms of the considered data mining approach in our case, clustering [20].

2.1.2 Data understanding

In the data understanding phase, the data is collected from different data sources, after which the data is explored and described. Describing the data implies giving e.g., the format of the data and number of datapoints, whereas, exploring data can be done by visualizing it in different graphs or investigating different characteristics in terms of basic statistics [22]. Finally, the quality of the data must be assessed e.g., noise in a signal or missing data points [20], [22].

2.1.3 Data preparation

In the data preparation phase, the selection of the final data for the modeling is performed based on defined inclusion and exclusion criteria [20]. In addition, any necessary manipulation to the data should be performed e.g., combining data sets, or computing new features from the raw data. In this phase any necessary data cleaning should be performed before the modeling part [20].

2.1.4 Modeling

In the modeling phase, the entire modeling process is described. Firstly, different modeling techniques are selected based on the objective of the research and the available resources, where it is important to motivate the choice of a specific technique. After selecting and motivating the choice of technique(s), the testing design is performed. The testing design implies e.g., dividing the data into a training and test set. After the designing the testing set up, the model itself is built. Model building requires choosing all necessary parameters for the model and explaining the algorithm of the model. Finally, the model must be assessed with respect to the requirements of the model [20].

2.1.5 Evaluation

After the model has been built and executed, the model itself and the process performed thus far must be evaluated with respect to the objectives set in the business understanding phase. In this phase the results are discussed and if the model does not meet the requirements, any necessary changes should be added by iteratively improving the model [20], [22].

2.1.6 Deployment

In the final phase of the methodology, is the deployment phase. Deployment of the model could be a final report or code. In this case, a final report will be produced, and code will be implemented based on the requirements of the company [20]. We do not address deployment in detail since the deployment of this work will include handing in this master thesis and code.

2.2 Machine learning and physiological signals

In this section, selected articles are presented to give an overview of the link between machine learning and physiological signals. These articles were found by using key words such as 'machine learning' 'pulse wave' 'clustering' 'doppler' 'pattern recognition' 'ppg' 'signal morphology' 'k-means' etc. These articles were chosen from many as examples on how artificial intelligence has been applied in the field of predicting and classifying different pathological conditions based on various physiological signals. Many other articles were found but not further analyzed.

- In a study by Miao et al. K-means clustering is used for clustering different features of the transcranial Doppler (TCD) waveform into either normal, abnormal, or borderline subclass of TCD spectral waveform. In this study a computer-based statistical pattern recognition system was developed through combining K-means clustering, canonical discriminant analysis and the Bayesian Gaussian classifier. This research extracted multi-dimensional features from the TCD waveforms, which were then used for classifying the spectral waveform as either normal, abnormal, or borderline subclass by means of the system [17].

- An example of a study using clustering of local extremes was performed by Gamage et al. [18]. More specifically, K-means clustering was used for classifying Seismocardiographic (SCG) signal events based on the morphology of the signal. The SCG signal is a measurement of vibrations caused primarily by inherent mechanisms of the heart e.g., closing and opening of the different heart valves and is measured at the surface of the chest [18]. The objective of this study was to cluster the time domain amplitude of the signal to investigate how different respiratory phases affect the SCG morphology, and through this analysis gain insight for improving the usage of SCG monitoring for detecting unwanted cardiac events e.g., heart failure [18]. This study is also an example of how clustering using an internal validation index (Silhouette index) for determining the optimal number of clusters can be used for clustering features of a physiological waveform, and thus, make predictions of a patient's physiological state.

- In a study by Slapničar et al [16] the photoplethysmogram (PPG) waveforms, together with the first and second order derivative waveforms were used as input in a new spectro-temporal residual neural network in order to model the relationship between PPG and blood pressure (BP). The objective was to use raw PPG signal segments and their respective derivatives for predicting systolic blood pressure (SPB) and diastolic blood pressure (DPB). The SPB and DPB were obtained from arterial blood pressure (ABP) signals by using a customized peak and valley detector. In addition, for comparison, the classical machine learning method Random Forrest was implemented, using several features from both the frequency and temporal domain constructed by hand, as input. In the end, the findings were that the deep-learning approach yielded better results over traditional machine learning [16].

Based on the overall review, we noted the following: (1) There seems to be a gap in research of using machine learning for **detecting** the actual landmarks associated with the waveform of interest, and instead the landmarks are computed beforehand as means for creating features, which then are used as input for prediction or classification tasks, (2) clustering is commonly used as an unsupervised learning approach on biological data, (3) machine learning of different variants were applied on a wide range of different physiological signals and therefore, this field is open for exploration.

2.3 Measurement process

Since this work uses measurement data collected from a study, some background information of performing measurements are given. This section is written based on information from Chapter 5 in the book *Research Methodology* written by Peter Pruzan [23].

In general, a measurement is a quantification of something that has an associated magnitude and unit e.g., weight in terms of kilograms or positional change in terms of meters per time unit [23]. The idea of performing measurements is to close the gap between how the physical world is seen and the actual physical world itself. When investigating this gap, one key concept is understanding the **precision** of the measuring instrument and the **accuracy** of the measurements. The formal definitions of accuracy and precision are the following:

- **Accuracy:** The accuracy of a measurement refers to its closeness to some external "truth" measurement [24]. With respect to the measurement instrument itself, the accuracy is the degree to which the new instrument manages to produce similar measurements when compared to measurements obtained by a "gold standard" measurement instrument [24]. Accuracy is quantified by the obtained bias [25].
- **Precision:** The precision of a measurement is associated with the ability to repeat a measurement with respect to a previous observation measured by either the same or different raters [24]. A precise measurement instrument would be able to produce repeated measurements all of which are close to each other in value. Precision is normally quantified as the resulting standard deviation of the measurements [25].

Based on these definitions one can conclude that if a measurement instrument is precise and the measurement process is accurate, then there is a higher chance of obtaining measurements that are uniformly distributed around the ground truth value [23]. Based on the book by Pruzan [23], there are three main criteria commonly used in literature when assessing the quality of measurements in a measurement process. These three criteria are *validity, reliability,* and *reproducibility/replicability,* all of which will be discussed as follows [23].

Validity of measurements refers to their respective trustworthiness. In other words, did the measurement process manage to measure what it was expected to measure. Again, validity of measurements is closely coupled with the precision of the measuring method and the accuracy of the obtained measurements. Even though the measurement instrument is precise, if it produces measurements far from the ground-truth, then the measurements shouldn't be considered valid. For example, invalid measurements would be considered measurements obtained by an un-calibrated measurement method. Based on these arguments, both precision and accuracy of the measurement instrument and process should be considered when addressing validity of measurements [23].

Reliability of measurements is associated with the consistency and stability of repeated measurements. Reliability of repeated measurements is more linked to the precision of the measurement instrument and the presence of random errors, both of which should be considered when assessing the degree of instability of the measurement instrument [23].

Reproducibility of measurements is the ability of another researcher to reproduce one's measurements and study. In other words, if someone is not able to replicate the measurement process and produce comparable results, then the measurements should not be considered reproducible. Reasons for lack of reproducibility of results could be due to mistakes made in the experiment, uncalibrated measuring instruments, or simply due to the level of skills and experience of the researcher [23].

Finally, we want to address the importance of understanding potential sources of measurement error. Measurement errors can be a consequence of many factors e.g., measurement process itself, outdated technology used for obtaining the measurements, or even misconception of the definition of what is being measured [23]. Typically, when analyzing measurement errors, random and systematic errors are commonly considered. *Random errors* or *unbiased errors* are errors of some degree which equally likely overestimate as underestimate the measurements. In other words, the errors are **inconsistent**. On the other hand, *systematic errors* or *bias* occur when the measurements are **consistently** underestimated or overestimated e.g., measurements obtained by a wrongly calibrated measurement instrument are most likely subjected to systematic error. The problem is that systematic errors may be difficult to detect and therefore, crucially affect resulting measurements. Therefore, it is essential to consider and evaluate the possible sources of systematic errors in advance [23].

2.4 Cardiac cycle

In this section, a description of the different phases of one cardiac cycle is given. Understanding the cardiac cycle plays a crucial role in this work since these different phases are expected to be reflected in the data, namely, the VFR signal. This in turn also aids in detecting the deviations in the waveforms due to underlying physiology.

The cardiac cycle refers to all events taking place in the cardiovascular system between the start of the current heartbeat to the start of the next [13]. The cardiac cycle is divided into two main phases, namely diastole which represents the period of relaxation, and systole which represents the period of contraction [13].
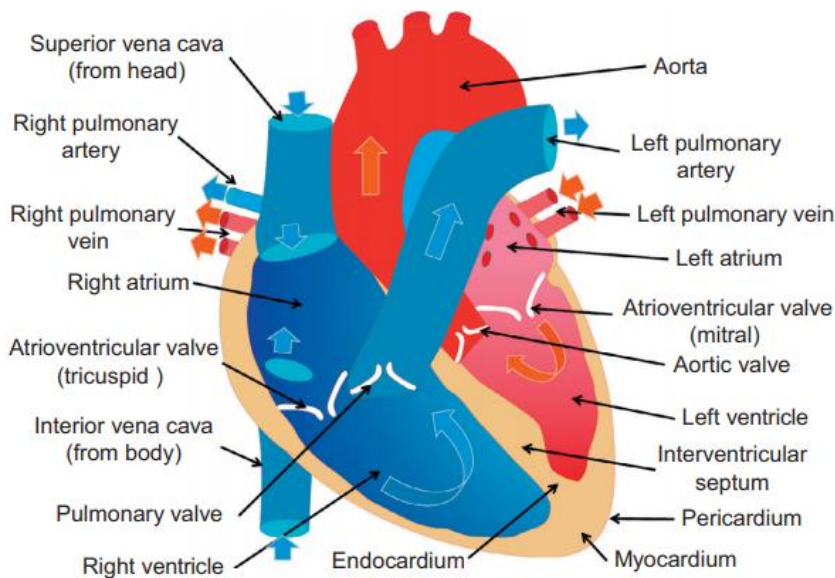
Figure 2. Illustration of the different chambers of the heart taken from Chapter 1 of the book Atherosclerotic Plaque Characterization Methods Based on Coronary Imaging by Athanasiou et al. [26].

In the diastolic phase, deoxygenated blood returns to the heart through the superior and inferior vena cava and fills up the right atrium. As a result of filling the right atrium, the pressure in this atrium increases. When the pressure in the right atrium exceeds the pressure in the right ventricle, the valve known as the **tricuspid** valve, opens and the blood flows into the right ventricle [26] In parallel, the oxygenated blood

from the lungs flow into the left atrium. Again, as the pressure increases in the left atrium, the valve known as the **mitral** valve opens resulting in the blood flowing into the left ventricle [26].

The systolic phase refers to the contraction of the heart, namely, when blood is ejected to the lungs from the right ventricle, and to the circulatory system from the left ventricle [13]. Beginning of systole is marked with closing of the Atrioventricular (AV) valves, namely the **mitral** and **tricuspid** valves. When the AV valves close the ventricles start to contract however, the semilunar valves (pulmonary valve and aortic valve) remain closed until the pressure is high enough to exceed the pressures in the pulmonary artery and aorta [13]. The phase just before the semilunar valves open is known as the **isovolumetric contraction** [26]. When the aortic pressure is exceeded, the semilunar valves open, resulting in that blood gets ejected into the circulatory system and the lungs [13]. Since this work analyses the blood flow in the CCA, this work is focused on the events happening in the left chambers of the heart, which are reflected in the VFR signal waveform.

The closing of the semilunar marks the end of systole and beginning of diastole [27]. The point in time when the semilunar valves close is known also known as the **dicrotic notch**. The location of the dicrotic notch has been used for early evaluation of diseases e.g., occlusion or arterial spasm [27].

3 Business understanding

In this section, all relevant information and preparation for the analysis is given, namely, background of the study, the available resources, associated limitations and chosen technologies and tools used for the modeling. Firstly, the objectives of the research are defined in Section 3.1. After the objectives are defined, the study from which the data was collected is explained in Section 3.2. The data used in this work were different physiological measurements measured by various hemodynamic measurement instruments. Therefore, a proper error analysis of the study must also be performed which is discussed in Section 3.3. In Section 3.4, the data mining goals are given. Finally, Section 3.5 describes the technical tools used in this work.

3.1 Objectives

This master thesis is a research conducted in collaboration with Philips Research. The goal for Philips Research was to gain insights from analyzing measurements of various hemodynamic parameters, which could be used for aiding the development of a non-invasive hemodynamic monitoring method. We believe that the goal can be realized by the research performed in this work.

The data used in this master thesis was collected in an animal study performed by Vrij University Medical Center (VUMC) in Amsterdam. The main goal of the study for VUMC was to investigate the effect of surgical and anesthesiologic interventions on perfusion of the liver, with the objective to gain insight of how these interventions might affect hemodynamically stable patients during liver surgery.

The signal of interest is the pulsatile signal representing volumetric blood flow rate (VFR), which was measured at the common carotid artery (CCA) by the Transonic flow sensor. In this research, related work associated with analyzing both Pulse Wave Doppler (PWD) signal waveforms and VFR waveforms are applied on the pulse signal obtained by the Transonic flow sensor. The main difference between the PWD waveform and the VFR waveform is that PWD measures the velocity of the blood (units *cm/s*), whereas the Transonic flow sensor measures the volume of blood passing the measurement point over time (units *mL/min*). It is feasible to apply the methods used for the PWD waveforms on the VFR waveforms since blood velocity can be transformed to flow by multiplying the velocity with the arterial cross-sectional area. The PWD signal was also measured in our study but is out of scope in this work.

The objective of this study is to automate extraction of universally recognized features or so-called **landmarks** of successive cardiac cycles from the VFR waveform. Capturing these landmarks can be used to describe the VFR waveform and this way provide insights about the blood flow in the carotid artery. The objective is that our model can be used as a component in developing a non-invasive hemodynamic monitoring method in the future.

3.2 The study

The study was conducted on 14 female Yorkshire pigs, where the animal is from now on referred to as subject. In the study, various hemodynamic measurement methods were used in different places on the subject for monitoring hemodynamic parameters.

Firstly, five Transonic flow sensors were placed in five different arteries. The five arteries were the descending aorta, v porta, a hepatica, common carotid, and femoral artery. In addition to the five flow sensors, the following measurement devices were used for data collection: PiCCO system and FloTrac system through arterial line in the femoral artery, Swan Ganz in the jugular vein, and fixed ultrasound (US) probe on the skin above the carotid artery.

There were two data collection sets in the study. The first set of measurements were divided into 4 blocks, where each block contained 4 steps that were performed in the same order each time. Each **block** was

associated with an administered medication and the **steps** were associated with positional change. In the first block no medication was administered, and the measurements were taken four times approximately 15 minutes apart.

The first medication to be administered was Nitroglycerin which is a vasodilator [28]. Vasodilators are used to widen the arteries which decreases systemic vascular resistance. By decreasing the systemic vascular resistance, the resistance that the heart must overcome to eject blood to circulatory system is lower and blood flow increases [28]. In a clinical setting, Nitroglycerin is commonly used for treatment of e.g., chronic heart failure and angina [28].

The second medication administered in the study was Adrenaline which was infused during the first three steps in the third block. As oppose to Nitroglycerin, Adrenaline constricts the arteries, making it a vasoconstrictor [29]. Adrenaline increases both cerebral and coronary perfusion pressures and has been used as a standard medication for many decades when performing cardiopulmonary resuscitation (CPR) [29].

Finally, in the fourth block, a combination of the aforementioned medications was administered. The effect of the combination was studied by Lurie et al. [30] with the objective of obtaining insight if the combination of the adrenaline, vasopressin and nitroglycerin would be more effective for increasing blood flow to the brain and heart when performing cardio pulmonary resuscitation (CPR), than using only adrenaline [30]. The authors found that the combination of the three drugs increased both the blood flow to vital organs and the coronary perfusion pressure when compared to only adrenaline.

The second set of measurements were performed in the end of the study. In this phase, the medication Lipopolysaccharide (LPS) was administered. The number of measurements in this phase differed per subject, but in general three measurements were obtained per subject from this phase.

Each subject was identified by a number associated with the study. The inclusion and exclusion criteria for the subjects were the following. We excluded the first two subjects as their data was collected in a test setting. We chose to exclude the first two subjects since we did not have information about the difference between the testing environment and the actual study. In addition, one more subject had to be excluded due an interruption in the study because of physiological reasons. This subject did not have available data. Therefore, we included the remaining 11 subjects that (1) did not participate in the testing of the study and, (2) had data available from the whole study period and for which the study was not interrupted for physiological reasons.

3.3 Sources of error in the study

In the study, different physiological measurements were obtained through various measurement instruments. In this section, the different sources of error are analyzed in a systematic way.

In this section, potential sources of measurement errors with respect to the measurement process are presented and discussed. In general, the reflection of these factors should be considered prior to the design of the measurement process, however, as the study has already been conducted, this section presents an analysis based on available documentation and discussions associated with the study, and literature.
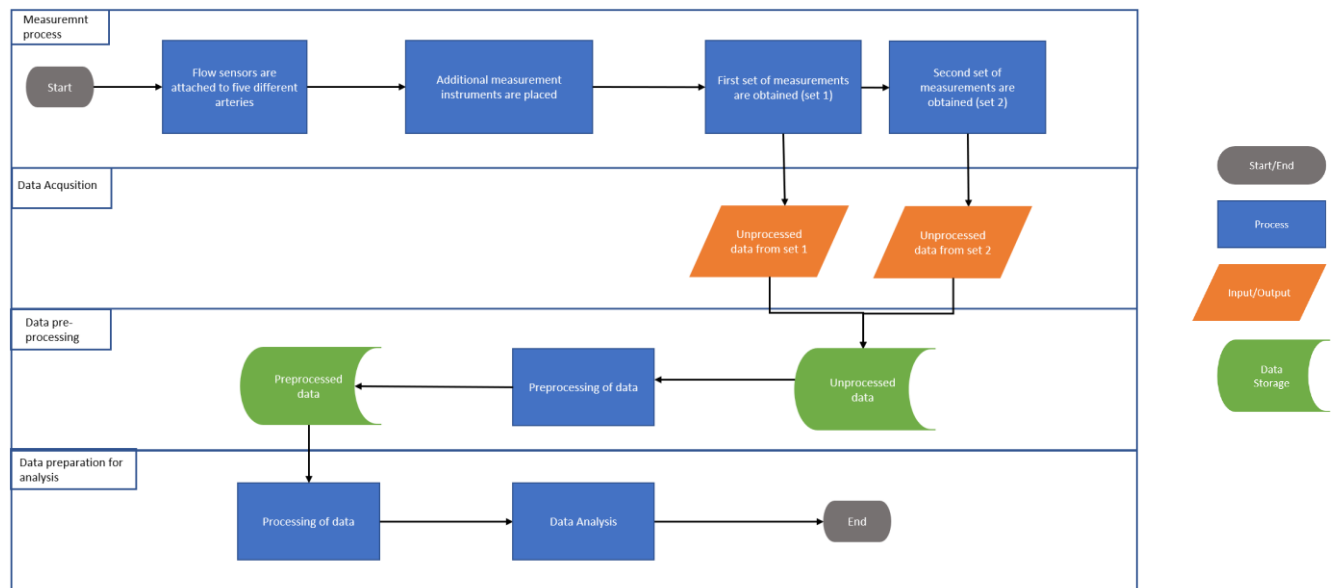
Figure 3. Flowchart showing an overview of the workflow from the measurement process to performing data preparation and analysis. These phases in the workflow also gives an overview where possible sources of error can occur.

The *measurement process* in Figure 3 illustrates the study on high level for one subject. As described in section 3.2, the process starts by attaching various measurement instruments. The measurement process was the same for each subject. By observing the flow of the measurement process, multiple sources of error can be identified.

After the surgery preparation of the subject, the measurement devices were placed. The following measurement instruments were used in the study: the Swan Ganz catheter, PiCCO system, FloTrac system for measuring CO, Transonic flow sensors (TFS) for measuring blood flow in five different arteries, and Lumify ultrasound probe (L12) for obtaining PWD velocity and B-Mode showing the arterial diameter in the carotid artery. In addition, Philips documentation of the study mentioned additional monitoring devices. These devices were oxygen saturation (SpO$_2$) sensors, attached to the tail of the subject, and electrocardiogram electrodes (ECG) on two different places for measuring heart rate. Analysis of the measurement instruments is essential for the error analysis and in this work, the measurement instruments of interest are the **PiCCO system** and the **Transonic flow sensor**, both of which will be presented and discussed as follows.

The **PiCCO** system measures cardiac output CO by using two techniques; continuous pulse contour analysis and intermittent transpulmonary thermodilution for calibration attached at a peripheral artery e.g., femoral [25]. Pulse contour analysis continuously monitors arterial pressure waveform from which it computes the beat-to-beat stroke volume [25]. The limitation of pulse contour analysis is that the arterial pressure waveform is highly dependent on the systemic vascular resistance, which is variable that varies between and within individuals [25]. The limitation resulting from changes in the systemic vascular resistance can be addressed by using transpulmonary thermodilution for calibration. Around the calibration points, the PiCCO system measures CO with a precision of <20% [25]. It is difficult to estimate the true accuracy and precision of the PiCCO system since there are many factors contributing to the variability of the results e.g., patient population, study methodology or the imprecision of the gold standard hemodynamic measurement method, Swan Ganz system, which PiCCO is often compared to [25].

The PiCCO system is of interest since the calibration points of the PiCCO system are used for computing signal segments for the analysis. The motivation for choosing the timepoints of the calibration points is that in the future, the blood flow in the carotid artery around the calibration point can be compared to calibrated cardiac output (CO) obtained by PiCCO. The calibration points of PiCCO were chosen over Swan Ganz calibration points because the PiCCO system was calibrated before the Swan Ganz system. How these signal segments are computed will be described later in the report.

Transonic flow sensor is a so-called perivascular flow sensor which is considered the gold-standard for invasive flow measurement [2]. These sensors consist of two ultrasonic transducers and one acoustic reflector [31]. These transducers exchange ultrasound signals between each other, and this way alternate the intersection with the flowing blood in both downstream and upstream directions [31] as depicted in Figure 4 [32]. The measurement of the flow sensor is the so-called *transit-time* which is a measure of the travel time for the ultrasound wave between the transducers [31]. The difference between the transit times between the downstream and upstream directions are then used for computing the blood volume over time which provides the measurement of blood flow.

The accuracy of the flow sensors used in this study was given in the specification document provided by Philips. The flow sensors had not been calibrated for approximately 10 years, yielding an absolute accuracy of ±15%. For example, for a measurement of 10L/min the value could be anywhere between 8.5L/min and 11.5L/min. Attempts to reduce the error were performed prior to the time of writing this master thesis, however, the results were inconclusive. The precision was not documented.

The Transonic flow sensors (TFS) were attached in five different arteries over the course of the experiment to measure blood flow rate. The raw signal is measured in volts, for which each flow sensor has a specific volt [V] to flow [ml/min] conversion factor depending on the size of the flow sensor. The largest flow sensor is normally attached to the largest artery, in this case the aorta. In addition, each flow sensor has an associated channel in the Transonic flow system.
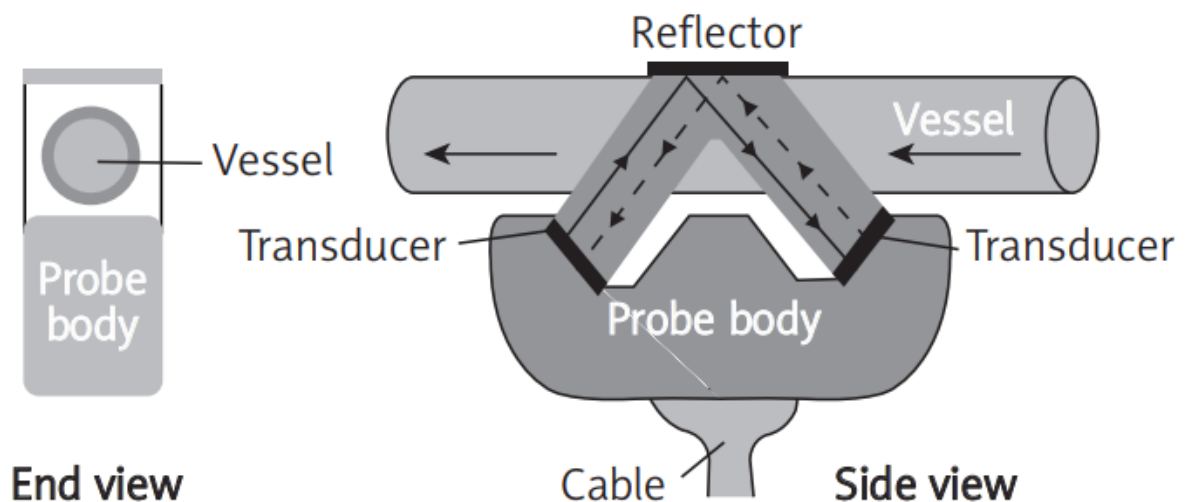
Figure 4 The transit-time ultrasound technology used in the Transonic flow sensor. Illustration is obtained from an article by Lee et al. [32]

From discussions with experts present during the experiments and documentation from the study, these flow sensors were attached surgically in the arteries. The attachment was not problem free in terms of finding the right location and fit around the artery. In addition, as also stated in the article by Mynard et al., [2] these sensors require proper acoustic coupling between the sensor and vessel wall. This is achieved by using different coupling agents e.g., coupling gel, which according to the specification of the sensor results in the highest accuracy. [33].

In summary, the main sources of error in the measurement process are (i) the measurement instruments and (ii) the procedure of attaching and placing these instruments. In addition, it should be mentioned that the physiology of the subject plays a crucial role in the error analysis. However, the sources of error in the data itself will be discussed later in this report, where possible errors caused by physiology are analyzed. However, based on this section, there are many factors adding to the complexity of the data with respect to the study and the measurement process.

3.4 Data mining goals

In this section, preliminary success criteria from a data mining perspective is given. The main data mining approach chosen for analyzing the data is **clustering**. The objective is to use clustering to group local extrema associated with different phases of the cardiac cycle to find so-called **landmarks** of the VFR waveform. We want to investigate if these landmarks can be found by applying a commonly used machine learning approach of clustering and this way automate the process without having to label the landmarks a priori.

In this work, we wish to detect and label these landmarks of one cardiac cycle, repeatedly over a segment of cycles of the Transonic flow sensor signal. We believe that landmarks of the VFR waveform during systole and diastole could be useful in characterizing and analyzing the blood flow in the common carotid artery (CCA), and later on used for predicting cardiac output (CO). Therefore, signal segments around PiCCO calibration points were computed such that later on, comparisons can be made to CO measurements measured by PiCCO. The segment length of the signal for the analysis was chosen to be one minute, evenly distributed around the point of calibration (±30 seconds on each side of the calibration points). This segment length was a period chosen by experts. The period of one minute was considered a suitable length since many features in hemodynamics are measured with respect to a period of one minute e.g., heart rate in units beats-per-minute (BPM).

For the unsupervised method, the same segment length was kept. Therefore, manually marking these landmarks would **not** be feasible since each subject has multiple segments, and each segment has multiple periods. This detection and labeling would have had to be automated somehow and still; the obtained landmarks would need to be verified by domain experts. In other words, marking these landmarks correctly would require more advanced domain knowledge and a specific tool for even detecting these landmarks, both of which are out of scope in this work.

With respect to domain knowledge of the heart functionality and the sensors, it is also difficult to know what we can expect from the data due to the various sources of error contributing to uncertainties in the data. Therefore, this work should be considered as an opportunity to explore the signal and iteratively reflect on the obtained domain knowledge for understanding the data better. As we are to explore the signal, we believe that the approach of using unsupervised learning is a more naïve approach in a sense that it is not restricted by uncertainties in the signals, whereas supervised learning would require more domain knowledge in advance.

Since we are going to use unsupervised learning, the extent to which our model manages to answer the research questions requires expert validation. Therefore, the results and their significance should be

validated by a domain expert to determine the extent of which the landmarks are detected and labeled correctly.

3.5 Technical tools

This research uses the Matlab version R2020a. Using Matlab was a request by Philips Research and has been used throughout the project. Therefore, all implemented data analysis and figures have been computed using Matlab.

4 Data understanding and preparation

The objective of this section is to build on the foundation of Chapter 3 by exploration and understanding the available data sets for the modeling part. The main data used in this research were the time points of PiCCO calibration timeseries stored in the Case Report Form (CRF) data set, and the VFR sensor signals stored in TDMS files. In addition, to understanding the data, some related work regarding analysis of the VFR and PWD waveforms will be presented. Finally, all necessary exploration, preparation, and cleaning will be explained.

4.1 Descriptors of the VFR waveform

To build on business understanding given in Chapter 3, some related work on how to describe both VFR and Pulse Wave Doppler (PWD) waveforms are given. To recap, PWD waveforms represent the blood velocity waveform measured by Ultrasonography using the phenomenon of Doppler effect [34].

In an expert consensus document by Kim et al. [19], a nomenclature is presented for arterial and venous Doppler waveforms with the objective to promote better communication with respect to terminology of the Doppler waveform among practitioners [19]. Initially, the description of peripheral arterial Doppler waveforms was based on (i) audibly recognizing if systolic and diastolic components of the cardiac cycle were present or absent; and (ii) displaying these components with respect to the zero-flow baseline. These two factors provided the basis for the original descriptors of the Doppler waveform, namely, *triphasic, biphasic* and *monophasic* waveforms [19].
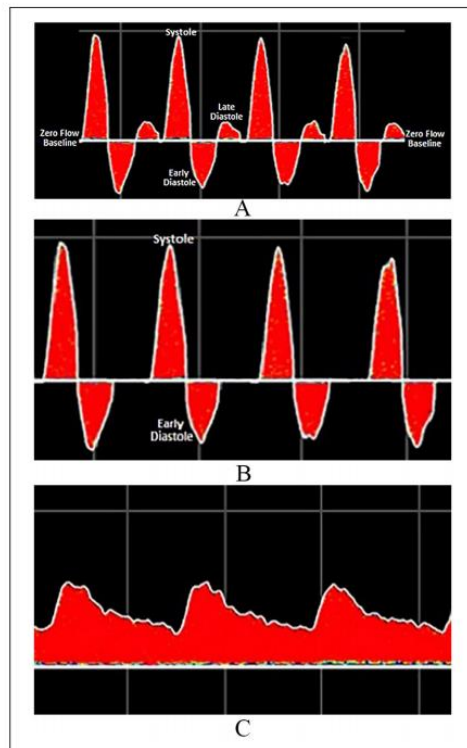
Figure 5. An illustration obtained from the article by Kim et al. [19]. Figure (A) shows a triphasic waveform (B) shows a bi-phasic waveform and (C) shows a monophasic Doppler waveform [19].

The *triphasic* waveform displayed three components of the cardiac cycle (1) systole; (2) early diastole reversal flow and (3) low forward flow in later diastole [19]. In the *biphasic,* component (3) is absent, whereas the *monophasic* waveform is characterized by no crossing of the baseline and therefore, no negative flow [19].

In the consensus document, the conclusions were that instead of using three descriptors for describing **phasicity**, two descriptors should be used instead, namely, *monophasic,* and *multiphasic*. *Monophasic* is used for waveforms that do not cross the zero-flow baseline and have a forward flow throughout the cardiac cycle, and *multiphasic* is used for when a flow waveform crosses the zero-flow baseline with both forward and reverse directions [19].

The second key descriptor was considered to be **flow direction**. Flow direction can be either defined as *antegrade* if the direction of flow is considered normal (forward flow), and *retrograde* if flow occurs against normal circulation (reversal flow) [19]. Two other types of flow direction were given but they were considered out of scope in this research.

For analyzing **resistance** of the waveform, *high-resistive* waveforms have a sharp upstroke followed by a rapid downstroke and can be either multiphasic or monophasic. *Low-resistive* waveforms are characterized by a downstroke that is prolonged in late systole. In addition, low-resistive waveforms have forward flow throughout the cardiac cycle, making them monophasic. Finally, the third resistance form is a hybrid that is monophasic but has features of both rapid downstroke with continuous forward flow over the whole diastolic phase. This hybrid type also contains an end-systolic notch which is the result of fast deceleration after which the diastolic acceleration starts. This type of waveform is called an *intermediate resistive* waveform [19].

In summary, the blood flow velocity waveform should be characterized through **flow direction**, **phasicity**, and **resistance**. Flow direction refers to either forward or backward flow, whereas phasicity indicates if there indeed is only forward directional flow, or both reverse and forward flow. Finally, the resistance can be investigated based on the steepness of the upstroke and downstroke and the phasicity. In this work, the analyzed waveform is not the PWD velocity waveform but the VFR waveform. However, since the volumetric flow rate can be computed using blood velocity, we believe that the VFR can also be characterized using these descriptors.

4.2 Detecting landmarks of the cardiac cycle

Characterizing VFR and PWD velocity waveforms over the cardiac cycle has been applied for defining baselines for modelling and assessing pathological changes [9], [10]. In previous studies, the PWD and VFR waveforms have been characterized by detecting features or as we call them, landmarks, inherent to the cardiac cycle [9]–[11]. Since in this work we wish to characterize the VFR waveform by detecting landmarks and investigate if these landmarks can be used to describe the waveforms in terms of descriptors in the consensus article, this section will discuss the state of the art with respect to these requirements and is an important component in the related work for this master thesis.

In a study by Holdsworth et al. [35], the landmarks of the velocity waveform measured by Pulse Wave Doppler US were used to characterize the waveform. The objective of the study was to find easy and well-defined features from individual waveforms and use these features for synthesizing an archetypal waveform and investigating cycle-to-cycle variability [35]. The landmarks were found on a cycle-by-cycle basis by using an automated routine [35]. For example, the systolic maximum and the maximum systolic acceleration were of interest and their validation was performed graphically.

In a study by Gwilliam et al., [9] temporal profiles of the volumetric flow rate (VFR) were used to investigate how the VRF waveform changes when pulse moves through the carotid three which were though to provide good input functions for modelling hemodynamics. This research adopted the methods from studies Holdsworth et al. [35] and Ford et al. [10], which were based on using the characteristics of individual flow waveform and averaging these features to create an archetypical waveform. In this study, the VFR was measured by phase-contrast (PC) magnetic resonance imaging (MRI) in the carotid arteries, including the CCA. The landmarks of interest in this study are shown in Figure 6 [9]. The points P1, P2, P3, M0, M1, M2 were noted manually, where the **global peak** P1 represented the portion of systole of the cardiac cycle and was considered as the initial point. Furthermore, the landmarks P2, P3, M0, M1 and M2 were computed based on change in sign of the waveform gradient. The rests were computed by means of a semi-automated algorithm, incorporating linear interpolation. The results from this study supported the findings from Holdsworth et al. [35] and Ford et al. [10] which was that the archetypical waveform can be used to regulate cycle-to-cycle variability. In addition, these waveforms were obtained from different locations along the carotid tree and carotid arteries. Since multiple carotid arteries in different locations were of interest, conclusions could be drawn about if there were statistically significant differences between the waveforms in these locations.
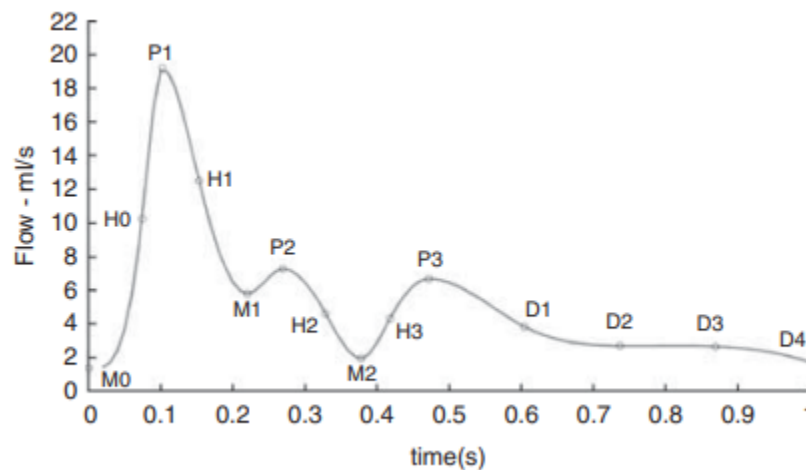
Figure 6.Figure obtained from the study by Gwilliam et al. [9], showing landmarks of interest in the study.

An additional study of interest was done by Rafati et al. [11], where waveform characteristics were investigated for characterizing atherosclerosis. Atherosclerosis is when plaque is formed on the inside arterial walls, which can result in e.g., occlusion of major arteries [26]. For evaluation of atherosclerosis, the main features given in this article were Peak Systolic Velocity (PSV), end diastolic velocity (EDV), peak diastolic velocity (V_D) and velocity of incisura between systole and diastole wave (V_I), as depicted in Figure 7 [11]. These landmarks were computed from the waveform which was obtained by an envelope detection algorithm called the *Modified Geometric Method.* From these features three parameters were derived namely, resistive index (RI), pulsatile index (PI) and dicrotic notch index (DNI) [11]. These indices have been previously used for prognosing cardiovascular diseases [11]. In this study, a semi-automated method was used to evaluate the diagnostic importance of these indices. The authors concluded that these parameters make useful means for evaluating carotid atherosclerosis development [11].
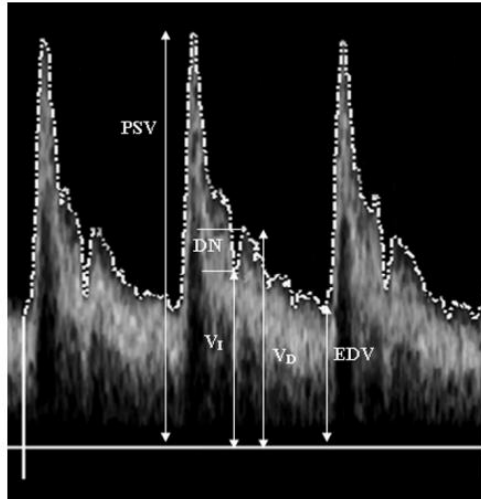
Figure 7. Illustration of the PWD waveform showing the landmarks of interest [11].

Based on previous research, features, or landmarks in terms of local extremes of a cardiac cycle have been used to evaluate development and status of cardiovascular and cerebral diseases. The following key observations were made based on these articles:

- Essential features of the velocity and VFR waveform that were often mentioned and identified were; maximum peak systolic velocity, end diastolic velocity, minimum velocity of the dicrotic notch, and peak diastolic flow [9], [11], [12], [35] and are commonly used to describe these waveforms and analyze pathological changes.

- For detecting these features, the authors have used customized algorithms or manual notation.

- Based on these articles only one cardiac cycle of the PWD and VFR signal is normally of interest per subject and detecting features over repeating cardiac cycles in a signal segment is lacking in the field.

4.3 Datasets

The main datasets used in this work were intermittent measurements documented in the Case Report Form (CRF) data and the sensor signals measuring VFR stored in TDMS files. Each subject had its own CRF dataset in MATLAB - data format. This data contained the measurements obtained at the calibration points of the Swan Ganz and PiCCO systems. The number of TDMS files containing the VFR signal segments varied per subject

As described in section 3.2, the study had two sets of data collection phases. The first data collection phase had four blocks with four steps in each, whereas the second data collection phase was one block with approximately three steps depending on the subject. In each of these blocks both the Swan Ganz and PiCCO system were calibrated and the cardiac output documented manually in the CRF. Therefore, the CRF dataset contained on average 18 calibration points per subject. Among all 11 subjects, 207 datapoints were available measured at the calibration points of both PiCCO and Swan Ganz systems.

In addition, the Transonic flow system also outputted instantaneous flow measurements, which were documented in the CRF at the time of calibration. These values turned out to be useful since they gave an indication of the magnitude of the blood flow at the point of calibration as captured by the Transonic flow

sensor. When exploring the VFR pulse signal segments computed around calibration points, these intermittent measurements gave an indication of what can be expected of the Area Under the Curve (AUC) over one minute around calibration points, as this would give the volume of blood passing the measurement location over one minute.

Finally, the VFR sensor signals were stored in segments of different lengths in so-called TDMS – files. The available data in these files will be discussed and described in more detail in the following sections.

4.3.1 Exploring VFR sensor signal in five different arteries (Channel 10 data)

As mentioned in section 3.2, the VFR was measured by Transonic flow sensors in five different arteries. The arteries were the hepatica, carotid, portal, aorta and femoral. In this section, the data obtained by the sensors of the so-called Channel 10 data are described. Channel 10 refers to that for each artery, 2 channels were reserved. Namely, one channel contained instantaneous pulsatile signal, and the other channel contained an averaged signal. 1

For each subject a set of files of format TDMS were available. The format TDMS stands for National Instruments Technical Data Management Streaming, and contains measurement data, recorded by National Instrument (NI) software. The number of files varied per subject but on average there were 15 files available, depending on the number of times the sensors were tested. Combining the signal data in the TDMS files yielded the full signal over the study period. Furthermore, each TDMS file contained respective metadata of the signals. Some TDMS files contained data from a test phase, which was sometimes indicated in the file name, but this was an exception not a rule.

The objective was to use the raw pulse signal to estimate the flow at calibration points. As mentioned before, each artery reserves two channels e.g., channel 1 and channel 2, where *even* channels contained the instantaneous pulse signal and the *odd* channel contained the average signal. As it is not documented how the average signal was computed, the raw pulse signals in the even channels were used for estimating the flow.

There were multiple uncertainties associated with the pulse signal. Firstly, the signal was measured in volts (V) and had to be converted to flow rate (L/min) or (mL/min). This calibration factor was sensor specific and is dependent of the size of the sensor. For each subject, a specific *look-up* table was provided. In addition, sometimes the electrodes of the sensors were swapped which meant that parts or even the whole signal could be inverted.

The idea was to process Channel 10 data, and then use the pulse VFR signal at the common carotid for modeling. The problem was that when calculating the area-under-the-curve (AUC) of the signal segment ±30 sec around the calibration points of CCA and aorta, these values could be negative. Based on domain knowledge, it is possible to have occasionally reversed flow (negative flow), however, having reversed flow for 1 minute is not possible. This statement was confirmed by experts. In Figure 8, the signal segments of all five arteries measured from Subject 5 at calibration point number 2 is shown. In this figure, the AUC of the CCA flow was -21 mL/min, whereas in the CRF the value 220mL/min.
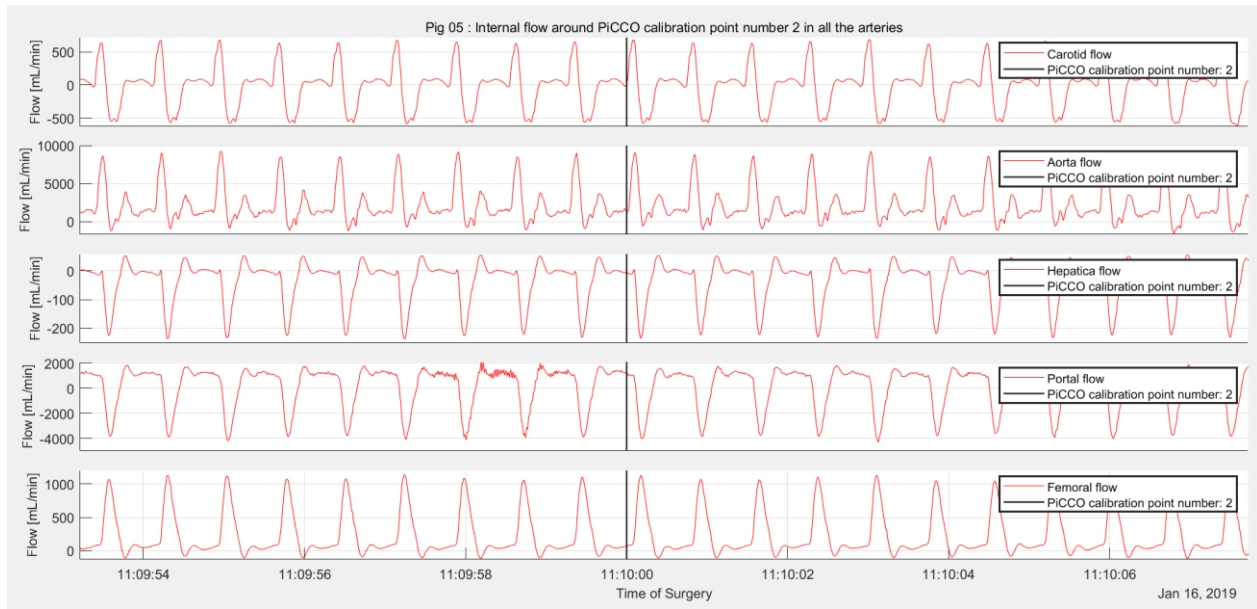
Figure 8. Alignment of the pulse signal in all the arteries of Channel 10 data around PiCCO calibration point number 2 of subject 5. Illustration produced by Matlab function [36].

As the pattern of finding unfeasible AUC values repeated itself, it turned out that Channel 10 – data would not be suitable for the remaining of the research. This is because (1) the flow values could not be matched with the intermittent sensor data in the CRF, and (2) AUC could obtain negative values. In the case of the example given above for Subject 5, inverting the signal segment would not help because (1) the waveform would look different than the remaining of the signal and (2) the value would still not match the one in the CRF. Therefore, the Channel 1 – data containing the sensor signal of only the carotid was considered. This data will be described in the following section. Figure 8 was created using an open source Matlab function [36].

4.3.2 Exploring VFR sensor signal in the common carotid artery (Channel 1 data)

As explained in end of the previous section, since the AUC of the signal segments of both the CCA and aorta in Channel 10 data could not be matched with the values in the CRF, only the CCA in Channel 1 data was considered. The same check as for Channel 10 data was performed on the CCA signal segments in Channel 1 data, namely, the AUC of the signal segment ±30 sec around the calibration point was computed. The AUC of these segments yielded the volume of blood passing the measurement point over 1 minute, which were comparable with the values in the CRF. The results for Subject 5 are presented in Table 1.

Calibration Point	AUC of sensor segment CCA (±30 sec) [L/min]	Flow CCA documented in CRF [L/min]
1	0.266	0.264
2	0.227	0.22
3	0.318	0.305
4	0.251	0.244
5	0.279	0.266
6	0.209	0.198
7	0.319	0.319
8	0.310	0.311
9	0.426	0.429
10	0.369	0.371
11	0.445	0.442
12	0.242	0.242
13	0.289	0.283
14	0.271	0.25
15	0.336	0.342
16	0.281	0.28
17	NaN	0.235
18	NaN	0.187

Table 1. Table showing the AUC of the signal segments around the calibration points compared to the flow of the CCA documented in the CRF. The two last values are NaN because no signal is available during these calibration points.

By observing the results in Table 1, the values at each calibration point differed on average by approx. 0.005 mL/min. Based on the results of this check, which was also performed on the remaining subjects and giving similar results for most of the subjects, the Channel 1 data was assumed to be correct. This assumption was also confirmed by scientists who had worked with the data prior to this work.

After verifying that the data was correct, every signal segment at each calibration point for each subject were generated, yielding on average 18 figures per subject. An example of a figure showing one of the signal segments around a calibration point is given below in Figure 9.
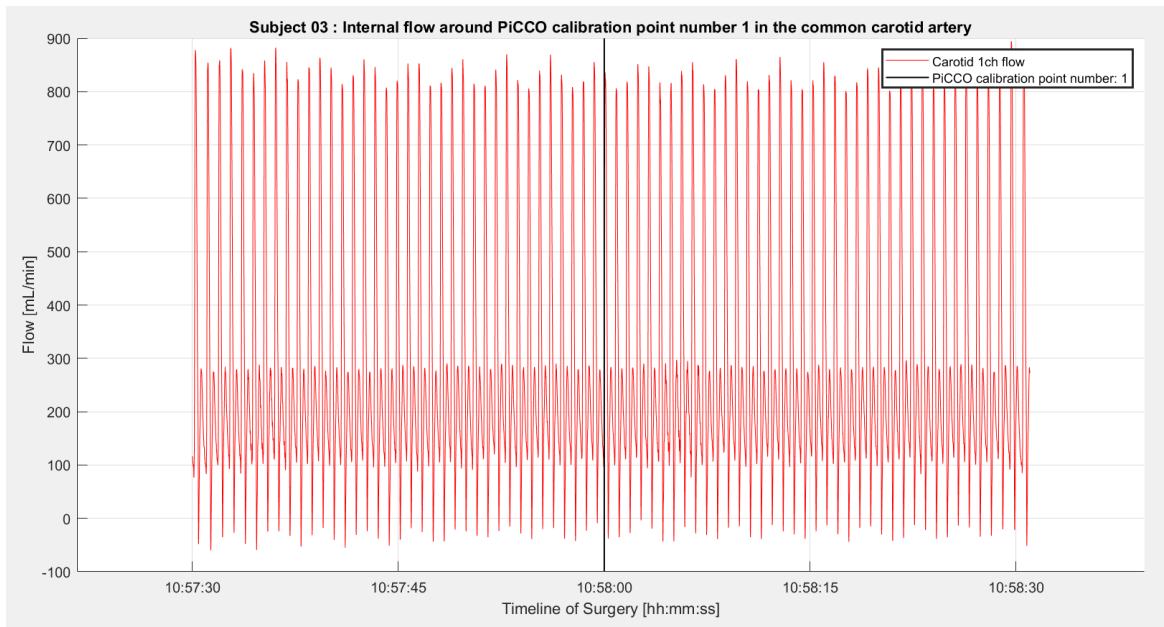
Figure 9. Example of the VFR sensor signal in the common carotid artery measured from Subject 3 at PiCCO calibration point 1.

28

By visually inspecting these figures (Figure 9), following questions were proposed without considering the underlying physiology of the signal:

I. ***What is the waveform morphology of the signal?*** Some signals might have more distinguishable local extrema than others, and maybe it differs based on the nature of the study. The following cases were considered based on speculations of the waveform morphology:

  o Local extrema are on the upstroke of the pulse wave.
  o Local extrema are on the downstroke of the pulse wave.
  o No clear local extrema are present.

II. ***Is there initial inherent noise in the signal due to the sensor itself?*** Some signals had indication of inherent noise in the signal throughout the surgery due to the sensor itself. Noise in the signal could also be present due to medication administration or positional change of the subject. These types of interventions could weaken the attachment of the sensors or alter the location of the sensor, which in turn could introduce temporary noise in the signal in the form of local noise. The following cases were considered:

  o There is no inherent noise due to initial attachment of the sensor.
  o There is inherent noise due to initial attachment of the sensor.

III. ***Are there interruptions because the signal is lost?*** Following question II. it should be determined if a potentially lost signal should be excluded. The following cases were considered:

  o The interruption occurs due to a lost signal and should be excluded from the data analysis.
  o The interruption occurs due to a potentially lost signal but should **not** be excluded from the data analysis.

IV. ***Is the signal inverted?*** In some cases, the VFR signal was inverted which resulted in negative flow over the one-minute window of interest. This could be verified by computing the area-under-the-curve (AUC) of the whole segment to get an indication of the volume of blood flowing in the CCA during that one minute. If this was negative, then the signal was inverted, since now the data is assumed to be correct.

V. ***What is the calibration factor from voltage to flow?*** As explained earlier the pulse wave obtained from the Transonic flow sensor was measured in volts. Therefore, a calibration factor had to be verified to convert the pulse wave from volt to flow (unit: liters per minute).

To the best of our knowledge, the waveform morphology has an upstroke, a downstroke, and local maxima and minima (local extrema) associated with either the upstroke, and global minimum and maximum for each cycle of the waveform. The strength and presence of local extrema differs per calibration point which indicates that the consequences of the interventions play an important role, as each calibration point is associated with an intervention. Furthermore, based on conversations with experts, there are various factors that might affect the signal e.g., the attachment of the sensor, the sensor itself and individual physiology of the subject.

These questions were proposed before considering any underlying physiology that might affect the VFR signal. Therefore, to analyze the flow rate signal, the expected waveform when including the physiology of the subjects will be defined. In addition to technical noise, there are physiological reasons contributing to the noise in the flow rate waveform, which will also be discussed in the upcoming section where the aim is to understand the VFR sensor signal.

4.4 Understanding VFR sensor signal in the common carotid artery (Channel 1 data)

In previous sections, the data to be used in this research was explored. In this section, the VFR waveform is explored further by also incorporating the domain knowledge. Firstly, the expected waveform and periodicity of the VFR waveform is discussed after which the landmarks of interest will be defined.

4.4.1 Expected waveform of the VFR sensor signal

In Section 2.3, the different phases of the cardiac cycle were discussed. In this section, the expected waveform of the VFR pulse signal measured by the Transonic flow sensor will be defined. The assumption is that the underlying physiology of the heart function can be captured by the VFR waveform. Therefore, a good starting point is to divide the waveform of one heartbeat into a systolic and a diastolic phase.

Based on domain knowledge of the cardiac cycle given in Section 3.1, the systolic phase starts after the Atrioventricular (AV) valves close. In terms of the waveform morphology of the VFR waveform, this would be the point in time just before the acceleration to the systolic peak. More specifically, this would represent the upstroke to the systolic peak, where the blood reaches its maximum flow. The peak systolic flow occurs during the rapid ejection after opening of the semilunar valves, which allows the blood to flow into the circulatory system. In the literature, the systolic peak is one of the main characteristics of the PWD/VFR waveform, defined as the **maximum** or global peak of one cycle in the PWD/VFR waveform [9], [12].

From the systolic peak, the waveform has a downstroke to the local minimum in the early diastole (Early - DF). Reverse flow is possible in the CCA and the deduction was made that if there is reverse flow and the zero-flow baseline has been crossed, the cardiac cycle has entered an early diastolic phase [19]. After speaking with professionals, the conclusions were that reversal flow in fact might occur during the closing of the semilunar valves which is also known as the **dicrotic notch**. However, in this work, Early-DF is used because it describes better the phase of interest in the cardiac cycle.

From the Early-DF, it is expected that a local maximum of the late diastolic phase of forward flow also known as the peak diastolic flow (PDF) follows with a short upstroke and positive acceleration from the local minimum of Early-DF. The PDF rises from a vascular elastic recoil in the diastolic phase [12], making it a local maximum.

Finally, from the PDF the diastolic phase ends in the end-diastolic flow (End-DF) which is defined as the end diastolic minimum flow [12], which is a local minimum before the start of the systolic phase of the next heartbeat [9], [10]. From the PDF to End-DF, blood flow declines and the acceleration drops before it increases again in the systolic phase.

In summary, the expected waveform of one heartbeat of the Transonic flow rate signal can be divided into systole and diastole, where three characteristics (local extrema) are expected from the diastolic phase and one global maximum in the systolic phase per cardiac cycle. Based on these characteristics, we wish to describe the waveform based on the consensus article by Kim et al. namely using key descriptors: (1) direction of flow; (2) phasicity, and (3) resistance. In Section 4.4.3, where the landmarks are formally defined, motivation for the choice of these specific landmarks are given.

4.4.2 Periodicity of the VFR waveform

Another essential part of the cardiac cycle and therefore, an essential factor of the VFR signal, is the inter-beat interval (IBI), which is defined as the time between sequential contractions of the heart [37]. Essentially, the IBI represents the **periodicity** of the VFR signal. This is an important factor in this work since two successive landmarks of the same kind are separated by periodicity.

To determine the IBI, a range of feasible heartrate values should be estimated for the chosen flow segment. The initial estimation of the IBI will be determined based on available literature, where similar studies on the same subject have been performed. Note that finding a study with the same experiment protocol and set-up is not feasible. Therefore, the objective was to review articles where (1) the same animal was investigated, and (2) similar medication was administered during the study. In addition, it is essential to note that for the subjects in our study, the hemodynamic parameters alter based on the inter- and intraspecies factors e.g., age, weight, and breed [38].

After reviewing studies [39]–[41], it is clear that when performing experiments such as the one in this work, reproducibility is difficult to achieve. In the reviewed studies, the breed, weight, or medication differed with our study. However, the objective of this review was to obtain an understanding of the range of feasible heartrates of the subject.

As already mentioned from the study description in Section 3.2, the subjects underwent both medication administration and positional change, implying that there are multiple sources contributing to the range for possible heart rates. The two drugs administered were adrenaline and nitroglycerin. However, when combined, what happens to the heart rate is unclear. In the reviewed articles, the heart rate range varied between the lower bound of the average heart rate, 50bpm, and the upper bound of the average heart rate, 170bpm.

In the end, the average upper bound of 170bpm was used as an initial estimation of the **periodicity** based on the study by Shen et al. [41], since adrenaline was also administered in the study. Furthermore, there is some additional heart rate variability (HRV) which might further increase the upper bound, however, the HRV is not known and therefore an **approximation** of the average heartrate is chosen based on literature. Notice that the approximated periodicity is a rough estimation and determining the upper bound for the heartrate would require analyzing the ECG signal obtained from the study which is out of scope of this master thesis.

The heartrate in beats-per-minute can be converted to datapoints per beat as the sampling rate of 120 Hz is known, and therefore, can be used as the initial estimation of periodicity in terms of number of timestamps.

4.4.3 Definitions of landmarks

Finally, the landmarks of the expected VFR waveform will be defined. There are two major contributing factors for defining the landmarks, namely the expected morphology of the waveform and periodicity. Periodicity implies that the same landmarks in successive heartbeats will be separated by a period that is approximately the average IBI. The definitions of the landmarks are the following:

Landmark 1 (Peak Systolic Flow): The peak systolic flow is defined as the global maximum of the heartbeat and a local maximum in the full signal segment. In other words, it is the highest value in one cardiac cycle and it is the only landmark representing the systolic portion [9], [10].

Landmark 2 (Early Diastolic Flow): This landmark occurs after the PSF and is defined as the local minimum of early diastole or as minimum flow in dicrotic notch [35]. A local minimum is the smallest value compared to neighboring values (set of values), however not the smallest value of all values in the signal. This

landmark occurs after a downstroke from the PSF and can be negative. As stated in Section 2.3, negative flow can occur in early diastole. Therefore, the assumption is that the landmark after the peak systolic flow in many cases represents the global minimum in the cardiac cycle.

Landmark 3 (Peak Diastolic Flow): This landmark occurs after an upstroke from the early diastolic minimum flow. It is the highest value in the diastolic phase [12]. Therefore, this landmark is defined as a local maximum flow rate between the minimum early diastolic flow and minimum end diastolic flow.

Landmark 4 (End Diastolic Flow): This landmark occurs after the downstroke from the peak diastolic flow. It marks the end of the diastolic phase and the start of the systolic phase of the next period, namely, it occurs just before the contraction of the heart. It is a local minimum in diastole [35].
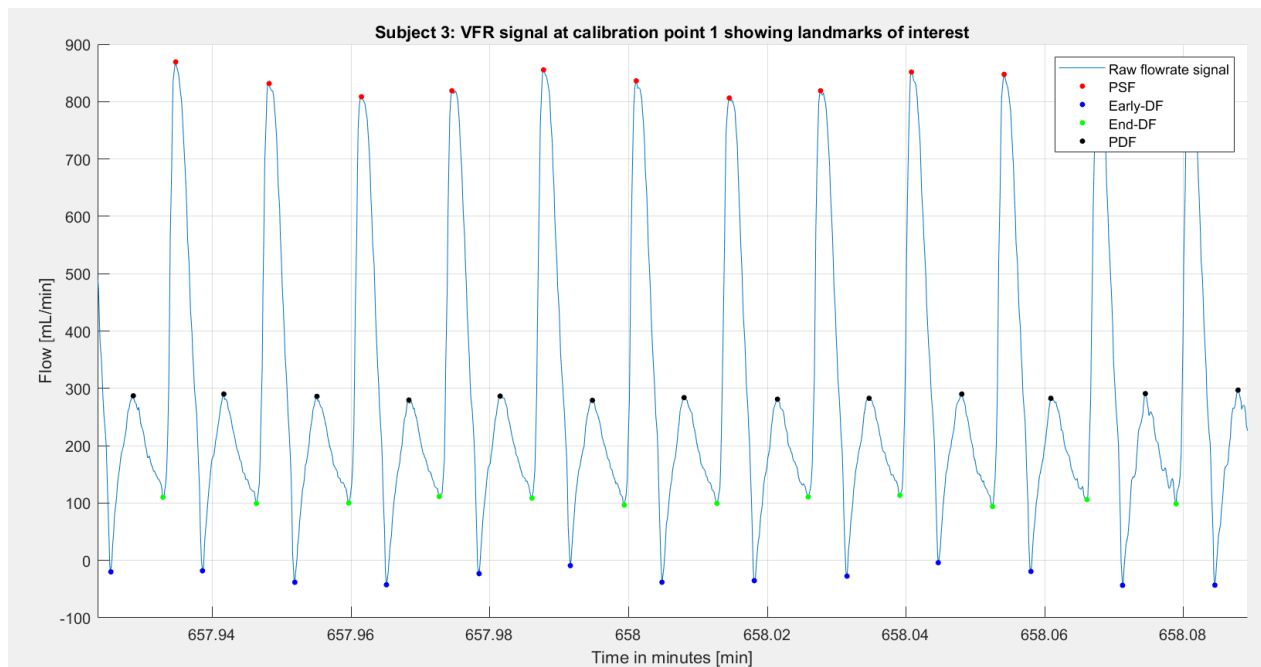
Figure 10. Figure showing the landmarks of interest. The red points represent the PSF landmarks, the blue points represent the Early-DF landmarks, the black points represent the PDF landmarks and finally, the green points represent the End-DF landmarks.

In summary, based on domain knowledge, the shape and therefore, the landmarks during one period of the VFR waveform are expected to occur in the following order: starting from the minimum end-diastolic flow (End-DF) represented by the green mark in Figure 10, the signal continues to a local maximum, also known as the peak systolic flow (PSF) represented by the red mark in Figure 10. For one period the PSF represents the global maximum. After the PSF, the (Early-DF) follows in the form of a local minimum, possibly negative, which is represented by the blue mark in Figure 10, finally the signal ends at the peak diastolic flow (PDF) which is represented by the black mark in Figure 10. From the PDF the cardiac cycle ends back at the End-DF.

The waveform shown in Figure 10 is what is expected from the signal. However, due to technical noise in the signal, interventions, and physiology, the morphology of the signal might differ in terms of the number of local minima and maxima together with their respective location. In other words, there can be multiple sources contributing to the noise of the signal. These possible sources of error will be discussed in the following section.

4.5 Sources of error

In this section the sources of error in the VFR sensor signal are discussed. The two major sources contributing to error in the VFR waveforms were identified as underlying physiology and technical noise.

4.5.1 Physiology

Firstly, it is essential to consider the underlying physiology of the subject itself. Since measurements are made at the common carotid artery (CCA) by the Transonic flow sensors, it is necessary to mention the effects of cerebral autoregulation. Cerebral autoregulation is an intrinsic functionality of the body which regulates cerebral blood flow by keeping the flow constant for a broad range of blood pressure values [42].

The porcine animal model is often used when studying the human brain due to similarities in e.g., development and anatomy of the brain [43]. Analyzing the effect of cerebral autoregulation is out of scope in this master thesis, however, it is essential to consider that the interventions and postural changes performed in the study might affect the measurements obtained by TFS at the CCA, however, the effect of cerebral autoregulation will be considered an **unquantifiable** source of error.

When exploring the segments around the calibration point, a specific deviation was noted in the signal. This deviation looked like a skipped heartbeat as depicted in Figure 11 at approximately time point 12:18:10. This phenomenon is called Ectopic heartbeat. Ectopic heartbeats are irregularities in the heart rhythm and can be noted as discontinuations in expected regular periodicity [44].
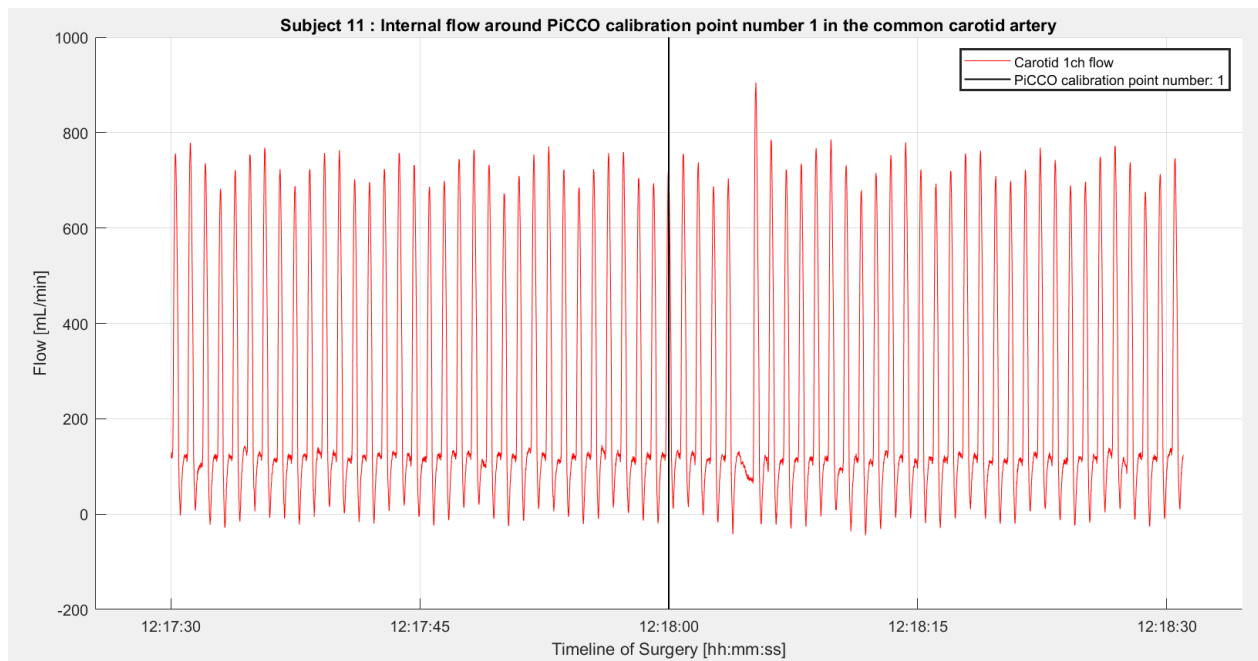
Figure 11. An example of a signal segment in which an Ectopic beat occurs.

Ectopic heartbeats can be noticed in the signal through absence of the systolic peak in the period. In other words, if there is a systolic peak missing over the period in the signal then there is a heartbeat missing.

In addition to Ectopic heartbeats, some waveforms show more fluctuation with respect to the systolic peaks and the early diastolic valleys. In Figure 12, the early diastolic flow shows rapid change in the amplitude between successive landmarks. This needs to be kept in mind when clustering local extremes, since the change in amplitude of these landmarks might result in that same landmarks get clustered into **separate** clusters.

33
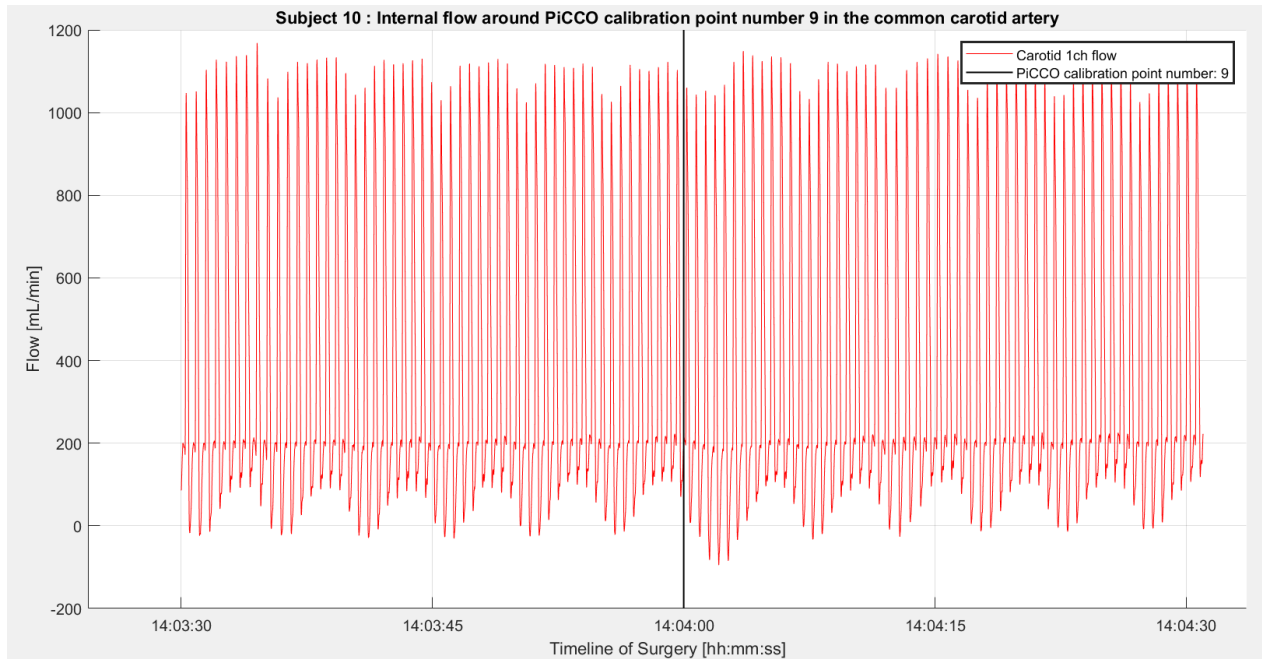
Figure 12. Signal segment with fluctuations in successive Early-DF landmarks in the bottom of the signal.

4.5.2 Technical noise

Technical noise introduced by the Transonic flow sensor (TFS) occurs in the signal as low frequency noise as depicted in Figure 13. More specifically, this type of noise can be defined as densely occurring local extremes (local minimum/maximum) around the landmarks of interest and are assumed to have no physiological significance but it simply represents a biproduct of the measuring process using the TFS.
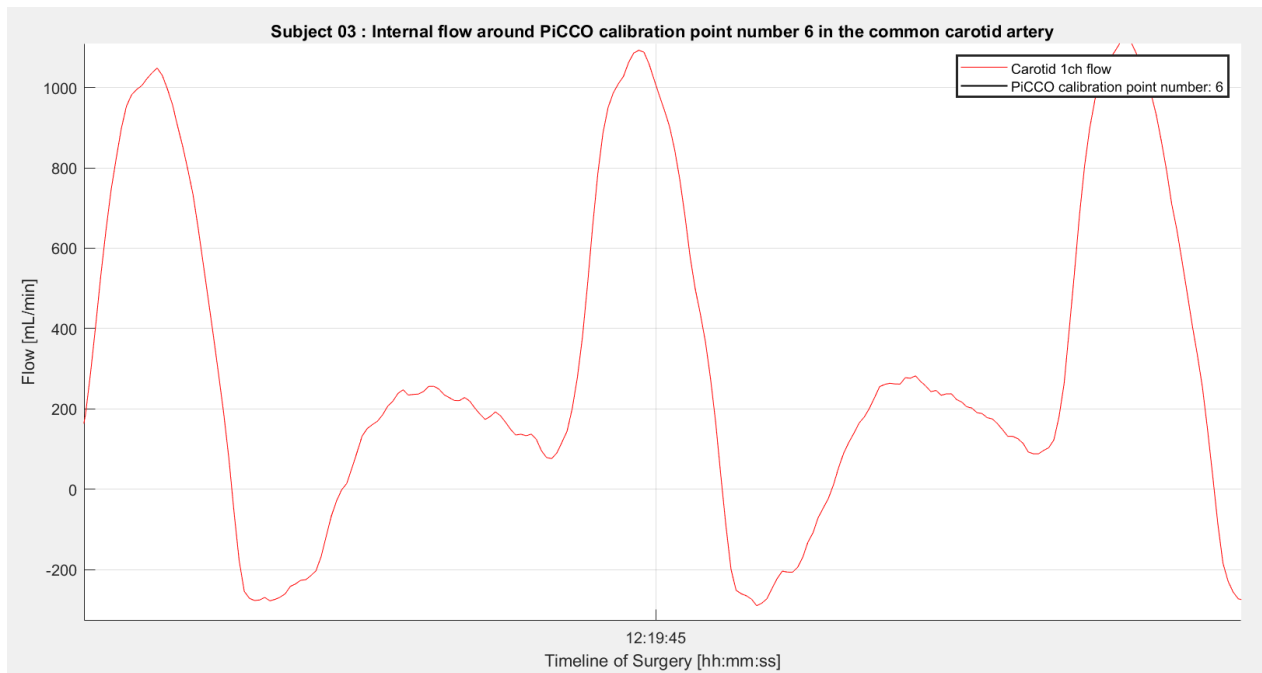
Figure 13. Technical noise may occur in the form of densely occurring local extremes in the waveform. It is assumed to be noise inherent to the Transonic flow sensor.

34

From discussions with experts present in the experiments and documentation from the surgery, these flow sensors were attached surgically in the arteries. The attachment was not problem free in terms of finding the right location and fit around the artery. In addition, as also stated in the article by Mynard et al., these sensors require proper acoustic coupling between the sensor and vessel wall [2].

In conclusion, the attachment of the flow sensors around the CCA may cause densely occurring local extremes which affects the detection of landmarks as these landmarks may be surrounded by noise. The factor that separates the noise from the actual landmarks is the **periodicity**, namely the inter-beat interval. In other words, two landmarks of the same type should occur at timepoints that differ by the periodicity of the waveform.

4.6 Data preparation

As explained in section 3.2., the VFR data were stored in TDMS files. As explained in the previous section, the TDMS files containing the so-called Channel 1 data is used in this work for which the following factors need to be considered. In this section, the data preparation phase for obtaining VFR signal segments around PiCCO calibration points is explained.

Firstly, the data stored in the TDMS - files had to be converted to Matlab data. A script by National Instruments (NI) was used to read the TDMS file into a Matlab structure. This script was provided by Philips Research to be used in this work. The obtained Matlab data was a structure that contained 12 fields. The data of each field are presented in a Table (see Appendix A) were the original names of each field were kept. Later, only the relevant data was stored in a separate structure when preparing for the modeling.

The data was converted separately for each subject to identify deviations in the measurement process and which TDMS files contained the relevant data. The following deviations were identified:

- TDMS file contained structure data with empty fields. If the fields were empty, then the TDMS file was excluded.
- TDMS file contained data from the test phase prior to the start of calibration points of PiCCO - and Swan Ganz systems. Sometimes a test phase could be indicated in the name of the TDMS file, but this also was inconsistent. The test files were excluded if the signal in the TDMS file ended before the first PiCCO calibration point.

Each TDMS file of Channel 1 data contained in general three signals, which had to be visually inspected to find the pulse signal due to inconsistent naming of the signals. These signals have been added to Appendix B.

After all empty and test files were excluded, the pulse signal had been verified, and the time segments were computed for each signal segment, all the TDMS files for the subject were combined and sorted based on time. At this point the signal was still measured in volts (units V). The conversion from volt to flow was done by using a calibration factor of 400mL/min defined by domain experts and documentation.

After the full signal had been converted to a volumetric flow rate (VFR) signal , the signal segments of ±30 seconds around each PiCCO calibration point. The idea is that the landmarks of each heartbeat in this segment can be used for analyzing blood flow in the carotid in future research.

After calibrating the signal and computing the signal segments used for modeling, the polarity of the sensors needed to be verified. Namely, based on domain knowledge, it is possible for the waveforms to be momentarily negative for physiological reasons (reversal flow) but in our case, also if electrodes of the sensors were swapped manually. After discussing with experts present in the study, it turned out that the electrodes of the sensors could be either occasionally swapped or swapped throughout the whole surgery.

In case the polarity of the electrodes was swapped, the signal was inverted and therefore also the AUC negative. Therefore, by computing the AUC of the signal segments over 1 minute, we were able to verify when the electrodes had been swapped.

4.7 Data cleaning

In this section, the necessary data cleaning part is given. Just like with any signal, we expect to have signal segments that cannot be used for the analysis due to noise inherent to the measurement process of using sensors. The objective is to develop a method to quantify when periodicity is violated such that the whole signal segment should be excluded.

At this point we cannot do this by investigating the periodicity itself since that would require knowing the landmarks, in particular the global maxima of each period in the VFR waveform. On the other hand, visual inspection of each signal segment is impractical. Therefore, we explore what can be considered feasible flow values in the sensor waveform and what can be considered clear deviations in these values. Again, there can be times when there are occasional deviations such as Ectopic heartbeats, however, the objective is to find when a large part of the signal or even the whole signal is corrupted.

We believe that by computing robust statistics of subsegments using a sliding window throughout the signal segment, results in a better understanding what can be considered feasible for the values in the waveform and for detecting when interruptions occur. The analysis is performed per subject due to inter subject dependencies. The chosen statistics are the **median**, the **25th** percentile and the **75th** percentile of the flow rate values captured in the sliding window. These statistics make robust estimates since extreme values are excluded.

The first step is to compute these subsegments using a sliding window through all the signal segments computed in the Section 4.6. The sliding window should cover a couple of heartbeats to capture the deviation occurring over a longer period and not only due to a physiological phenomenon such as an Ectopic heartbeat, which we believe occurs in this signal only during one period. Since each signal segment contains 1 minute of measurements, a feasible window size could be using the ventilation rate, namely, how many breaths the subject took per minute. Based on the study protocol, the ventilation was 12-15 breaths/minute. This indicated that one respiration cycle was 4-5 seconds. We chose the shorter period as window length. Since the average number of calibration points is 18, this would imply approximately 270 windowed data segments per subject. After this, the 25th percentile, median and 75th percentile of each data segment were computed.

To investigate the nature of the flow rate values, each computed statistic of all subsegments was plotted in its own histograms as depicted in Figure 14. No assumptions of the distribution were made since it is not known how underlying physiology and interventions affect the flow rate measurements.
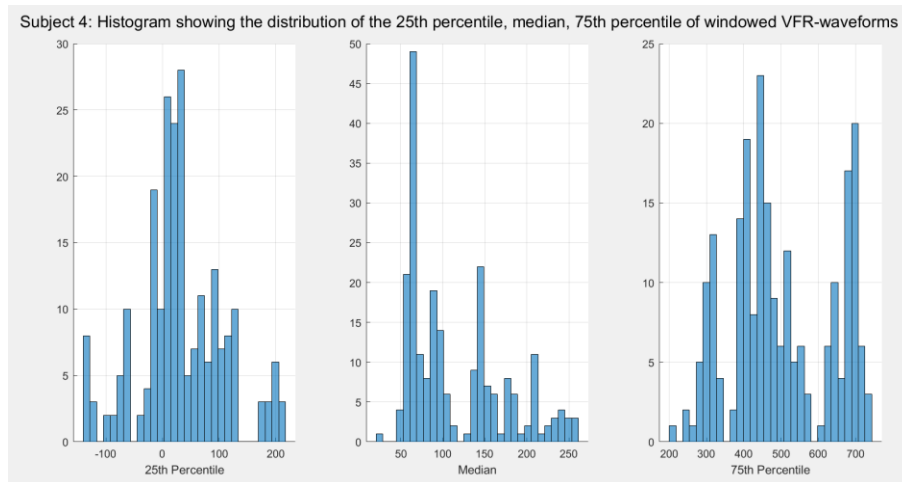
Figure 14. Histograms showing the distribution of the 25th percentile, median and 75th percentile of the flow rate of the subsegments for Subject 4. The bin size is chosen to be 30.
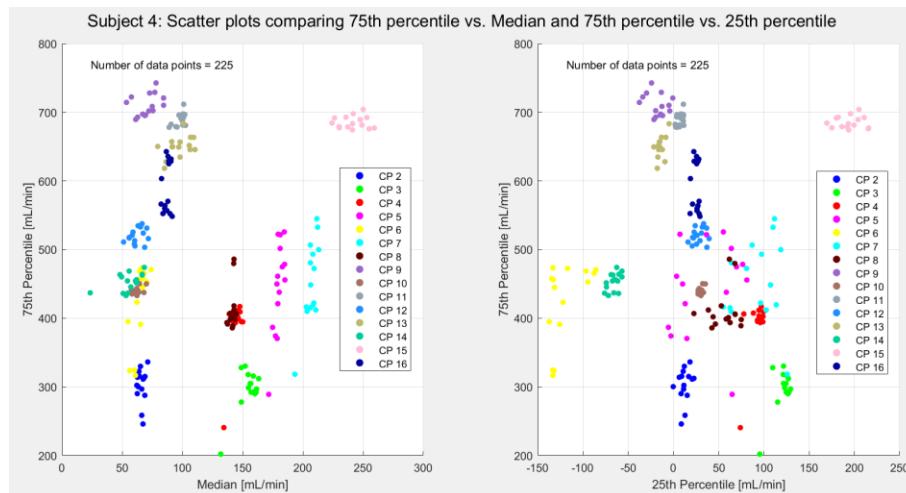
Figure 15. Scatter plots comparing the 75th percentile of each subsegment with both the median and 25th percentile of each subsegment. The color of the datapoints indicate the original signal segment which is associated with a calibration point which is abbreviated as CP in the legend. This plot shows each subsegment of Subject 4.

Figure 14 shows the distribution of the data obtained from the above described approach for Subject 4. From the figure, it is clear that for this subject the 75th percentile of the flow rate in the windowed data is around 500 mL/min however, sometimes higher (around 700 mL/min) and sometimes lower (around 300 mL/min). This is the result of the different interventions and physiology contributing to the change of flow rate. For the median flow rate, around 70 mL/min was measured most frequently. Finally, the 25th percentile indicated that sometimes negative flow occurred, and the most frequent value was around 0. From the domain knowledge, occasional negative flow is feasible. Based on this plot, no deviating or suspicious values were identified. In addition, the scatter plots show well grouped datapoints, with some groups containing slightly more variability than others, which can be the result of variating respiration rate.

Next, we demonstrate how deviating flow rate values were detected. The subject with the noisiest signal segments was Subject 9, which will be used as example. Again, the histograms showing the distribution of

the median, 25th percentile and 75th percentile of the flow rate values in the windowed data were computed and plotted .
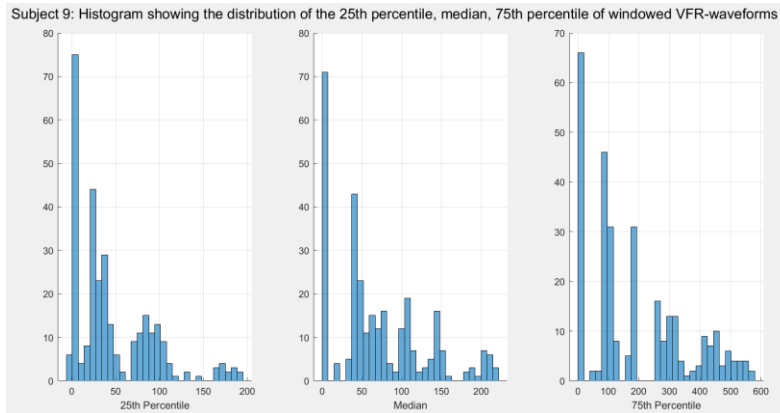
Figure 16. Histograms showing the distribution of the 25th percentile, median and 75th percentile of the flow rate of the subsegments for Subject 9. The bin size is chosen to be 30.

Compared to Subject 4 in Figure 14, the most frequent values for **all** statistics of interest is around value 0. This seems strange since the waveform is expected to be periodic, which implies that there should be distinction between the statistics of the windowed data, especially for the 25th and 75th percentile. As was concluded from Figure 14, it would make sense that the 25th percentile can obtain values close to 0, however, having all three statistics being most frequently around 0 is not feasible.

To identify which signal segment(s) contains the deviating values, we extracted the values from the first bins of each histogram and checked around which calibration point this windowed data was measured. In addition, scatter plots were created showing how the windowed data behaves per calibration point and if there are cases when whole signals are around zero. In this case there should be data points close to the origin.
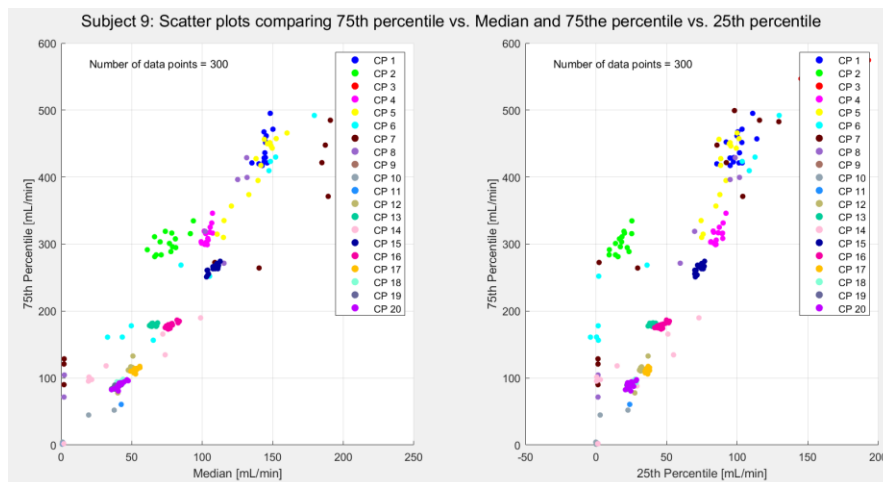
Figure 17. Scatter plots comparing the 75th percentile of each subsegment with both the median and 25th percentile of each subsegment. The color of the datapoints indicate the original signal segment which is associated with a calibration point which is abbreviated as CP in the legend. This plot shows each subsegment of Subject 9.

The main deviation is also captured in the scatter plot e.g., when observing CP 14 (light pink). For these data points all statistics, namely, median, 25th percentile and 75th percentile obtain flow rate values around 0. This example also has some points scattered across the plot, indicating occasional interruptions in the pulse signal. This same holds for CP 7, CP 8, CP 10, and CP 11. In addition, it seems like CP 9 is completely interrupted which is indicated by no datapoints being visible in the scatter plot, since all are overwritten by measurements at later calibration points e.g., CP 11 and CP 14. Based on the figures of the histogram and the scatter plot, we can get indication of when there are interruptions in the signal segments. For example, when visually inspecting the signal segments at CP 11 and CP 14 in Figure 18, it is clear that the expected waveform is violated in both the left figure and right figure. The left figure shows no periodic signal whereas the right figure shows periodic data in the beginning of the signal, before the calibration point, after which the signal is interrupted.
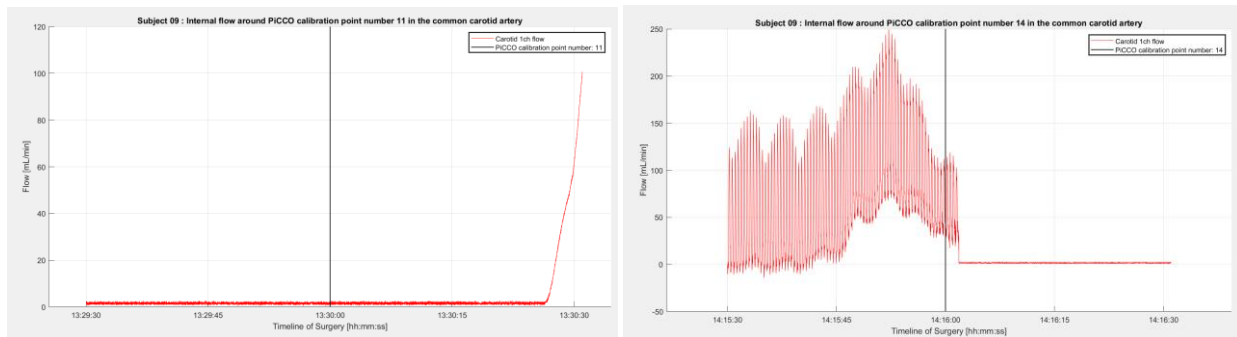
Figure 18. Interrupted flow waveforms for Subject 9. Examples are given at calibration point 11 (left) and at calibration point 14 (right).

Due to limited domain knowledge of the signal waveform with respect to feasible flow rate values, we shouldn't exclude a signal without verifying that there indeed are multiple missing periods resulting in that the three statistics of interest are around 0. By performing this analysis, we obtain indication about which signal segments could contain missing periods that are not for example Ectopic heartbeats. By visually inspecting the signal, we check if the waveform lacks periodicity in the form of **multiple** missing peaks, similar to the examples shown in Figure 18, such that there are periods during which the flow rate measurements are continuously close to the x-axis.

If there is only one missing systolic peak, like depicted in Figure 11, this signal segment shouldn't be excluded. However, based on the length of the window, the subsegments should contain multiple periods and therefore, also capture if the signal contains more than one missing period.

If the waveform meets the exclusion criteria, we exclude the complete signal segment. Manually excluding signal segments through visual inspection can be used in data cleaning of physiological signals, due to the uncertainties associated with underlying physiology itself and measurement processes. By using this data cleaning approach, we can find the signal segments with interrupted periodicity, which can then be excluded from the analysis. We performed this data cleaning approach for each subject.

Based on the lessons learnt in this project, the following noise detection method can be used for identifying when the signal might contain missing periods. To achieve this, the following steps were taken:

1. For each subject, divide the signal segments into **subsegments** of length l, where l contains the signal over 4 seconds. This segment length is expected to contain multiple heartbeats and therefore captures the periodicity of the signal even in the presence of physiological deviations e.g., Ectopic heartbeats where one heartbeat is missing.
2. Compute the 25th percentile, median and 75th percentile for each subsegment.
3. Inspect the three histograms showing the 25th, the 50th and the 75th percentiles of all subsegments per subject and detect deviations from expected values. If one of the statistics obtain multiple subsegments with too low or too high values, then there is a high chance that the periodicity cannot be detected, and the signal remains e.g. close to the x-axis.
4. Create scatter plots comparing the 75th percentile to both the median and the 25th percentile. This approach is chosen because when periodicity can be detected in the signal, then the 75th percentile obtains significantly higher values than the other two. It is also expected that the statistics of subsegments from the same signal segment are scattered densely in groups. Some groups can have more variability than others depending on fluctuations in the signal segment. If there are groups close to the origin belonging to the same signal segment, then the compared statistics indicate missing periods in that signal segment. The same argument applies for groups that are scattered around significantly higher values than the rest of the groups.
5. Based on these plots, identify the signal segments with missing periods. Visually inspect these signal segments to determine if this indeed is the case. If the signal segment contains multiple missing periods consecutively, we exclude the whole signal segment since we do not know what uncertainties and errors it might introduce in the modeling.

Finally, we discuss briefly what kind of limitations our method might introduce in the modeling part. Based on the way we estimated the window size it could be that we have overlooked some spikes in the data. The term spikes refer to significantly higher flow rate values than the neighboring peaks. In case these spikes occur only ones in the window, then the chosen statistics will not capture this deviation as the high value of the spike might be only visible in the 90th or 95th percentile. Therefore, we cannot determine based on this approach if there is high frequency noise in the data in the form of spikes occurring irregularly in the signal segment. This limitation must be kept in mind in the modeling phase since we do not know its effect on the results.

5 Modeling

In this chapter we address the first research question which is how we can automate detecting and labeling landmarks. We do this by identifying the requirements for our model, testing two model candidates, and evaluating them. In the terms of the CRISP-DM methodology, this section can be divided into the following subsections: (1) selecting modeling technique(s); (2) building the model(s) and (3) assessing and evaluating the model(s) [22].

5.1 Select modeling technique(s)

When selecting a modeling technique, the expected output and the requirements should be set. The goal of the algorithm is to detect and label the defined landmarks to be used for characterization of the VFR signal and future analysis. The following **requirements** should be met by the model:

    I.   The landmarks of each period should be detected and labeled.
    II.   The landmarks should be separated from the technical noise present in the signal.
    III.   The model should detect when Ectopic heartbeats occurs.

The objective is to use machine learning for finding the landmarks of the VFR signal from each cardiac cycle, from now on referred to as **period**, and asses if these landmarks can be used to describe the signal segment in terms of (1) phasicity (2) direction of flow and (3) resistance.

Based on the first requirement, namely that landmarks from each period should be detected and grouped together, applying machine learning for this task seems like a feasible approach. As opposed to supervised learning, unsupervised learning does not require labeling of landmarks *a priori*. In many previously conducted research articles presented in Section 4.2, the landmarks are either manually labelled by experts or by using a custom-made algorithm. In addition, the waveform of **one** period (cardiac cycle) per subject is normally of interest, whereas in this work the objective is to automate the labeling of landmarks of all periods occurring over one minute around all calibration points for all subjects.

Based on the scope of this work, it is not feasible to label landmarks manually for a supervised learning approach because: (1) it is not doable to label all landmarks for such a large number of periods, and (2) there is not enough domain knowledge to ensure that the landmarks are labeled correctly. Therefore, an unsupervised learning algorithm should be considered for clustering landmarks.

A commonly used unsupervised learning technique is clustering, which is a method for clustering data into groups based on their similarities. It is common enough that an article was written for the soul purpose for addressing common mistakes when clustering biomedical data [45]. Further, after inspecting the data, we thought that using clustering would make a great starting point. In the following section, an overview of different clustering methods is given with respect to the above given requirements.

5.1.2 Clustering algorithm for detecting landmarks

In this section, the different clustering algorithms will be evaluated with respect to the requirements set to our model. The four commonly used algorithms are Hierarchical clustering, K-means clustering, DBSCAN clustering, and statistical methods e.g., Gaussian mixture models [45].

Hierarchical clustering creates clusters in a tree looking structure also known as a dendrogram. A dendrogram groups similar data in a tree shaped structure where the root represents the entire dataset. The branches of the tree then form the clusters. Hierarchical clustering is useful when data contains clusters within clusters, or when the data may have nested relationships [45]. There are two ways to perform hierarchical clustering, namely **agglomerative** hierarchical clustering, and **divisive** hierarchical clustering [46], [47]. The agglomerative hierarchical clustering method uses bottom-up approach, namely

starting from the leaves and merging clusters based on a chosen distance metric up until the root is reached. In general, agglomerative is more used in applications [46] and is the approach chosen for this work. The divisive hierarchical clustering method uses a top-to-bottom approach and starts from the root down until all single data instances have been reached [46].

For the VFR waveform, hierarchical clustering was mainly considered since we expect nested structure in the local extremes due to the presence of technical noise (presented in Section 4.5.2) in the flow rate signal. For calculating the distances between clusters, the Ward linkage method was used. The Ward linkage is commonly used in hierarchical clustering as it computes the clusters based on the incremental sum of squares when merging clusters. In other words, the data is clustered in such a way that when joining clusters, the increase of the within-cluster sum of squares is minimized. The reason for choosing this linkage is that the Ward linkage not only considers the distance between clusters but also aims to minimize the within cluster variability [47].

The Ward's linkage is calculated in the following way [46], [47]:

$$Ward(S_i, S_j) = \frac{n_{S_i} n_{S_j}}{n_{S_i} + n_{S_j}} d\left(c_{S_i}, c_{S_j}\right),$$

Where S_i and S_j are two clusters to be merged and $n_{S_i} = |S_i|$ and $n_{S_j} = |S_j|$, and

$d\left(c_{S_i}, c_{S_j}\right) = \left\|c_{S_i} - c_{S_j}\right\|^2$ is the distance between centroid c_{S_i} of cluster S_i and centroid c_{S_j} of cluster S_j.

K-means clustering algorithm clusters data based on the distance of the datapoint to the center of the cluster, also known as a centroid based clustering algorithm [45]. This results in the clusters that are roughly spherical in shape. The main parameter in K-means is the **number of clusters**, where the choice of this parameter may significantly affect the end-result of the algorithm [45]. In addition, the K-means algorithm performs poorly on irregularly shaped data [45] e.g., half-moon shaped clusters.

K-means was considered due to its simplicity and **intuition** of the expected number of clusters. With intuition, we mean that ideally the local minima are clustered in two separate clusters, and the local maxima are clustered in two separate clusters. However, due to the uncertainty of the noise in the waveform, choosing the right number of clusters for separating the landmarks is essential. For example, if we were to choose *K = 2* for clustering local minima, and there is some local noise in the form of a local minima close to the systolic peak, this results in that any local minima on the bottom of the signal will be clustered in the same cluster, if they are considered more similar in value than the local noise on the top of the signal. Therefore, due to the occurrence of local noise in the waveform, it is not certain what the optimal number of clusters will be to distinguish these landmarks. In addition, no assumptions should be made about the shape of the clusters, which is assumed to be spherical for K-means clustering.

DBSCAN clustering is a density-based algorithm and is useful for identifying densely connected data and for finding complex structures in lower dimensional data [45]. This algorithm has two main parameters: (1) *epsilon* and (2) *minimum number of points*.

Epsilon sets the density of the cluster, whereas *minimum number of points* literally indicates the minimum number of datapoints in each cluster [48]. The minimum number of data points can be estimated based on periodicity, namely through estimating the heart rate. On the other hand, the DBSCAN is useful for excluding outliers of the data, making the right choice of *epsilon* essential . However, due to uncertainties in the signal such as fluctuations where the amplitude of successive landmarks introduces more variability of the flow rate measurements, the choice of epsilon becomes specific for each signal segment. In Figure

15, an example of a fluctuating signal is shown, where the variance of amplitude between local minima in the bottom of the signal is high. This could result in clustering landmarks as outliers if *epsilon* is wrongly estimated. Therefore, if we choose to use DBSCAN, epsilon will need to be set manually for each signal and if chosen wrong, some landmarks might be classified as outliers which is not desirable.
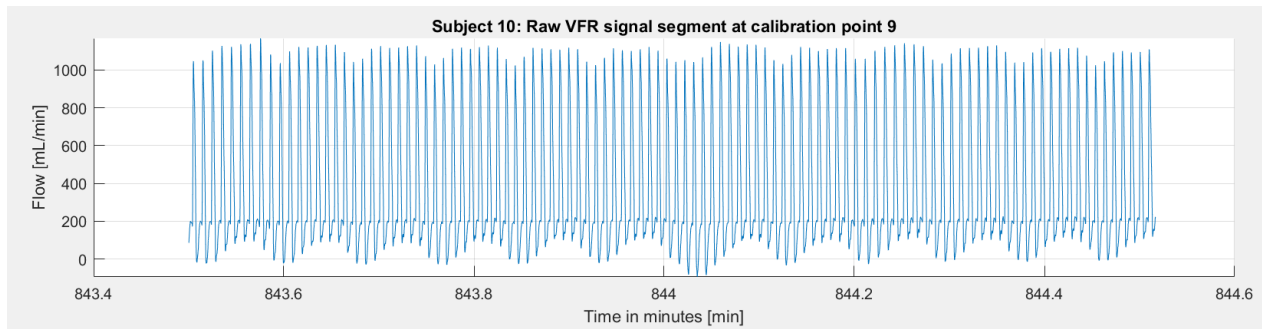
Figure 19. Example of a signal segment where fluctuation occurs. This is a scenario when the DBSCAN clustering algorithm might cluster landmarks as outliers if the density parameter epsilon is incorrectly estimated.

Statistical methods cluster data based on the fitting different statistical distributions to the data e.g., self-organizing maps and Gaussian mixture models [45]. This approach was not considered suitable for our purpose since no assumptions were made of the distribution of the local extrema.

After assessing the different clustering algorithms, the *hierarchical* clustering algorithm was considered the most suitable clustering algorithm for the objective of this research. Regarding the requirements set in the beginning of this section, the reasons for choosing the hierarchical clustering algorithm is the following:

- Hierarchical clustering can be used when there is nested structure in the data, which is the case with the noisy local extremes/technical noise.
- No specific number of clusters need to be set.
- The Ward linkage finds clusters by minimizing the incremental sum-of-squares of merging clusters. It is useful because it not only considers the between cluster distance but also the within cluster distance. Minimizing the variance within clusters will aid in grouping the noise around the landmarks into the same cluster after which the actual landmarks can be identified in these clusters by choosing either the maximum or minimum value depending on if a local maximum or local minimum is of interest, respectively.

In the next section we describe how we optimize hierarchical clustering.

5.1.3 Choosing the optimal number of clusters

For the hierarchical clustering the specific number of clusters were NOT defined beforehand and therefore, we needed an internal validation index to find the optimal number of clusters. If no internal validation index is used for determining the number of clusters, a threshold or cut-off value with respect to the distance between clusters would need to be defined. When considering only one signal segment, setting the threshold is not a tedious task since only the cutting point of the dendrogram need to be determined. However, this threshold could differ per signal segment and the cutting point would have to be chosen manually for each segment based on visual inspection of a dendrogram, and if chosen wrong, possibly exclude local minima or local maxima.

For an internal validation index, the Silhouette validation index was used. The Silhouette index for a datapoint indicates the strength of the membership of that point in the cluster. The Silhouette index is computed in the following way [49]:

For a point i in a cluster C. Firstly, the average distance $a(i)$ to all other data points in cluster C is computed. Then the average distance $d(i, B)$ is computed to all other values in any cluster B where $C \neq B$. From here, the value $b(i)$ is computed:

$$b(i) = min_{C \neq B} d(i, B)$$

Using $b(i)$ and $a(i)$ the Silhouette index $s(i)$ for point i can be computed:

$$s(i) = \frac{b(i) - a(i)}{\max \{a(i), b(i)\}}$$

The value $s(i)$ ranges from -1 to 1, where the closer the value is to 1 the better this datapoint i belongs to its own cluster. Finally, the average of the $s(i)$ of all points indicates the optimal number of clusters [18]. The closest value to 1 then determines the optimal number of clusters. This validation index was used since it had been noted in a previous article [18]. Later in the evaluation this index turned out to be effective, so no further validation indices were considered, however, we make note in future work that other validation could also be explored.

5.1.4 Separate landmarks from local noise

After choosing the method for clustering local extremes of the flow rate measurements, the requirement of separating the landmarks from the noisy local extremes is discussed. This should be done using a characteristic inherent to the expected waveform. We believe that by an inherent characteristic reflects on the true quality of the signal.

Based on the choice of clustering algorithm (Section 5.1.3), it is expected that densely occurring local noise around the actual landmarks get clustered in the same cluster. In addition, what separates the landmarks from each other and from local noise is **periodicity**. Therefore, the inter-beat interval (IBI) estimated in Section 4.4.2 can be used as an estimate of periodicity for separating the local extremes from noise. This is done by taking either the minimum or maximum value if the number of timestamps between successive extremes in the same cluster is smaller than the defined periodicity. We believe that periodicity should be robust since it is expected to be consistent throughout the signal segment.

5.1.5 Detect physiological deviations

In Section 4.5.1 we identified some physiological anomalies in the VFR signals. One noted anomaly was the Ectopic heartbeat. The Ectopic heartbeat should be considered since it could be impacting the effectiveness of the model.

The Ectopic heartbeat can be detected when a systolic peak is missing and with hierarchical clustering, it is expected that the peak systolic flow values of each heartbeat get clustered in the same cluster. Then by calculating the time points between successive peak systolic flow values, the inter-beat interval (IBI) can be calculated. If there is one systolic peak missing during one cardiac cycle, namely, roughly twice the IBI, then we believe that an Ectopic heartbeat has occurred.

5.2 The first iteration of the model

In this section, the model for computing the landmarks using hierarchical clustering is presented. The approach is based on clustering local minima and maxima of the VFR waveform, with the objective of detecting and labeling local maxima as either peak systolic flow (PSF) or peak diastolic flow (PDF), and local minima as either early diastolic flow (Early-DF) or end diastolic flow (End-DF).

The goals of this model are:

(1) to cluster the four landmarks in their own clusters
(2) separate the landmarks from noise
(3) detect deviations in the signal, namely Ectopic heartbeats

The idea is to first cluster local minima and maxima of the raw signal **separately** into clusters and this way give them labels. Then the model uses periodicity of the waveform for excluding local noise for detecting the landmarks. From now on any local minima are referred to as **valleys** and any local maxima are referred to as **peaks.**

In the case of the VFR waveform, 1D clustering of the original flow rate values turned out to be the best and simplest option, since adding additional dimensions did not contribute to the end results of the clustering. For example, dimensions such as the change in amplitude or time passed between two successive local maximum/minimum.

The inputs of the model are the **peaks** and **valleys** of the raw VFR signal segment f, which is a timeseries of the flow rate values of a windows size of ±30 seconds around PiCCO calibration points, the **sampling rate** which in the case of the VFR signal is 120 Hz, and finally, an approximation of the highest average heartrate BPM_{max} based on literature in Section 4.4.2. BPM_{max} is used for calculating the minimum periodicity between values in the same cluster.

There are 4 main functions in the first iteration of the model:

(1) ***Cluster*** peaks and valleys separately.
(2) ***Exclude*** local noise from clusters expected to contain the global peaks and global valleys of each period in the signal segment.
(3) ***Merge*** clusters in cases there are fluctuations in the signal causing landmarks of the same group to be clustered in different clusters. An example of when clusters require merging is given in Figure 20. These functions are discussed in further detail in following subsections.
(4) ***Identify*** remaining landmarks.

5.2.1 Cluster peaks and valleys

Firstly, the model computed all local minima and maxima flow rate values (peaks and valleys) in the raw VFR signal. After this, hierarchical clustering was implemented for clustering separately **peaks** and **valleys**, using the Ward linkage as the distance metric and the Silhouette evaluation index for determining the optimal number of clusters. When all peaks and valleys had been clustered, the centroids were computed for each cluster. The centroid of a cluster was defined as the mean of the values in that specific cluster.

The model started by investigating two clusters, namely, cluster $C_{peaksMax}$ and cluster $C_{valleysMin}$. Cluster $C_{peaksMax}$ was the cluster with the largest centroid and containing peaks, whereas cluster $C_{valleysMin}$ was the cluster with the smallest centroid and containing valleys.

Based on landmark definitions and the expected waveform, the assumption was that the values in $C_{peaksMax}$ and $C_{valleysMin}$ contain the PSF landmarks and Early-DF landmarks, respectively. The reasons for investigating the aforementioned clusters first were the following:

- It is uncertain which clusters contain the values of End-DF and PDF, namely local extrema of each period. Therefore, it is natural to start searching for the landmarks of PSF and Early-DF as they are assumed to represent the global maximum and minimum of each period, respectively.

- The values in $C_{valleysMin}$ can answer the question if the cardiac cycles of the flow rate segment contain **monophasic** or **multiphasic** phasicity and if the flow direction of the cardiac cycle are **antegrade** or **retrograde**. If the cluster with the smallest centroid contain negative values, then there are cardiac cycles that are **multiphasic** and **retrograde**.

- The global maxima of each period are expected to be clustered in $C_{peaksMax}$. These landmarks are important for deciding the resistivity of the segment since the upstroke and downstroke need to be analyzed.

- By determining the global peaks and valleys of each period, both PDF and End-DF can be found by finding the largest and smallest values in the window ranging from the Early-DF landmark of a period the PSF landmark of the next period. The PDF and End-DF is used for analyzing resistivity.

- If the cluster number of both PDF and End-DF are different to the cluster number of both PSF and Early-DF, then the clustering algorithm has managed to cluster the landmarks into four clusters which is expected from the algorithm.
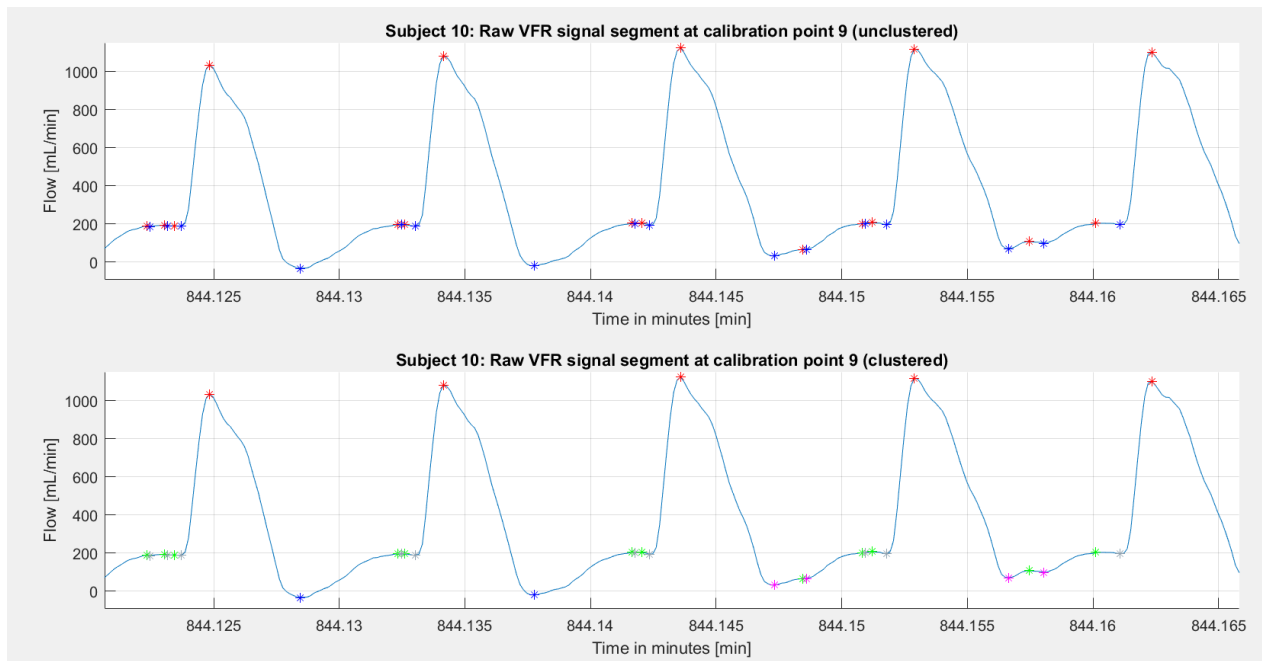
Figure 20. Example of a VFR signal when fluctuation in the signal results in the valleys of Early-DF of each heartbeat to be clustered in different clusters (pinks and blue clusters). In this case the pink and the blue cluster in the below figure should be merged.

5.2.2 Exclude local noise

As concluded in section 4.5.2, the Transonic flow sensors introduce technical noise that is visible in the waveform as local noise/extrema around the actual landmarks. After computing clusters $C_{valleysMin}$ and $C_{peaksMax}$ containing the assumed PSF and Early-DF landmarks, any technical noise should be excluded in order to find the desired landmarks.

The estimated periodicity is calculated by using the maximum heartrate BPM_{max} (beats/minute) which is chosen based on similar studies such as the one considered in this work (given in Section 4.4.2). Knowing BPM_{max} and the **sampling frequency** allows us to estimate a lower bound of the inter-beat interval (IBI). To generalize the term IBI, we call the estimated periodicity *period* which is calculated using equation:

$$period = 60 \sec \times \frac{sampling\ frequency}{BPM_{max}} \tag{1}$$

In our model, the function excluding local noise is implemented in the following way:

1. Compute the number of timestamps between successive values in the same cluster. Successive values are defined as values occurring after each other with respect to the occurrence of their time stamps in the signal segment.
2. If the number of timestamps between successive values differ with less than the estimated periodicity, exclude either the smaller or the larger value. Choosing which value to exclude depends on if $C_{valleysMin}$ or $C_{peaksMax}$ is considered. If $C_{valleysMin}$ is considered, then the **maximum** value of two successive values is excluded from $C_{valleysMin}$. If $C_{peaksMax}$ is considered, then the **minimum** value of the two successive flow values is excluded from $C_{peaksMax}$.
3. Step 1 and step 2 are repeated until there are no more successive values in the same cluster that differ with less than the estimated periodicity.

5.2.3 Merge clusters

The Early-DF landmark and PSF landmark per period can be missing if there are fluctuations in the VFR signal (Figure 20), resulting in that values of PSF or Early-DF might be clustered in separate clusters. Therefore, the model needs to check if clusters should be merged. Again, the objective is to use periodicity of successive values in clusters $C_{valleysMin}$ or $C_{peaksMax}$ to determine if there are landmarks missing from these clusters.

Figure 20 shows a case where the blue and the pink cluster should be merged, since landmarks belonging to the Early-DF have been clustered in separate clusters. However, the tricky part is to recognize when there are actually values missing from the Early-DF or PSF, and not just one missing heartbeat due to physiology (Ectopic heartbeat), example can be seen in Figure 21 for subject 11 calibration point 1.

When talking about merging clusters for detecting missing global maxima (PSF) of each period, we mean that if there are global maxima missing, then cluster $C_{peaksMax}$ should be merged with the cluster containing peaks and having the second largest centroid. Respectively, if there are values missing in cluster $C_{valleysMin}$, then this cluster should be merged with the cluster containing valleys and having the second smallest centroid.

The following cases for merging clusters were identified:

Case 1: If successive values in a cluster are separated by a period indicating missing values occurring **non-sequentially** throughout the signal. This is when there is regular/periodic fluctuation in the signal e.g., due to respiration.

Case 2: If successive values in a cluster are separated by a period indicating missing values occurring **sequentially** in the **beginning** of the signal. This is when there are higher/lower global extrema in the beginning of the signal.

Case 3: If successive values in a cluster are separated by a period indicating missing values occurring **sequentially** in the **end** of the signal. This is when there are higher/lower global extrema in the end of the signal.

Next, an assumption must be made of when the clusters should be merged. It is important that all the values from PSFs and Early-DFs are found, therefore, the chosen number of beats to be missed is one, which can happen when an Ectopic heartbeat occurs, as depicted in Figure 21 at approximately 738.075 minutes. If there is one heartbeat missing between two successive PSF landmarks, the time between these landmarks would be approximately two times the periodicity.
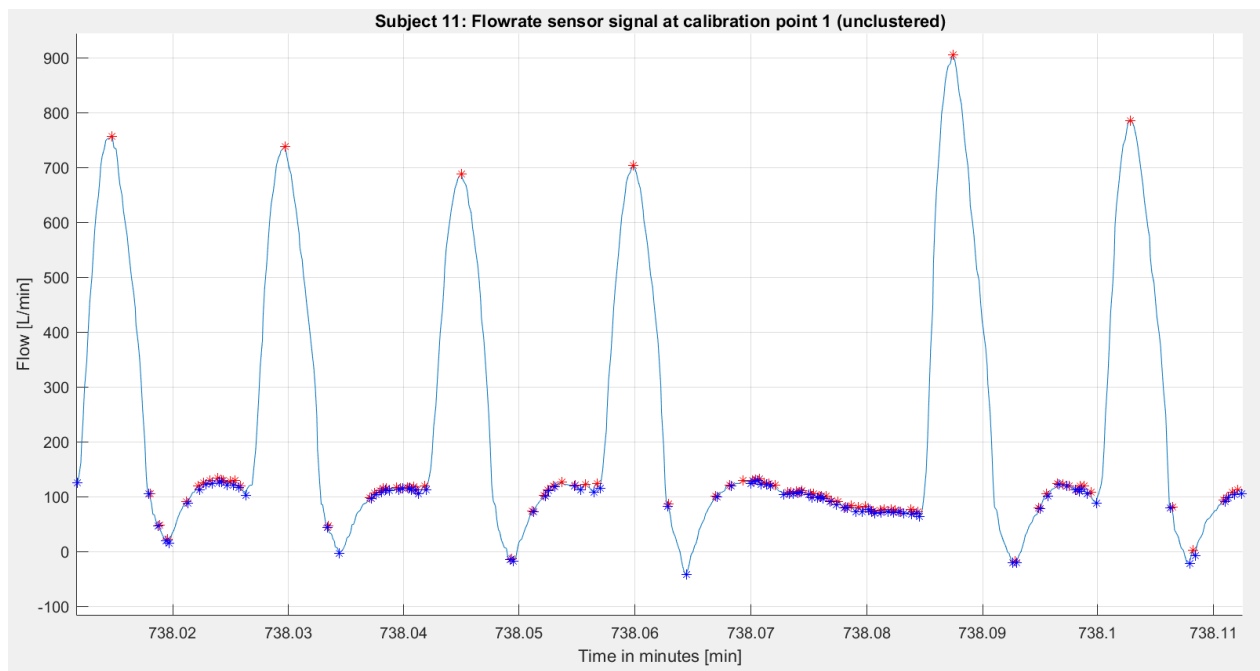
Figure 21. Example of an occurrence of Ectopic heartbeat at time in minutes 738.07 in the VFR signal. The red stars represent the peaks, whereas the blue stars represent the valleys.

If there exists an interval that is approximately three times the periodicity, then the signal has skipped at least 2 heartbeats successively, which is an indication that landmarks have been clustered in separate clusters due to fluctuation.

Therefore, the assumption for the VFR signal is that **2** heartbeats shouldn't be missing sequentially. This results in that we chose the factor for the upper bound of missing periods to be **3**. In other words, two successive values in the same cluster should not be separated by approximately 3 times the periodicity.

Now, since local noise has been excluded by using the estimated period based on maximum heartrate from literature, the minimum period between successive values in a cluster is at *least* the **period** obtained

by using Equation 1. Therefore, a new estimation of the periodicity can be made by finding the minimum difference in timestamps between successive values from the same cluster.

As mentioned before, the assumption now is that landmarks are missing if the time difference between successive landmarks is 3 times the minimum periodicity. This value is from now on referred to as **maximal allowed periodicity (MAP).** With respect to Case 1, Case 2 and Case 3 described above the following checks were made:

- Case 1: the model checks if any difference of number of timestamps between successive values from the same cluster is larger than MAP. If yes, then merge with the next smallest/largest cluster.
- Case 2: the model checks if the difference of number of timestamps between the **first time point** of the signal segment and the flow rate value from the cluster occurring **first** in the signal segment is larger than MAP. If yes, then merge with the next smallest/largest cluster.
- Case 3: the model checks if the difference of number of timestamps between the **last time point** of the complete signal segment and the flow rate value in the cluster occurring **last** in the signal segment is larger than MAP. If yes, then merge with the next smallest/largest cluster.

If any necessary merging has been performed, we might now have merged a cluster without any local noise with a cluster that contains local noise. Therefore, we repeat the steps given in section 5.2.2. and section 5.2.3 until none of the cases (Case 1, Case 2, and Case 3) occur.

5.2.4 Identify remaining landmarks

After the necessary merging and cleaning of the clusters were performed, the PSF and Early-DF landmarks of each period were expected to be found. These values were then used for finding the remaining landmarks namely end diastolic flow (End-DF) values and peak diastolic flow (PDF) values. Firstly, the local maxima representing the PDF landmarks were computed by using the timestamps of successive End-DF and PSF values. Then, the local minima of the End-DF are computed by using the timestamps of successive PDF and PSF. How these landmarks were computed are explained in more detail as follows.

Firstly, the model ensures that the forward search starts from an Early-DF landmark of the **current** period and ends in the PSF landmark of the **next** period. Then the model finds all the peaks in this window that are **not** clustered in the same cluster containing the PSFs. This check is performed since we expect that PDF and PSF landmarks are clustered in separate clusters. Then from all these peaks detected in the window, the **maximum** peak is labelled as the PDF landmark of that period. This procedure is then repeated through all cardiac cycles, until all the PDF landmarks are obtained.

For finding End-DF landmarks, the previously computed PDF landmarks and PSF landmarks were used for estimating the window in which the End-DF landmark of a period is expected to occur. The model then paired the PDF of the current period and the PSF of the next period to find the **smallest** valley between these values. This value was labelled as End-DF landmark of the current period. This procedure was repeated throughout all cardiac cycles in the signal segment. An example of how the model managed to label and detect landmarks is given in Figure 22.

After the remaining landmarks (PDF and End-DF) were computed, the next step is to evaluate the model.
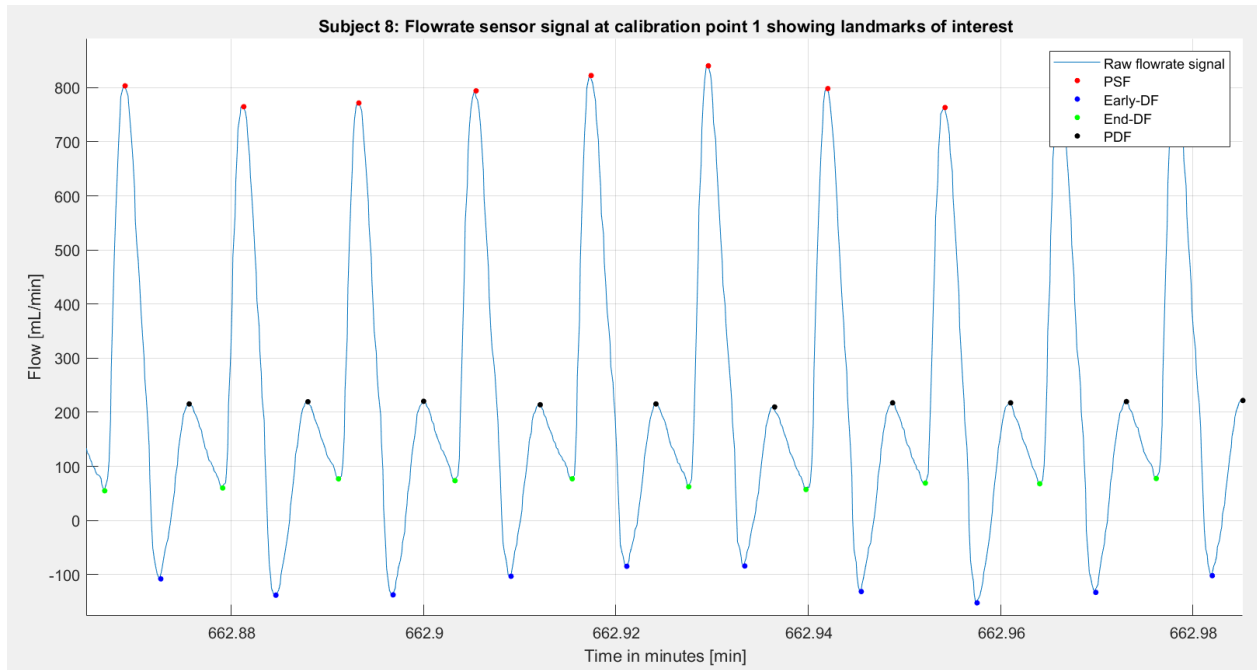
Figure 22. Final result of the clustering algorithm for subject 8 in the signal segment around PiCCO calibration point 1 where the landmarks have been labelled and detected.

5.2.5 Evaluation of the first model iteration

In this section, the model presented in the previous section is evaluated to determine its effectiveness. The CRISP-DM methodology is based on iteratively improving the model, based on identified limitations in the model evaluation. Two main limitations were identified in this approach:

Limitation 1: It is possible to miss a global minimum of a period which violates the assumptions of the expected waveform and underlying physiology since this would imply that there is no diastolic phase.

Limitation 2: It is possible that no local minima or maxima occurs between Early-DF landmark of the current period and the PSF landmark of the next period, implying that we won't find remaining landmarks.

When considering limitation 1, there are two factors to account for; (1) the requirement of obtaining separate clusters for Early-DF and End-DF is not feasible as can be depicted in Figure 23, (2) consequently, the choice of **periodicity** used for excluding local noise might result in global minimum of a period being excluded completely which violates the expected waveform.

These factors were discovered when the order of occurrence of the landmarks was investigated. More specifically, after the model had computed all the landmarks, the landmarks were sorted based on the time of occurrence. Consequently, the cluster labels of the sorted landmarks were used for (1) determining the number of clusters, (2) the order of occurrence of the landmarks during each period. If there were four clusters, then the assumption was that the model had managed to distinguish between four landmarks. If the there are two clusters, the algorithm has managed to find the global peaks and valleys of each period.

If the algorithm finds **three** clusters, either PSF and PDF are clustered in the same clusters, or Early-DF and End-DF are clustered in the same cluster. This is not desirable; however, it can be that the values of Early-DF and End-DF are similar in flow rate value such that hierarchical clustering still clustered these landmarks in the same cluster.

50

In the end, finding four unique clusters did not necessarily mean that all the landmarks were computed correctly. Therefore, the order of occurrence of the landmarks were assessed. Based on domain knowledge of the cardiac cycle, both systole and diastole should be possible to identify in the VFR signal. Firstly, the PSF represents the global maximum of the period in systole and the whole cardiac cycle. From the PSF, the signal should continue to a point in the period where the sign of the first order derivative will change from negative to positive in order to enter the phase of diastole, after which the systole starts again and we reach the global maximum of the next cardiac cycle. Therefore, we must assume that each period has at least one global peak and one global valley. This implies that there needs to be one landmark between two successive peak systolic flow landmarks.

In the example of subject 3 at calibration point 15 (shown in Figure 23), limitation 1 of the current model can be identified. Limitation 1 is explained in the following steps:
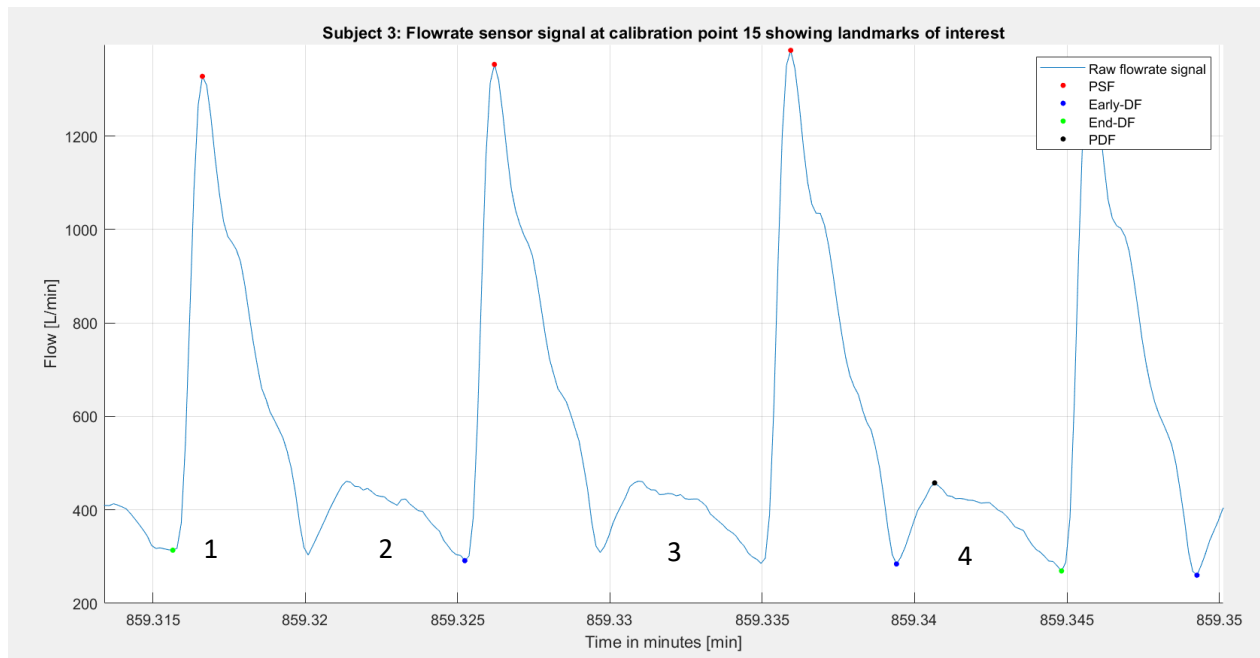
Figure 23. Limitation 1 of the current model showing the steps used for identifying how the model failed to label the desired landmarks. The steps are indicated by numbers 1-4.

The steps illustrated in Figure 23 are explained as follows:

Step 1: Starting from End-DF (green point) as labelled by the algorithm, the next landmark is PSF, after which the downstroke from PSF marks that the cardiac cycle enters diastole in the period.

Step 2: Now, since landmarks of Early-DF and End-DF turned out to be clustered in the same cluster, when excluding local noise based on the estimated **periodicity**, the model excluded the landmark of Early-DF because the End-DF of the respective cardiac cycle was smaller and these values were separated by less than the **periodicity**. This implies that the model will not find a PDF landmark in the window between End-DF landmark of the current period and PSF landmark of the next period because there are no local maxima on the upstroke to the PSF. Consequently, no "End-DF" will be found either since this landmark has been wrongly labelled as Early-DF.

Step 3: The problem continues since the End-DF is the global minimum of the period in Step 2 and is labelled as Early-DF. Now, if the landmark of Early-DF in Step 3 is **larger** than the End-DF in Step 2 and the

time between these two points are less than the estimated **periodicity**, no Early-DF will be found in Step 3. Successively, no other landmarks of the period in Step 3 will be found. This issue was detected since the order of landmarks will have two PSF landmarks in sequence. This violates the assumption of the flow rate signal waveform and the model excludes landmarks which should be detected based on the requirements.

Step 4: Since no valleys were detected in Step 3, the landmark in Step 4 will be labelled as Early-DF correctly since the number of time stamps between the wrongly labelled Early-DF in step one is surely larger than the estimated periodicity. When the Early-DF is labelled correctly, the two remaining landmarks will be labelled by the algorithm.

From this example, two main conclusions were drawn: (1) the periodicity estimated by the maximum possible heartrate in the literature might exclude landmarks in the case that landmarks belonging to different landmark groups have been clustered in the same cluster, (2) the initial assumption of the signal was wrong and the intuition that the landmarks can be clustered into four clusters, two for valleys and two for peaks, is not feasible since landmarks of Early-DF and End-DF can be clustered in the same cluster and therefore, be separated by a period less than the estimated period. This already is an indication that the model will not work for all signal segments.

When considering **limitation 2**, there can be cases when there are no local extremes between the Early-DF of a current period and the PSF of the next period. Limitation 2 was noticed based on cases like the one shown in Figure 24. In these cases, the number of unique clusters was 4, however, some cardiac cycle did not have any local extremes in the window ranging from an Early-DF landmark of the current cardiac cycle and the PSF of the next cardiac cycle. This was noticed when simply checking the number of values in the in each cluster.

Limitation 2 can be explained in the following steps as shown in Figure 24:
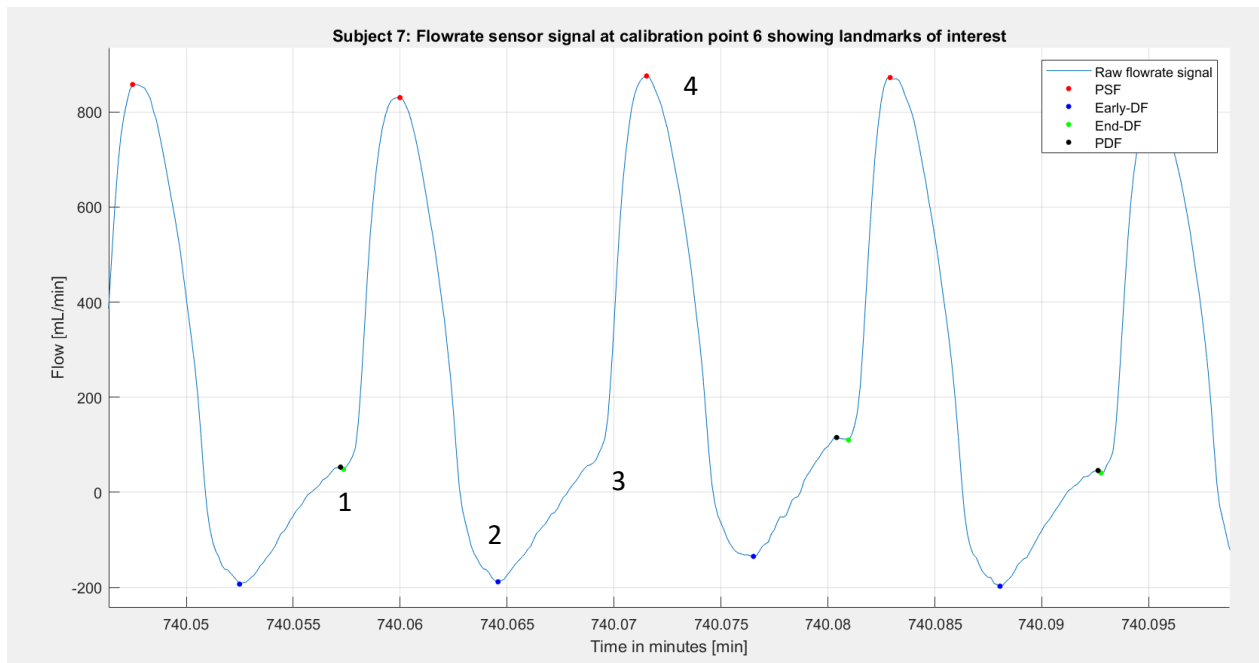
Figure 24. Limitation 2 of the current model showing the steps used for identifying how the model failed to label the desired landmarks. The steps are indicated by numbers 1-4.

Step 1: Starting from End-DF (green point) as labelled by the model, the next landmark is PSF (red point), after which the downstroke from PSF marks that the cardiac cycle enters diastole in the period.

Step 2: The landmark after PSF (red point) is Early-DF (blue point) as labelled by the model.

Step 3 and Step 4: From Early-DF (blue point), we expect to find PDF landmarks (black point) and End-DF landmarks (green point). However, there are no local extremes on the upstroke from Early-DF (blue) to the next PSF (step 4). The model should find an End-DF landmark. For this type of signal, it is difficult to say if the local minima and maxima found in the previous and successive cardiac cycle are due to technical noise in the signal which introduces local extremes.

In summary, the following conclusion were made from the evaluation of the first iteration of the model. Firstly, the initial assumptions of the waveform were incorrect regarding landmarks of local minima that were expected to be clustered in separate clusters. Namely, in some cases Early-DF and End-DF are too similar in value and may therefore end up in the same cluster. As a result, by using the estimated periodicity for excluding local noise, Early-DF or End-DF landmarks may be excluded.

Finally, in some cases there are waveforms with no local extremes between an Early-DF landmark in the current period and a PSF landmark in the next period. This implies that the model will not detect End-DF and PDF landmarks. In other words, the landmark End-DF might not be a local minimum. Specifically, we need to find End-DF in order to compute the upstroke to the PSF landmark which is used for describing the resistance of the waveform. Namely, if the artery had high, intermediate, or low resistance. As the model failed to meet **Requirement I** in Section 5.1, namely that the landmarks of each period should be detected and labeled, the conclusion is that the current model needs to be improved. In conclusion, there is too much uncertainty in the signal for only using a naïve approach of clustering for finding all the landmarks. The improvements to the model given in this section will be presented in the following section.

5.3 The second iteration of the model

Based on the evaluation of the first iteration of the model, in this section we present what we did to improve it. In order to improve the first model, an additional layer between clustering peaks and valleys, and labeling landmarks needed to be added. With respect to the CRISP-DM methodology, the limitations of the first iteration gave us a better understanding of the VFR waveform. What we learned from the first iteration of the model is summarized as follows:

- Landmarks of Early-DF and End-DF can be clustered in the same cluster, and Early-DF is not necessarily the global minimum of each period for these signal segments.
- The period based on the estimation of the maximum heart rate from literature is not a feasible estimation for excluding noisy local extrema since this period might exclude desired landmarks if two groups are clustered in the same cluster (illustrated in Figure 23).
- End-DF is **not** necessarily a local minimum (illustrated in Figure 24).

Based on these findings, using an estimated periodicity for excluding local noise, merging clusters, and investigating the order of occurrence and number of clusters will not be sufficient for finding landmarks. Based on previous work presented in Section 4.3, using the first order derivative has been applied for finding landmarks. In this work, we combine the approach of computing derivatives of the VFR waveform with hierarchical clustering for detecting and labeling landmarks.

In Section 4.4.1, the expected waveform of the VFR signal was described. Based on the expected waveform, the characteristics of the expected first order derivative function of one period in the VFR - waveform can be described. From now on the first order derivative will be referred to as the first order derivative (FOD) function of the VFR signal.

Again, the starting point of the period (cardiac cycle) is the End-DF landmark, which marks the point in time where the diastolic phase ends, and the systolic phase begins. After this point, a steep upstroke to the systolic peak (PSF landmark) occurs, the maximum first order derivative (FOD) of the period is achieved during this upstroke. From the PSF landmark, the FOD waveform starts to slow down. Around the point of the PSF, the FOD of the signal crosses the x-axis and the sign changes from positive to negative. After this point, the steep downstroke starts from the PSF landmark to the Early-DF landmark. During the downstroke, the minimum FOD of the period will be achieved. After the minimum FOD, the slope of the FOD waveform starts to increase, and around the Early-DF landmark, the FOD waveform will cross the x-axis and the sign changes from negative to positive. After the crossing of the x-axis, the FOD remains positive until a possible PDF landmark, where the velocity waveform would cross the x-axis from positive to negative. After this point, the FOD remains negative until the End-DF, where the FOD waveform crosses the x-axis from negative to positive marks the area of the end of diastole and start of the next cardiac cycle.

The FOD is calculated using an open source function in Matlab [50] which fits a low order polynomial regression model in a sliding window. We use this function since it overlooks noise in the signal. In the next section we explain how we calculate the window size of the sliding window.

5.3.1 Estimating window size

In this section we describe how we estimated the window size used to computed FOD. For all the signal segments we plan to use the same window size. The way the window size is calculated needs to be effective for all segments.

To meet these requirements, the window was estimated based on the steepness of the upstroke and downstroke to and from the systolic peak, respectively. In other words, the steepest incline and decline of each cardiac cycle in the signal should be captured with the estimated window size. Therefore, an approach was implemented where landmarks were marked manually in three periods of three different signals, after which the fraction of the period that is dedicated to both the upstroke to the PSF and downstroke from the PSF were calculated. The minimum fraction was then used to estimate the window size.

Three VFR signal segments were chosen at the **first** calibration point based on the objective of finding the three segments with the least amount of technical local noise. These signals were chosen since no medication had yet been administered at this point, which excluded an additional source possibly altering one period.

Subject	Timestamp End-DF (previous EndDF)	Timestamp PSF (current PSF)	Timestamp Early-DF (current EarlyDF)	Timestamp End-DF (current EndDF)	Period of one cardiac cycle (Period CC)	Fraction upstroke (FU)	Fraction downstroke (FD)	Minimum(FU, FD) (Min Percentage)	Number of Timestamps (Num Timestamps)
Subject 3	2639	2653	2680	2736	97	0.14	0.28	0.14	14
Subject 5	2660	2675	2704	2750	90	0.17	0.32	0.17	15
Subject 8	3079	3093	3120	3168	89	0.16	0.30	0.16	14

Table 2. This table shows the necessary data for computing the window size used for calculating the first order derivative of the VFR waveform.

The columns shown in Table 2 are explained as follows. Column 1 represents the subjects from which the signal segments were used for estimating the window size. Column 2 represents the timestamp of the End-DF landmark of the previous cycle (previous End-DF). Column 3 represent the timestamp of the PSF landmark of the current cardiac cycle (current PSF). Column 4 represent the timestamp of the Early-DF landmark of the current cardiac cycle (current Early-DF). Column 5 represent the timestamp of the End-DF of the current cardiac cycle (current End-DF). Column 6 represents the period of one cardiac cycle

54

(Period CC). Column 7 represents the fraction of the upstroke from previous End-DF to current PSF (FU). Column 8 represents the fraction of the downstroke from current PSF to the current Early-DF (FD). Column 9 is the minimum between FD and FU. Column 10 is the number of timestamps of the cardiac cycle that makes up the minimum percentage.

The period of one cardiac cycle which is shown in Column 6 is computed in the following:

$$Period\ CC = current\ EndDF - \ previous\ EndDF$$

The fraction dedicated to the upstroke from the previous End-DF landmark to the current PSF-landmark in the cardiac cycle shown in Column 7 is computed in the following way:

$$FU = \frac{current\ PSF - current\ EndDF}{Period\ CC}$$

The fraction dedicated to the downstroke from the current PSF landmark to the current Early-DF landmark in the cardiac cycle that is shown in Column 8 is computed in the following way:

$$FD = \frac{current\ EarlyDF - current\ PSF}{Period\ CC}$$

The minimum percentage $minimum\ (FU, FD)$ in Column 9 can then be used to compute the number of timestamps in the cardiac cycle that the window size should **at least** cover. This number of timestamps in Column 10 is computed in the following way

$$Num\ Timestamps = min(FU, FD) \times Period\ CC$$

Table 2 shows that the window size should be roughly ~14-15 timestamps. However, it is better to underestimate than overestimate the window size since we want to capture the rate of change of each cardiac cycle where the VFR waveform changes abruptly. Therefore, the window size is chosen to be 10 timestamps by taking the floor of the average estimated window sizes:

$$window\ size = \lfloor avg(Num\ Timestamps) \rfloor$$

The alternatives of how this window can be explored is discussed more in future work.

5.3.2 Computing landmarks using first order derivative
In this subsection, the second iteration of the model is explored

As shown in the first iteration of the model, clustering local minima of the VFR signal segment did not work due to wrong assumptions of the waveform. In previous work, landmarks were detected and labeled based on analysis of the first order derivative (FOD) of the waveform. The global peak was in general noted **manually** as the initial point from where backward- and forward search for timestamps of sign change of the first order derivative for one period started [9], [10]. Therefore, instead of performing this task manually, we want to automatize finding the global peaks of each period for all periods in the signal segment by using the hierarchical clustering of peaks explained in Section 5.2. The PSF landmarks are therefore computed using the first model. After the PSF landmarks have been obtained, we analyze the first order derivative waveform of the signal to find the remaining landmarks.

In Section 5.3.1, the window size used for fitting a low order regression model for computing first order derivative waveform of the whole VFR signal segment was defined. Again, this window size was chosen to be 10 timestamps. The following steps were performed in order to detect and label landmarks:

1. Use the first iteration of the model explained in Section 5.2 for clustering peaks, excluding local noise, and merging clusters to find global maximum of each period. We know based on definition that the global maximum in the cardiac cycle is the PSF landmarks, as opposed to the global minimum which can be either Early-DF landmarks or End-DF landmarks based on previous results. Therefore, it is feasible to assume that hierarchical clustering returns the landmarks of PSF.

2. After the PSF landmarks have been computed, start from a PSF landmark. Perform forward search and find the **first** point in time where the FOD waveform changes sign from negative to positive. Take the minimum value in the window between this timestamp and the PSF landmark where the search began. This marks the landmark Early-DF.

3. Go back to the **next** PSF landmark. Perform backward search and find the **first** point in time where the FOD waveform changes sign from negative to positive. Take the minimum value between this time stamps and PSF landmark where the search began. This marks the landmark End-DF.

4. Take the window between the Early-DF landmark and the End-DF landmark and find the maximum value in this window. This marks the landmark PDF.
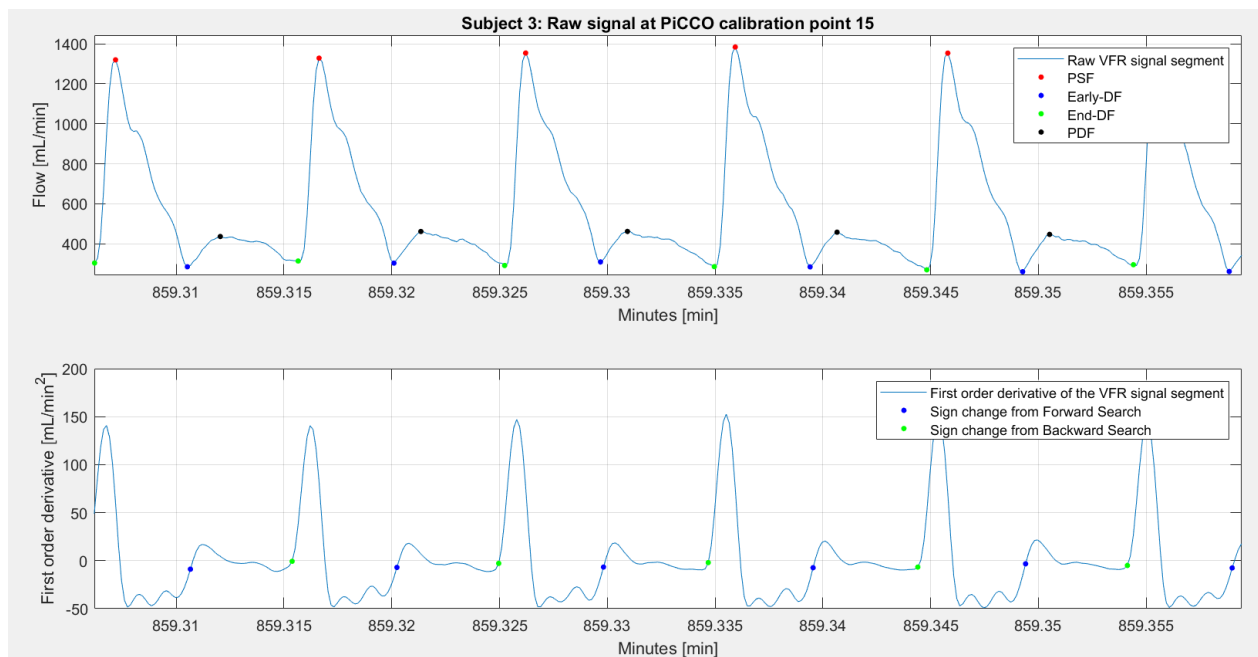
Figure 25. In this figure the results of the model when using the added component of FOD for Subject 3 at calibration point 15. Compared to Figure 23, the model managed to detect and label the landmarks correctly.

Compared to Figure 23, where **limitation 1** of the first iteration of the model was illustrated, Figure 25 shows that by using the new iteration of the model, limitation 1 will be addressed. However, this approach would not address **limitation 2**.

The reason for this is that when End-EDF is not a local minimum, then it might be that the first order derivative function crosses the x-axis from negative to positive only once during the cardiac cycle. This implies that when performing backward search from a systolic peak, the forward search from the previous systolic peak will result in the same sign change. In other words, performing backward search from a current systolic peak should return End-DF landmark and forward search from a previous systolic peak should return Early-DF landmark, whereas in this case, only Early-DF landmark is returned. Now, the number of times the first order derivative function crosses the x-axis is directly correlated with the chosen window size, which introduces more uncertainty to this approach. However, a smaller window size could result in capturing the technical noise explained in Section 4.5.2. instead of the actual landmarks. Therefore, the approach for estimating the window size given in Section 5.3.1 was chosen.

In conclusion, limitation 1 may be addressed using **only** the first order derivative of the VFR waveform. This is because even though Early-DF and End-DF are similar in value, if there is a peak diastolic flow in between, the FOD-function will cross the x-axis from negative to positive at least twice resulting in finding Early-DF by forward search and End-DF by backward search. However, if there are no local extremes on the upstroke between the Early-DF landmark of the current period and the PSF landmark of the next period, then using only the FOD-function will not be sufficient. In the following subsection, the last step of the second iteration of the model is given, where the second order derivative (SOD) of the VFR waveform is computed in order to address limitation 2.

5.3.3 Computing landmarks using second order derivative
In this section, the approach for addressing limitation 2 presented in Section 5.2.5 will be discussed. To recap, limitation 2 is the case when no clear local extrema occur on the upstroke from Early-DF landmark to the next PSF landmark. If this the case, the first iteration of the model will not detect the remaining landmarks (PDF and End-DF). This limitation could neither be addressed by computing the first order derivative explained in Section 5.3.2. Therefore, a final component to the model had to be added, where using the second order derivative of the VFR waveform was incorporated.

Using a combination of hierarchical clustering and the first order derivative function of the VFR waveform allows us to compute **at least** the following landmarks; (1) the PSF landmarks representing the global maximum of each period and (2) the Early-DF landmark which is obtained forward search from a PSF landmark. However, finding both Early-DF landmarks, End-DF landmarks and PDF landmarks are essential for describing resistivity of the artery, which is one of the key descriptors in the resent consensus article by Kim et al. [19]. On the other hand, the Early-DF landmarks are important for using the two remaining descriptors: flow direction and phasicity.

This final component of the model is the function of the second order derivative (SOD) of the VFR waveform shown in Figure 26. The SOD was computed by differentiating the first order derivative obtained in Section 5.3.2.
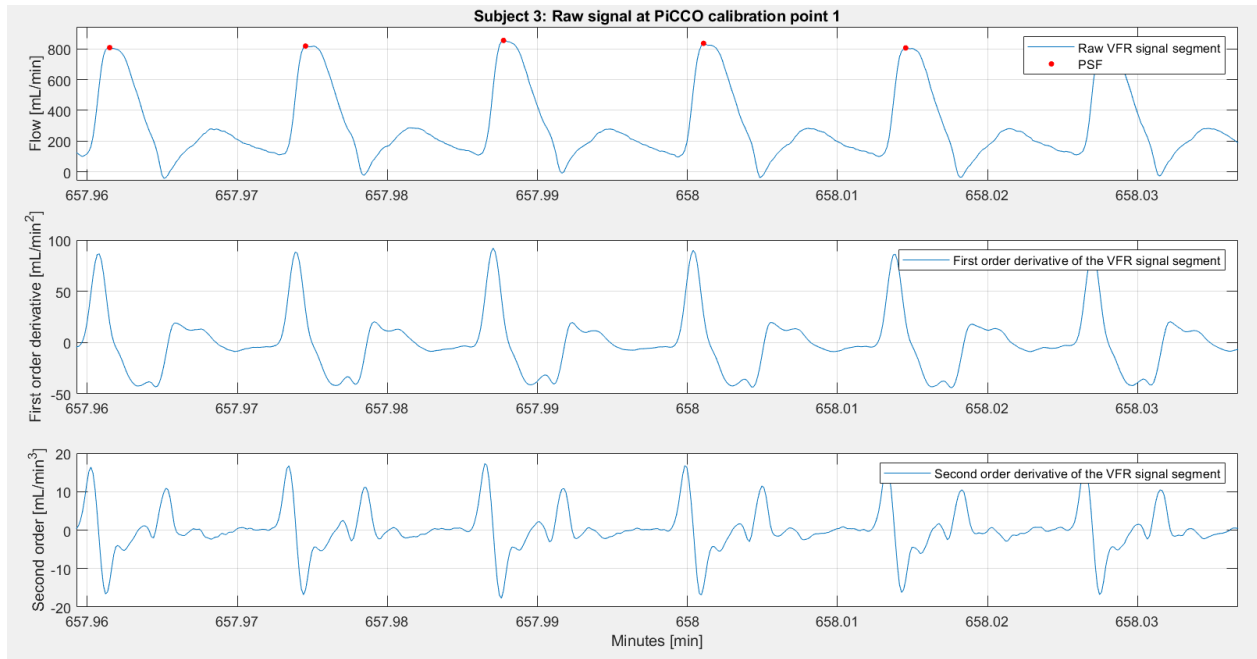
Figure 26. In this figure all the necessary components for finding the landmarks are shown. The top illustration shows the raw VFR waveform together with the PSF landmarks detected and labelled by using hierarchical clustering. The middle illustration shows the first order derivative of the raw VFR waveform which was estimated through a first order regression model in sliding window throughout the signal segment. Finally, the bottom illustration shows the second order derivative of the waveform which is the final component in the model and is used for computing the End-DF landmark.

Based on the domain knowledge with respect to the cardiac cycle, the diastolic phase ends and the systolic phase begins in the End-DF landmark. In the beginning of the systolic phase, we know that the rapid ejection is visible in the VFR waveform as a steep upstroke to the systolic peak. The start of the rapid ejection is also when the maximum acceleration of that period is achieved. In addition, there is a short time segment in the systolic phase which happens before rapid ejection which is called the isovolumetric phase. As we do not know the time period for the isovolumetric phase, we assume that this is the timestamp **prior** to the maximum acceleration of the blood flow in the systolic phase. Therefore, we redefined the End-DF landmark as the flow at the timestamp prior to the **maximum** second order derivative of the VFR waveform in each cardiac cycle. In other words, the End-DF landmark is estimated as the time point before the maximum acceleration in the window between the first time point that the FOD changes sign from backward search of the systolic peak and the systolic peak itself. This definition was also confirmed by experts to be a feasible time point of the End-DF landmark.
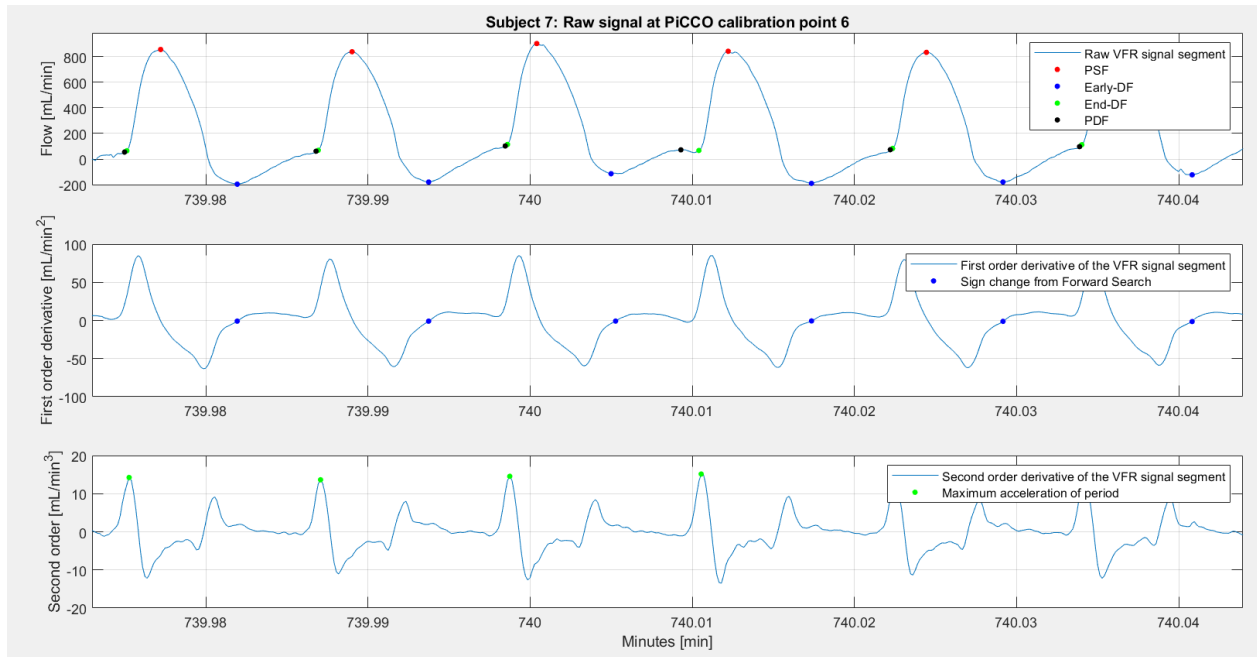
Figure 27. This figure showing the desired landmarks by obtained by the model. The top illustration shows all the desired landmarks. The middle illustration shows the first order derivative of the raw VFR signal segment and the time point of the sign change from negative to positive which is used for defining a window in which we expect to detect the Early-DF landmark. The bottom illustration shows the second order derivative of the raw VFR signal segment and the time point prior to the maximum acceleration of the cardiac cycle. This point in time is used for defining a window in which we expect to detect the End-DF landmark.

As illustrated in Figure 27, the model managed to address limitation 2 defined in Section 5.2.5. which was identified for Subject 7 at calibration point 6. We believe that by using this model we are able to detect the defined landmarks. In the following section, the final model evaluation is performed.

5.3.4 Evaluation of the second model iteration

In this section the second iteration of the model will be evaluated. This will be done by re-visiting all the requirements set to the model in Section 5.1. and discussing systematically if the requirements were met.

The first requirement is that **the landmarks of each period should be detected and labeled**. By using the second model iteration, the landmarks are believed to be detected and labeled correctly based on the functions described in the previous section. This is checked again by evaluating the periodicity between successive landmarks in each group. Since the model is expected to separate the landmarks from technical noise, second requirement can also be evaluated using this evaluation method. The second requirement is that **the landmarks should be separated from the technical noise present in the signal**.

Before the periodicity between landmarks is investigated, a simple check can be performed regarding the number of landmarks in each cardiac cycle (period) in the waveform of the signal segment. It is expected that each cardiac cycle has the same number of landmarks, namely, one PSF landmark, one Early – DF landmark, one PDF – landmark, and one End-DF landmark. Since finding Early-DF and End-DF is based on analyzing the FOD waveform and SOD waveforms in a window ranging between two successive PSF landmarks, we can expect that if hierarchical clustering has found n number of PSF landmarks in a signal segment of 1 minute, then for all remaining landmark groups, we expect $n – 1$ number of landmarks in

59

each group. If this is not the case, then the model has missed landmarks. Therefore, we first check that each signal segment has the expected number of points.

We observed two signal segments with missing PDF landmarks for Subject 14, namely, at calibration points 4 and 10. The reason for this was that for these signal segments there still remains high frequency noise that was not captured in the data cleaning. This indicates that also the window size for computing the FOD and SOD is too large for noisy signals. In these cases, the time point of the maximum SOD which was used to compute End-DF landmark is the same time point of the first sign change of the FOD used for computing Early-DF. Since the End-DF is the time point **prior** to the maximum acceleration, the End-DF might get labeled at a time point before Early-DF. If this happens then the PDF will not be detected. This is a limitation of the data cleaning part, indicating that more extensive signal processing should have been performed, for example by using low pass filtering.

These two signal segments for Subject 14 were then excluded from the remaining model evaluation because if there are landmarks missing, we cannot assume that the other landmarks have been computed correctly. The following step in the model evaluation was performed in the following way. Firstly, the periodicity between successive landmarks per group were computed. If the landmarks have been detected and labelled correctly, it is expected that the periodicity between landmarks in successive cardiac cycles is approximately the same length between successive PSF landmarks, successive Early-DF landmarks, successive End-DF landmarks, and successive PDF landmarks. Figure 28 shows how the periodicity between successive landmarks has been calculated.
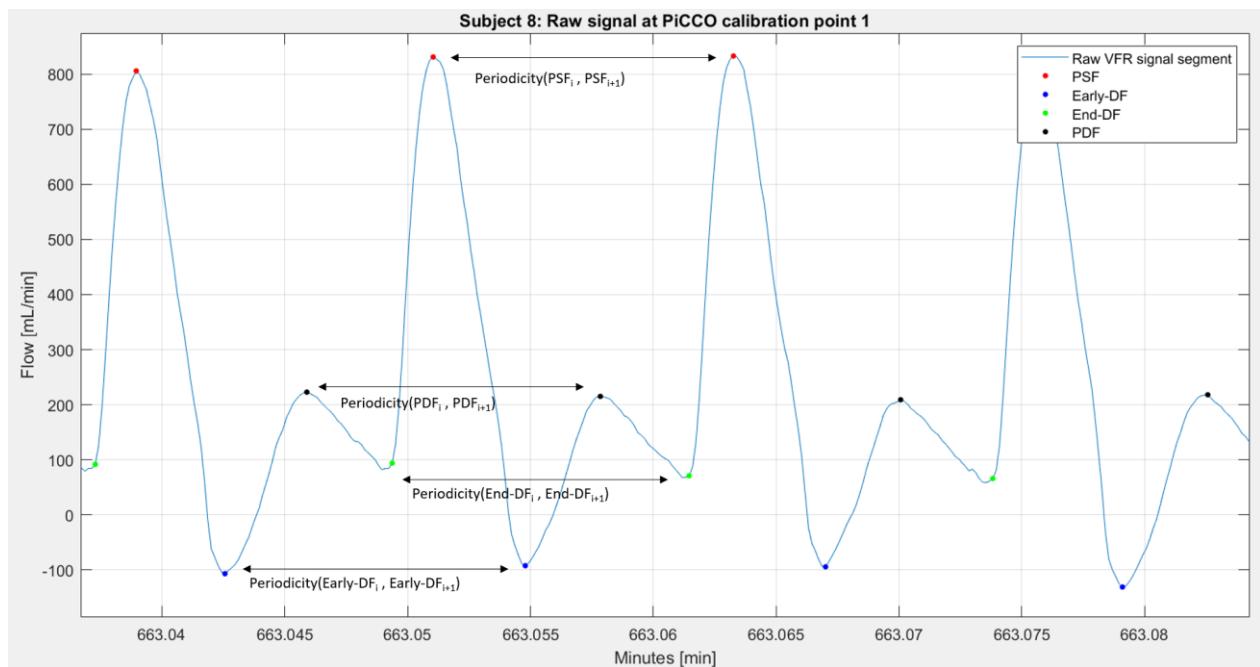
Figure 28. This figure shows how the periodicities of successive landmarks per landmark group are estimated for model evaluation.

After the periodicity has been computed between successive landmarks per group, we perform a comparison of the periodicities. As stated before, it is expected that these periods are approximately the same length. For example, **Periodicity(End-DF$_i$, End-DF$_{i+1}$)** should be approximately the same length as **Periodicity(PSF$_i$, PSF$_{i+1}$).** Therefore, the difference between these periodicities in each cardiac cycle should obtain a value around 0. The unit for the periodicities is the **number of timestamps**. Since the PSF are considered the initial time points for finding the remaining landmarks, we compute pairwise the difference between the periodicity between successive PSF landmarks and the periodicity between successive landmarks in the remaining groups, namely, Early-DF landmarks, End-DF landmarks and PDF-landmarks.

After the differences have been computed, the distributions of these differences were plotted. Again, we explore this distribution per subject to better understand the inter-subject variability. As examples in this model evaluation, we show the distribution for Subject 5 and Subject 14 in Figure 30.
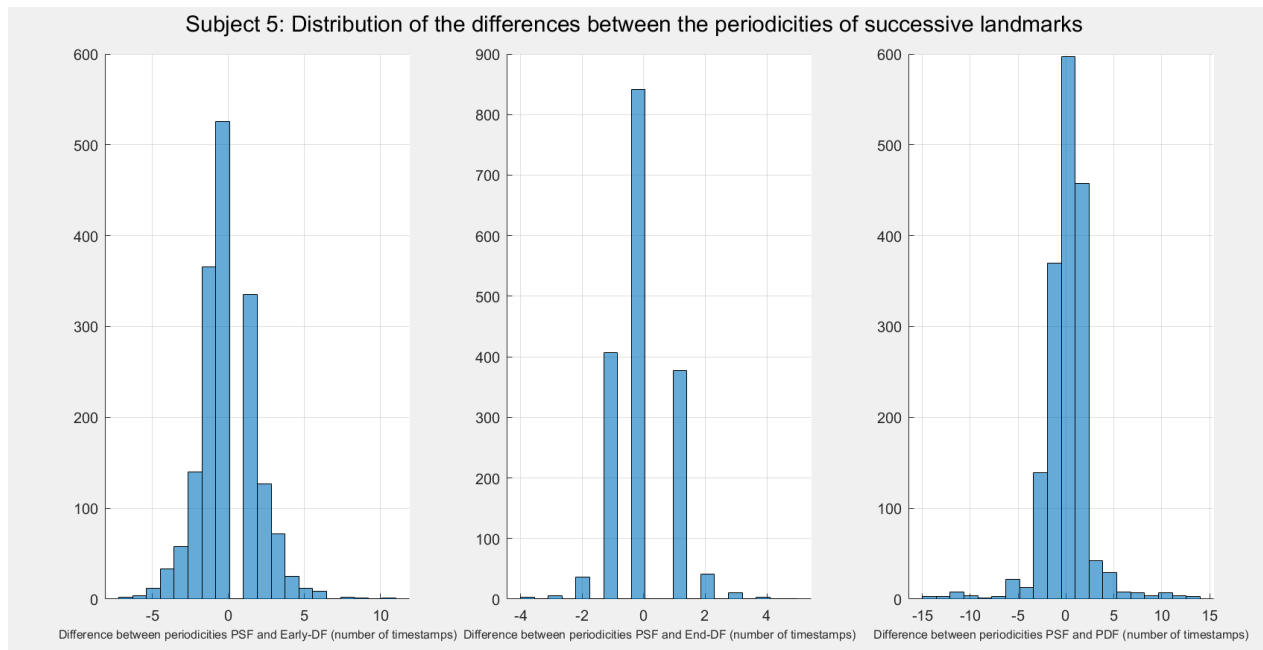
Figure 29. This figure shows the distributions of the differences between the periodicities of the landmark classes. The illustration on the left shows distribution of the differences between the periodicities of successive PSF landmarks and the periodicities of successive Early-DF landmarks detected and labeled in all signal segments for Subject 5. The illustration in the middle shows distribution of the differences between the periodicities of successive PSF landmarks and the periodicities of successive End-DF landmarks detected and labeled in all signal segments for Subject 5. The illustration on the left shows distribution of the differences between the periodicities of successive PSF landmarks and the periodicities of successive PDF landmarks detected and labeled in all signal segments for Subject 5. The unit of the periodicities are the number of number of timestamps.
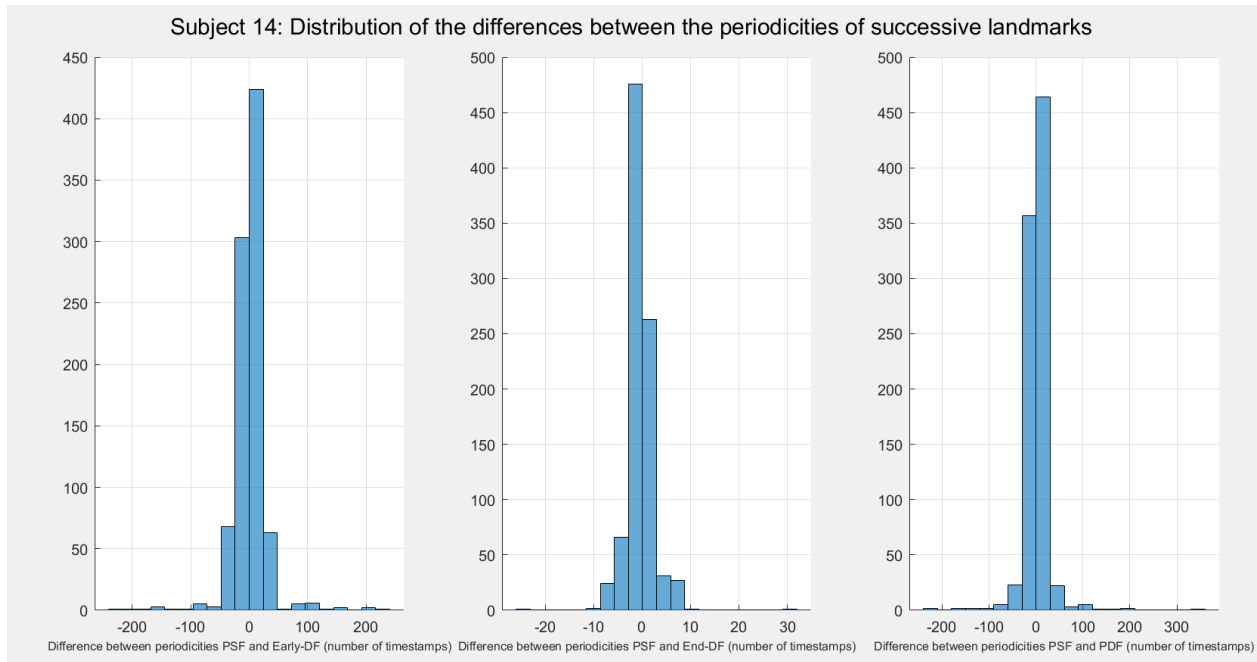
Figure 30. This figure shows the distributions of the differences between the periodicities of the landmark classes. The illustration on the left shows distribution of the differences between the periodicities of successive PSF landmarks and the periodicities of successive Early-DF landmarks detected and labeled in all signal segments for Subject 14. The illustration in the middle shows distribution of the differences between the periodicities of successive PSF landmarks and the periodicities of successive End-DF landmarks detected and labeled in all signal segments for Subject 14. The illustration on the left shows distribution of the differences between the periodicities of successive PSF landmarks and the periodicities of successive PDF landmarks detected and labeled in all signal segments for Subject 14. The unit of the periodicities are the number of number of timestamps.

As depicted in Figure 29 and Figure 30, it is clear that the model performed worse for detecting and labeling landmarks in the signal segments of Subject 14 (Figure 30) than for Subject 5 (Figure 29). This can be concluded by inspecting the variability of the distributions. By looking at the illustration of Subject 5, the variabilities in the distributions of the differences are much smaller, indicating that the model performed better in detecting the landmarks since successive landmarks in each group occurred approximately with regular frequencies. However, when looking at the illustration of Subject 14, there can be cardiac cycles where the periodicity between two successive PSF landmarks is approximately 300 time stamps larger than the periodicity of two successive PDF landmarks.

Subject 5 and Subject 14 were chosen as examples because the histogram of Subject 5 shows results were the model managed to detect and label landmarks such that the variability of the differences between landmark periodicities remained relatively low, whereas the histogram for Subject 14 showed high variability especially when considering the periodicities of the PDF landmarks. In general, the periodicities varied the most for the PDF landmarks when analyzing the histograms of the other subjects as well. The histograms per subject can be found in the Appendix C.

It is difficult to say why there is more variability for some subject and it would require us to visually inspect these signal segments. However, we expect that there still remains high frequency noise in the signal which leads to that both the FOD and SOD waveforms become too noisy for estimating the correct time points

62

used for determining the time range containing the landmarks. This is the result of uncertainties inherent to measuring physiological signals using sensors and physiology itself. As an example, we show the results of the model for signal segment at calibration point 9 of Subject 14 in Figure 31. This signal segment contains difference that obtained a lot of variability in the periodicities (including the example of the difference of approximately 300 timestamps between the periodicities of PSF landmarks and PDF landmarks).
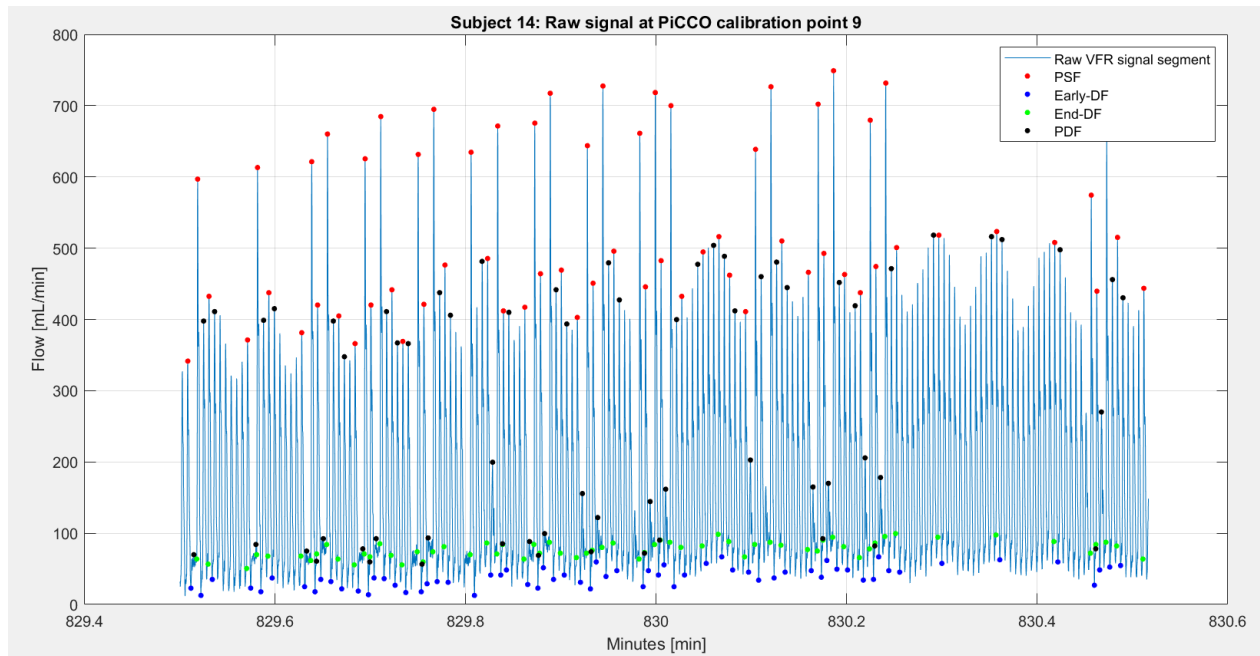
Figure 31. Example of a signal segment which failed to detect and label the landmarks as expected by the model.

As can be depicted from Figure 31, this signal contains high frequency noise, which results in that the hierarchical clustering failed to detect the PSF landmarks. This noise is not the sort of technical noise of local extremes around the actual landmarks as we explained in Section 4.5.2, but it is noise which looks like a biproduct of the sensor being ill attached. In Figure 31, some peaks are much higher than others and therefore, using the functions that exclude noise and merge clusters by using the first model iteration could have excluded some of the global peaks in a similar manner to **limitation 1** presented in Section 5.2.5. When we further investigated the FOD and SOD, the window size is too large for this signal segment and when performing forward search of the Early-DF landmarks, the sign change was also missing for multiple periods making detection of Early-DF landmarks infeasible. This is also an example of the limitation presented in Section 4.7.

In conclusion for evaluating requirement 1 and requirement 2 set to our model, it is difficult to know beforehand what to expect from the signal. Finding signal segments containing high frequency noise, like the one depicted in Figure 31, could be addressed by using more advanced signal processing approaches.

Finally, for the third requirement, **the algorithm should detect when Ectopic heartbeats occur,** is checked by again using the periodicity between PSF landmarks, global peaks of each cardiac cycle. Now, as defined previously, an ectopic heartbeat implies that the number of time stamps between two PSF landmarks is approx. 2 times the actual periodicity. In addition, the heart rate variability (HRV) must be considered

when analyzing periodicity. HRV is commonly computed as the standard deviation of the normal-to-normal (NN) intervals obtained from QRS complexes in ECG-signals [51]. This data is not in the scope of this work and therefore, the standard deviation of the periods computed between all the successive PSF landmarks will be used as an estimation of HRV in a specific signal segment.

The ectopic heartbeats were estimated setting an upper bound for the allowed periodicity. This upper bound was calculated by taking the average periodicity of all periods computed by taking the number of timestamps between successive PSF landmarks after which the standard deviation (HRV) was subtracted from this value. Finally, this value was multiplied by 2. Mathematically, if **P** contains all periodicities p_i where **i ∈ {1…,n-1}** *and* **n = number of PSF landmarks**, then the upper bound **UB** for an inter-beat interval (period) between successive PSF landmarks is shown in Equation 2:

$$UB = 2 \times \big(avg(P) - std(P)\big)$$
(**2**)

If the periodicity is above the upper bound it is labelled as an Ectopic heartbeat. This is a rough estimation for which more domain knowledge would be required to determine if this is a feasible way to determine if an Ectopic heartbeat occurred. The intuition of the method based on the available resources was confirmed feasible by a domain expert. Therefore, we can conclude that our model could also be used for detecting Ectopic heartbeats in the signal segment.

6 Model validation

In this chapter, the model validation is presented. Model validation in this work is done together with a scientist who has been involved in this work from the beginning as a supervisor from Philips Research. In Section 6.1, the execution of the model validation is given. In Section 6.2, the results are discussed systematically based on the model validation session. Finally, in Section 6.3 a short discussion of the model validation regarding the requirements of the model is given.

6.1 Execution

The objective of the model validation is to determine if the landmarks were detected and labelled correctly and if these landmarks can be used in the future for describing the VFR waveform in terms of phasicity, resistance, and flow-direction. Understanding the VFR – waveform and the landmarks require experience and domain knowledge; therefore, the model and the findings should be validated by an expert.

The data used for the model validation was chosen as follows. Firstly, five subjects were chosen at random from the total of 11 subjects. Then for each five subjects, one signal segment (±30 seconds around calibration point) was also chosen at random. Again, on average each subject has 18 signal segments. Finally, for each signal segment one cardiac cycle showing the landmarks is chosen and shown to the scientist in the form of a figure in a slide deck. For consistency, the full cardiac-cycle closest to the calibration point was chosen for the model validation.

These five illustrations were shown to the scientist and the following question was asked per illustration:

Question 1. Can we conclude that the detected landmarks in the figure represent the true landmarks, namely Peak Systolic Flow, Early-Diastolic Flow, Peak Diastolic Flow and End-Diastolic Flow?

After all the five illustrations were shown the second question was asked, with the objective of determining if the landmarks could be used to describe the waveform. The second question was the following:

Question 2. Can we use these landmarks for describing the waveform in terms of phasicity, flow direction and resistance?

Since **Question 2** is a more generic question which can be summarized for all illustrations the answer to this question will be given in the end of Section 6.2, whereas, more detailed answers to **Question 1** will be presented per illustration in separate subsections.

6.2 Results

Five figures were shown to the scientist for model validation. In this section, these five figures are presented together with remarks made by the scientist regarding **Question 1**. The cardiac cycle shown in each illustration starts and ends at successive End-DF landmarks. The start and end of each cardiac cycle is indicated in each figure.

6.2.1 Subject 6 at PiCCO calibration point 10

In this subsection, the first cardiac cycle showing the landmarks of interest is discussed. Firstly, the scientist noted that it seemed like Early-DF has been correctly detected and labeled even though there were some other extremes on the downstroke. This indicates that the window size used for computing the first order derivative (FOD) used for finding Early-DF through forwards search made a good estimate, since the first

sign change from negative to positive of FOD occurs in the bottom of the signal and not at prior local extremes on the downstroke from the systolic peak.
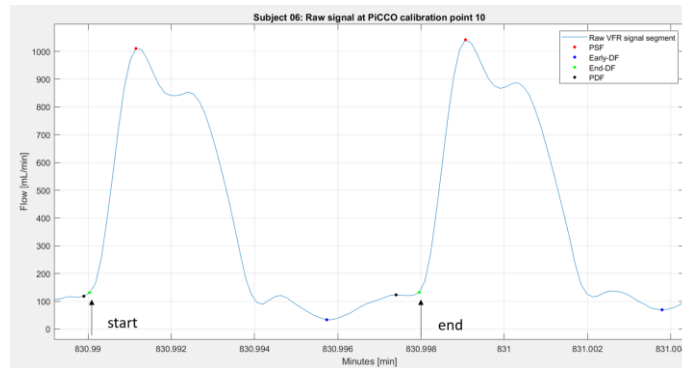
Figure 32. First cardiac cycle for model validation

What was pointed out by the scientist is that the sensor itself contributes to noise and inaccuracies in the signal. This is uncertainty affects mainly the task of detecting and labeling PDF. This claim was also confirmed by the scientist who remarked that the PSF, Early-DF and End-DF landmarks seem to obtain correct values, whereas it is difficult to say if the PDF landmark is the actual landmark or noise.

6.2.2 Subject 11 at PiCCO calibration point 13

The second cardiac cycle to be discussed is around the 13th PiCCO calibration point for subject 11. During this cardiac cycle, there is a clear systolic peak and no disturbances on the downstroke or upstroke, resulting in that the FOD can capture the desired sign change.
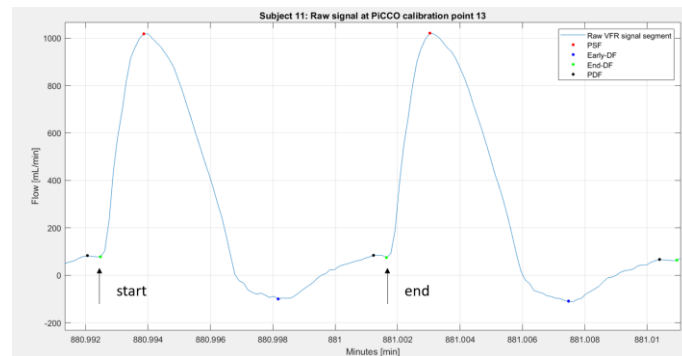
Figure 33. Second cardiac cycle for model validation

Again, the same remark was made by the scientist, namely, that landmarks of PSF, Early-DF and End-DF are correctly detected but it is difficult to determine if the PDF landmark has been detected correctly because of the noise in the signal.

6.2.3 Subject 10 at PiCCO calibration point 1

In this subsection, the second cardiac cycle showing the landmarks of interest is discussed. This cardiac cycle represents the cardiac cycle closest to the calibration point of the signal segment chosen at random.

This signal segment shows a one-minute signal segment around the 1st PiCCO calibration point for subject 10.
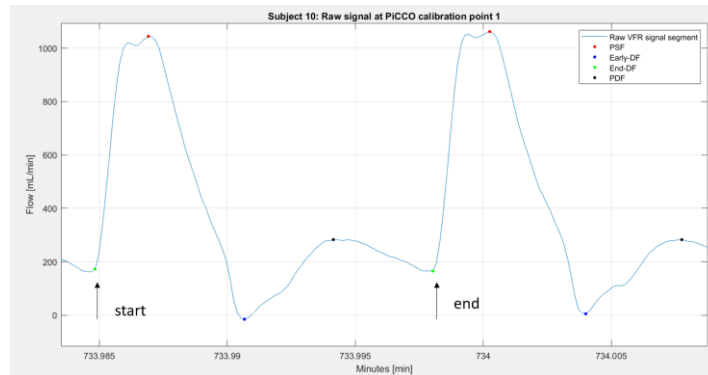
Figure 34. Third cardiac cycle for model validation

Figure 34 is an interesting example of the difficulty of determining the correct landmarks. Based on the definition of the PSF, this landmark represents the global maximum of one cardiac cycle. However, by looking at the systolic portion of this cardiac cycle, there are two local maxima in the top of the waveform. For the PSF landmark, the maximum of the two is chosen. However, it might be that due to noise introduced by the sensor, the actual PSF is in between these two local maxima. Another possibility could be that the local maxima occurring prior to the detected PSF, is the correct PSF landmark and the second local maxima is again noise introduced by the sensor. The scientist noted that this is a main challenge when measuring physiological signals using measurement instruments with their inherent limitations.

For the rest, the PDF in this signal seems to have been detected and labeled correctly, as oppose to previous cardiac cycles shown in Section 6.2.1 and Section 6.2.2. where it is uncertain if the PDF were found. The detected Early-DF and End-DF landmarks are labeled correctly.

6.2.4 Subject 5 at PiCCO calibration point 15
In this subsection, the fourth figure (Figure 35) showing the landmarks of interest is discussed, namely, the one cardiac cycle measured for subject 5 at calibration point 15. In the scientist again made a remark about the PDF, the other landmarks were correctly detected and labeled.
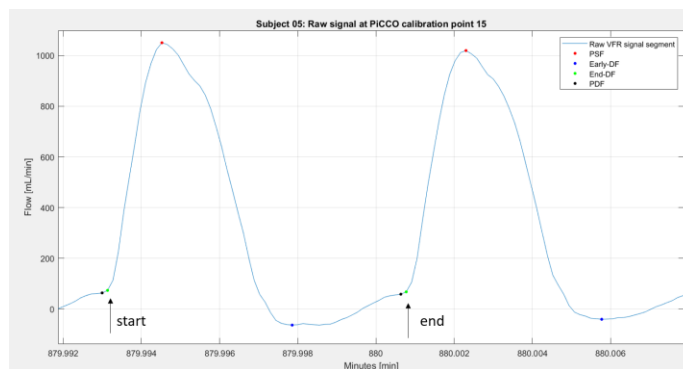
Figure 35. Fourth cardiac cycle for model validation

6.2.5 Subject 7 at PiCCO calibration point 4

The final example presented to the scientist is the cardiac cycle measured at PiCCO calibration point 4 for Subject 7. In Figure 36, the desired landmarks are shown and discussed. Again, the conclusions of the scientist were that the PSF, Early-DF and End-DF landmarks were correctly detected and labeled by the model, whereas, the PDF landmark is not necessarily detected correctly.
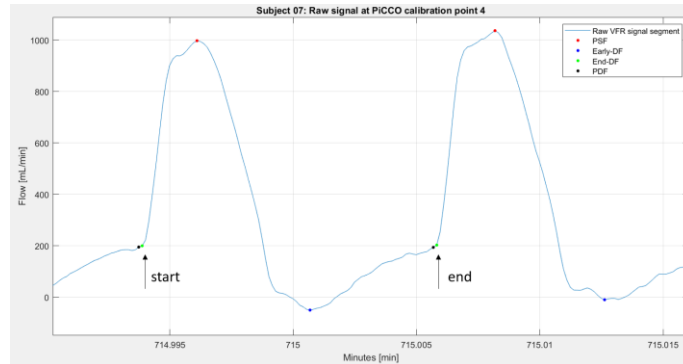
Figure 36. Fifth cardiac cycle for model validation

6.3 Discussion

Finally, remarks made by the scientist on **Question 2** were that these landmarks indeed can be used for describing the waveform in terms of the key descriptors. As for **Question 1,** the main limitation of the model concluded from the model validation is the way the model computes the PDF landmark. Namely, due to the noise inherent to the sensors, it is difficult to say if the peak diastolic flow (PDF) detected by the model is actually the landmark or noise. The way this limitation affects this work is when trying to determine the resistance of the artery, mainly for determining if there is intermediate resistance which has an end systolic notch as trademark.

Based on the model validation session, the scientist is more confident about the way the model is computing the PSF, End-DF and Early-DF landmarks. For future work, the way to determine peak diastolic flow (PDF) landmark should be further investigated. We believe that this would require more domain knowledge which is out of the scope of this thesis.

7 Conclusion

In this chapter we conclude this master thesis by giving an overview of the research, the contribution of this work with respect to state of the art, after which, we discuss the main limitations of the approach together with possibilities of future work with respect to the limitations. Finally, we conclude by providing the final words of this work.

7.1 Summary

The objective of this thesis was to create a method using unsupervised learning for detecting and labeling landmarks. In addition, we explored the possibility of using the detected landmarks for describing the waveform in terms of key descriptors defined in a consensus article by Kim et al. [19], namely, flow direction, phasicity, and resistance of the artery.

This objective was based on an identified gap in related work, where the two main conclusions were:

(1) machine learning is mainly used for making predictions of pathological states and in many cases, parameters derived from landmarks or whole physiological signal segments are used as input.

(2) when detecting and labeling landmarks, only one cardiac cycle is normally of interest where the landmarks are either manually marked or by using a customized algorithm.

The result of this thesis is a model for detecting and labeling landmarks inherent to the VFR waveform. This model is based on VFR signals measured by Transonic flow sensors and collected from a study with 11 subjects. Specifically, signals were split into segments measured over 1-minute time period around each PiCCO calibration point per subject.

To evaluate the findings, we computed the periodicities between successive landmarks in each group per subject. We analyzed each subject separately since we believed that inter-subject dependencies might affect the results. Based on domain knowledge, the expectations were that the periodicities between successive landmarks in successive cardiac cycles would obtain approximately the same periodicity. Therefore, we computed the differences between the periodicities of successive PSF-landmarks and the periodicities per remaining groups. These differences were then plotted in histograms to investigate the variability of these differences. The expectations were that the distribution would be centered around 0 and the variability would be low. We found that:

(1) for some subjects there was more uncertainty in the waveforms

(2) the landmark for which the periodicities differed the most was the PDF-landmark. This finding was also made in the model validation.

The model validation was performed in a session with a domain expert, where five randomly chose cardiac cycles containing the landmarks were shown and results were validated. The main remark was that it is hard to determine if the PDF landmark was the actual landmark or a local peak of noise introduced by the sensor. Specifically, due to the noise inherent to the sensors, it is difficult to say if the PDF landmark was detected by the model is actually the landmark or noise. In addition, the conclusions were that the since the Early-DF landmarks were detected correctly, the waveform could be described by commenting on if the waveform was **multiphasic** or **monophasic** and if the flow direction was **retrograde** or **antegrade**. The **resistance** was more difficult to comment on due to the uncertainty of the PDF landmark, since deciding if the resistance is intermediate requires us to know the location of this landmark.

All in all, we managed to answer both our research questions. For research question 1, we found that by combing hierarchical clustering with derivative analysis we were able to effectively develop an augmented unsupervised learning algorithm to successfully detect and label selected landmarks in signal segments measuring VFR. In addition, according to the model validation, it was concluded that these selected landmarks could be used for describing the VFR waveform in terms of state-of-the-art descriptors. We believe that this method is a good step towards finding a method which detects landmarks that can be used in the future for developing a non-invasive hemodynamic monitoring method.

Although this is a solution for filling the identified gap, there are many improvements that could be made which will be discussed in the following section.

7.2 Limitation and future work

Below we address different steps that could be taken to improve or expand certain aspects of the model, which were encountered while developing the method following the CRISP-DM process model. We list the ideas from most relevant to least relevant.

One of the main components in our model was hierarchical clustering. For optimizing our approach, we had to choose an internal validation index for determining the optimal number of clusters since otherwise this would have had to be determined based on visual inspection of each dendrogram for each signal segment. For this task, the Silhouette index was chosen. Since using this validation index was considered to fulfill the requirements set to the model, we did not further explore other validation indices. However, for future work, other validation indices e.g., Davies Boudin index or Calinski-Harabasz index [45] could be used to compare the results obtained by using the Silhouette index.

In the second iteration of the model, we estimated a window to fit a low regression model for computing the first order derivative (FOD) of the signal segment after which the second order derivative (SOD) was computed from the FOD [50]. The choice of the window size might have contributed to the **high** variability of the differences between periodicities of the different landmark groups presented in the model evaluation. An example illustrating this was Subject 14 (Figure 30), where the length of periodicities could differ by the second order of magnitude. This subject even had two signal segments where landmarks were missing. This was due to high frequency noise still being present in the signal segments. This was a limitation in the data cleaning part presented in Section 4.7, where signal segments were excluded only if there were missing periods in the segments. An idea that didn't get implemented is applying low pass filtering on the signal segments or other more advanced signal processing methods. For determining which advanced methods could be used would require more domain knowledge in the field of signal processing.

In the model validation session, we encountered a waveform where two local maxima were present in the top of the signal (Figure 34). The conclusions were that it is difficult to say which one of the peaks represent the PSF-landmark due to noise in the signal. One idea is applying a smoothing filter e.g., Gaussian filter. If the waveform is smoothed, the position of this PSF-landmark would likely get shifted somewhere in between these two values, which violates the definition of this landmark being the global peak of the cardiac cycle. The possibility of using smoothing for estimating the position of the landmarks would have to be further investigated.

For evaluating the model, comparing results obtained by other physiological signal (ECG or PPG) peak detection algorithms could be explored and applied on the VFR signal. This would require work in (i) understanding these different physiological signals, and (ii) acquiring more experience with signal

processing. In addition, there are general peak detection algorithms available for any type of signals. However, using these general algorithms would require manually setting parameters such as the threshold for both the height and the distance between peaks which consequently would require exploration of different peak heights and periodicities.

In addition, using these models for finding the correct landmarks a priori would allow us to explore other supervised learning. However, the labeling of the landmarks would still need to be verified by experts since analyzing these signals require more advanced domain knowledge.

Another idea is to explore recurrent neural networks (RNNs), specifically, the Long Short-Term Memory (LSTM) architecture. RNNs using LSTM-architecture are commonly used in sequential data processing based on time points [52]. With respect to our domain, one physiological signal for which LSTM models have been explored is the electrocardiogram (ECG) signal [52], [53]. More specifically, LSTM models have been used for segmenting, detecting and predicting P-wave, QRS-complex, T-waves in the ECG signal which then could be used for making or confirming diagnoses [52], [53]. Since we can use the order and position of the landmarks of the VFR waveform, using RNNs incorporating the LSTM architecture could be used for automating detection and labeling these landmarks.

7.3 Final words
In this work, I gained experience in working within the field of applied data science. This was a great learning process as I had to perform research in the field of cardiology which was a completely new topic for me. In addition, this work was performed under unordinary circumstances introduced by the pandemic.

With respect to the project, I learned that understanding the domain and the data takes time since there are so many factors e.g., physiology and sensor characteristics, contributing to the quality of the data that finding the best method can be difficult, and most likely there were some factors that were overlooked due to lack of domain knowledge.

It is also important to understand that sometimes the chosen method doesn't work out the way it was expected and that this is the nature of working with data and applying different approaches. In addition, working with physiological signals was also a new field for me, where so many sources of error may contribute to the end results. Therefore, the CRISP-DM methodology turned out to be a good choice for this project since it is suitable for revisiting steps in the process from business understanding to model evaluation, to support the findings.

Finally, I am grateful to have been part of the team at Philips Research and knowing that my research has contributed to the development of a non-invasive hemodynamic monitoring technique which is an important project in the field of medicine.

References

[1] "Cardiovascular diseases (CVDs)." [Online]. Available: https://www.who.int/news-room/fact-sheets/detail/cardiovascular-diseases-(cvds)#:~:text=Cardiovascular%20diseases%20%28CVDs%29%20are%20a%20group%20of%20disorders,supplying%20the%20arms%20and%20legs%3B%20Meer%20items...%20. [Accessed: 24-May-2021]

[2] J. P. Mynard, A. Kondiboyina, R. Kowalski, M. M. H. Cheung, and J. J. Smolich, "Measurement, Analysis and Interpretation of Pressure/Flow Waves in Blood Vessels," *Front. Physiol.*, vol. 11, 2020, doi: 10.3389/fphys.2020.01085. [Online]. Available: https://www.frontiersin.org/articles/10.3389/fphys.2020.01085/full. [Accessed: 11-May-2021]

[3] M. R. Pinsky, "Hemodynamic Evaluation and Monitoring in the ICU," *CHEST*, vol. 132, no. 6, pp. 2020–2029, Dec. 2007, doi: 10.1378/chest.07-0073. [Online]. Available: https://journal.chestnet.org/article/S0012-3692(15)52483-5/fulltext. [Accessed: 24-May-2021]

[4] J. Muller, J. Kennard, J. Browne, A. Fecher, and T. Hayward, "Hemodynamic Monitoring in the Intensive Care Unit," *Nutr. Clin. Pract. Off. Publ. Am. Soc. Parenter. Enter. Nutr.*, vol. 27, pp. 340–51, Jun. 2012, doi: 10.1177/0884533612443562. [Online]. Available: https://www.researchgate.net/publication/224972320_Hemodynamic_Monitoring_in_the_Intensive_Care_Unit

[5] D. D. Backer and J.-L. Vincent, "Noninvasive Monitoring in the Intensive Care Unit," *Semin. Respir. Crit. Care Med.*, vol. 42, no. 1, pp. 40–46, Feb. 2021, doi: 10.1055/s-0040-1718387. [Online]. Available: http://www.thieme-connect.de/DOI/DOI?10.1055/s-0040-1718387. [Accessed: 14-May-2021]

[6] M. Gassner, K. Killu, Z. Bauman, V. Coba, K. Rosso, and D. Blyden, "Feasibility of common carotid artery point of care ultrasound in cardiac output measurements compared to invasive methods," *J. Ultrasound*, vol. 18, no. 2, pp. 127–133, Nov. 2014, doi: 10.1007/s40477-014-0139-9. [Online]. Available: https://www.ncbi.nlm.nih.gov/pmc/articles/PMC4504859/. [Accessed: 12-Oct-2020]

[7] J.-L. Vincent *et al.*, "Clinical review: Update on hemodynamic monitoring - a consensus of 16," *Crit. Care*, vol. 15, no. 4, p. 229, 2011, doi: 10.1186/cc10291. [Online]. Available: https://www.ncbi.nlm.nih.gov/pmc/articles/PMC3387592/. [Accessed: 13-May-2021]

[8] A. D. Hughes, K. H. Parker, and J. E. Davies, "Waves in arteries: A review of wave intensity analysis in the systemic and coronary circulations," *Artery Res.*, vol. 2, no. 2, pp. 51–59, Apr. 2008, doi: 10.1016/j.artres.2008.02.002. [Online]. Available: https://www.atlantis-press.com/journals/artres/125937690. [Accessed: 14-May-2021]

[9] M. N. Gwilliam *et al.*, "MR Derived Volumetric Flow Rate Waveforms at Locations within the Common Carotid, Internal Carotid, and Basilar Arteries," *J. Cereb. Blood Flow Metab.*, vol. 29, no. 12, pp. 1975–1982, Dec. 2009, doi: 10.1038/jcbfm.2009.176. [Online]. Available: https://doi.org/10.1038/jcbfm.2009.176. [Accessed: 11-May-2021]

[10] M. D. Ford, N. Alperin, S. H. Lee, D. W. Holdsworth, and D. A. Steinman, "Characterization of volumetric flow rate waveforms in the normal internal carotid and vertebral arteries," *Physiol. Meas.*, vol. 26, no. 4, pp. 477–488, Apr. 2005, doi: 10.1088/0967-3334/26/4/013. [Online]. Available: https://doi.org/10.1088/0967-3334/26/4/013. [Accessed: 12-May-2021]

[11] M. Rafati, E. Havaee, H. Moladoust, and M. Sehhati, "Appraisal of different ultrasonography indices in patients with carotid artery atherosclerosis," *EXCLI J.*, vol. 16, pp. 727–741, May 2017, doi: 10.17179/excli2017-232. [Online]. Available: https://www.ncbi.nlm.nih.gov/pmc/articles/PMC5547385/. [Accessed: 12-May-2021]

[12] A. Azhim *et al.*, "Exercise Improved Age-associated Changes in the Carotid Blood Velocity Waveforms," *J Biomed Pharm Eng*, vol. 1, Jan. 2007 [Online]. Available:

https://www.researchgate.net/publication/242482090_Exercise_Improved_Age-associated_Changes_in_the_Carotid_Blood_Velocity_Waveforms#:~:text=The%20aerobic%20exercise%20increases%20whole%20velocity%20waveforms%20in,after%201-month%20exercise%20in%20previously%20sedentary%20young%20men.

[13] J. W. Calvert and D. J. Lefer, "Chapter 6 - Overview of Cardiac Muscle Physiology," in *Muscle*, J. A. Hill and E. N. Olson, Eds. Boston/Waltham: Academic Press, 2012, pp. 57–66 [Online]. Available: https://www.sciencedirect.com/science/article/pii/B9780123815101000065. [Accessed: 11-May-2021]

[14] S. Sundararajan, "Carotid Artery," in *Encyclopedia of the Neurological Sciences (Second Edition)*, M. J. Aminoff and R. B. Daroff, Eds. Oxford: Academic Press, 2014, pp. 600–601 [Online]. Available: https://www.sciencedirect.com/science/article/pii/B9780123851574011271. [Accessed: 14-May-2021]

[15] E. Kaniusas, "Fundamentals of Biosignals," in *Biomedical Signals and Sensors I: Linking Physiological Phenomena and Biosignals*, E. Kaniusas, Ed. Berlin, Heidelberg: Springer, 2012, pp. 1–26 [Online]. Available: https://doi.org/10.1007/978-3-642-24843-6_1. [Accessed: 15-May-2021]

[16] G. Slapničar, N. Mlakar, and M. Luštrek, "Blood Pressure Estimation from Photoplethysmogram Using a Spectro-Temporal Deep Neural Network," *Sensors*, vol. 19, no. 15, p. 3420, Jan. 2019, doi: 10.3390/s19153420. [Online]. Available: https://www.mdpi.com/1424-8220/19/15/3420. [Accessed: 11-May-2021]

[17] J. Miao, P. J. Benkeser, and F. T. Nichols, "A computer-based statistical pattern recognition for Doppler spectral waveforms of intracranial blood flow," *Comput. Biol. Med.*, vol. 26, no. 1, pp. 53–63, Jan. 1996, doi: 10.1016/0010-4825(95)00029-1. [Online]. Available: https://www.sciencedirect.com/science/article/pii/0010482595000291. [Accessed: 11-May-2021]

[18] P. T. Gamage, M. Khurshidul.Azad, A. Taebi, R. H. Sandler, and H. A. Mansy, "Clustering Seismocardiographic Events using Unsupervised Machine Learning," in *2018 IEEE Signal Processing in Medicine and Biology Symposium (SPMB)*, 2018, pp. 1–5, doi: 10.1109/SPMB.2018.8615615 [Online]. Available: https://ieeexplore.ieee.org/document/8615615

[19] E. S. H. Kim *et al.*, "Interpretation of Peripheral Arterial and Venous Doppler Waveforms: A Consensus Statement From the Society for Vascular Medicine and Society for Vascular Ultrasound," *J. Vasc. Ultrasound*, vol. 44, no. 3, pp. 118–143, Sep. 2020, doi: 10.1177/1544316720943099. [Online]. Available: https://doi.org/10.1177/1544316720943099. [Accessed: 12-May-2021]

[20] C. Schröer, F. Kruse, and J. M. Gómez, "A Systematic Literature Review on Applying CRISP-DM Process Model," *Procedia Comput. Sci.*, vol. 181, pp. 526–534, Jan. 2021, doi: 10.1016/j.procs.2021.01.199. [Online]. Available: https://www.sciencedirect.com/science/article/pii/S1877050921002416. [Accessed: 11-May-2021]

[21] F. Martínez-Plumed *et al.*, "CRISP-DM Twenty Years Later: From Data Mining Processes to Data Science Trajectories," *IEEE Trans. Knowl. Data Eng.*, pp. 1–1, 2019, doi: 10.1109/TKDE.2019.2962680. [Online]. Available: https://ieeexplore.ieee.org/document/8943998

[22] "CRISP-DM," *Data Science Project Management*. [Online]. Available: https://www.datascience-pm.com/crisp-dm-2/. [Accessed: 12-May-2021]

[23] P. Pruzan, "Measurement," in *Research Methodology: The Aims, Practices and Ethics of Science*, P. Pruzan, Ed. Cham: Springer International Publishing, 2016, pp. 115–135 [Online]. Available: https://doi.org/10.1007/978-3-319-27167-5_5. [Accessed: 11-May-2021]

[24] D. L. Streiner and G. R. Norman, "'Precision' and 'Accuracy': Two Terms That Are Neither," *J. Clin. Epidemiol.*, vol. 59, no. 4, pp. 327–330, Apr. 2006, doi: 10.1016/j.jclinepi.2005.09.005. [Online]. Available: https://www.sciencedirect.com/science/article/pii/S0895435605003409. [Accessed: 21-May-2021]

[25] E. Litton* and M. Morgan, "The PiCCO Monitor: A Review," *Anaesth. Intensive Care*, vol. 40, no. 3, pp. 393–408, May 2012, doi: 10.1177/0310057X1204000304. [Online]. Available: https://doi.org/10.1177/0310057X1204000304. [Accessed: 11-Sep-2020]

[26] L. S. Athanasiou, D. I. Fotiadis, and L. K. Michalis, "1 - Introduction," in *Atherosclerotic Plaque Characterization Methods Based on Coronary Imaging*, L. S. Athanasiou, D. I. Fotiadis, and L. K. Michalis, Eds. Oxford: Academic Press, 2017, pp. 1–21 [Online]. Available: https://www.sciencedirect.com/science/article/pii/B9780128047347000014. [Accessed: 11-May-2021]

[27] S. Nara, M. Kaur, and K. Verma, "Novel Notch Detection Algorithm for Detection of Dicrotic Notch in PPG Signals," *Int. J. Comput. Appl.*, vol. 86, Dec. 2013, doi: 10.5120/15081-3520. [Online]. Available: https://www.researchgate.net/publication/262979985_Novel_Notch_Detection_Algorithm_for_Detection_of_Dicrotic_Notch_in_PPG_Signals

[28] M. Abdollahi and A. F. Behboudi, "Nitroglycerin," in *Encyclopedia of Toxicology (Third Edition)*, P. Wexler, Ed. Oxford: Academic Press, 2014, pp. 569–572 [Online]. Available: https://www.sciencedirect.com/science/article/pii/B9780123864543011428. [Accessed: 11-May-2021]

[29] C. J. R. Gough and J. P. Nolan, "The role of adrenaline in cardiopulmonary resuscitation," *Crit. Care Lond. Engl.*, vol. 22, no. 1, p. 139, May 2018, doi: 10.1186/s13054-018-2058-1. [Online]. Available: https://ccforum.biomedcentral.com/articles/10.1186/s13054-018-2058-1

[30] K. G. Lurie *et al.*, "Combination drug therapy with vasopressin, adrenaline (epinephrine) and nitroglycerin improves vital organ blood flow in a porcine model of ventricular fibrillation," *Resuscitation*, vol. 54, no. 2, pp. 187–194, Aug. 2002, doi: 10.1016/S0300-9572(02)00096-5. [Online]. Available: https://www.resuscitationjournal.com/article/S0300-9572(02)00096-5/abstract. [Accessed: 11-May-2021]

[31] "Transit-time Ultrasound Theory of Operation," p. 2 [Online]. Available: https://www.transonic.com/resources/research/tech-notes/transit-time-ultrasound-theory-of-operation/

[32] B. Y. Lee, N. Al-Waili, and G. Butler, "The effect of adrenergic β2 receptor agonist on paraplegia following clamping of abdominal aorta," *Arch. Med. Sci. AMS*, vol. 7, no. 4, pp. 597–603, Aug. 2011, doi: 10.5114/aoms.2011.24128. [Online]. Available: https://www.ncbi.nlm.nih.gov/pmc/articles/PMC3258778/. [Accessed: 23-May-2021]

[33] "keys-to-accurate-perivascular-flow-measurements-with-transit-time-ultrasound.pdf." [Online]. Available: https://www.transonic.com/resources/research/tech-notes/keys-to-accurate-perivascular-flow-measurements-with-transit-time-ultrasound/. [Accessed: 11-May-2021]

[34] M. A. Quiñones, C. M. Otto, M. Stoddard, A. Waggoner, and W. A. Zoghbi, "Recommendations for quantification of Doppler echocardiography: A report from the Doppler quantification task force of the nomenclature and standards committee of the American Society of Echocardiography," *J. Am. Soc. Echocardiogr.*, vol. 15, no. 2, pp. 167–184, Feb. 2002, doi: 10.1067/mje.2002.120202. [Online]. Available: https://www.onlinejase.com/article/S0894-7317(02)45599-X/abstract. [Accessed: 12-May-2021]

[35] D. W. Holdsworth, C. J. D. Norley, R. Frayne, D. A. Steinman, and B. K. Rutt, "Characterization of common carotid artery blood-flow waveforms in normal human subjects," *Physiol. Meas.*, vol. 20, no. 3, pp. 219–240, Jan. 1999, doi: 10.1088/0967-3334/20/3/301. [Online]. Available: https://doi.org/10.1088/0967-3334/20/3/301. [Accessed: 12-May-2021]

[36] B. Mitch, *Ben Mitch (2021). Panel (https://www.mathworks.com/matlabcentral/fileexchange/20003-panel), MATLAB Central File Exchange. Retrieved May 24, 2021.* [Online]. Available: https://www.mathworks.com/matlabcentral/fileexchange/20003-panel. [Accessed: 24-May-2021]

[37] J. R. Jennings, "Heart Rate*," in *Encyclopedia of Stress (Second Edition)*, G. Fink, Ed. New York: Academic Press, 2007, pp. 274–277 [Online]. Available: https://www.sciencedirect.com/science/article/pii/B9780123739476001884. [Accessed: 12-May-2021]

[38] P. P. Lelovas, N. G. Kostomitsopoulos, and T. T. Xanthos, "A Comparative Anatomic and Physiologic Overview of the Porcine Heart," *J. Am. Assoc. Lab. Anim. Sci. JAALAS*, vol. 53, no. 5, pp. 432–438, Sep. 2014 [Online]. Available: https://www.ncbi.nlm.nih.gov/pmc/articles/PMC4181683/. [Accessed: 24-May-2021]

[39] M. P. Izco *et al.*, "Ivabradine in acute heart failure: Effects on heart rate and hemodynamic parameters in a randomized and controlled swine trial," *Cardiol. J.*, vol. 27, no. 1, pp. 62–71, Feb. 2020, doi: 10.5603/CJ.a2018.0078. [Online]. Available: https://www.ncbi.nlm.nih.gov/pmc/articles/PMC8086495/. [Accessed: 12-May-2021]

[40] B. S. Orozco, K. M. Engebretsen, J. S. Holger, and S. J. Stellpflug, "A Swine Model of Severe Propranolol Toxicity Permitting Direct Measurement of Brain Tissue Oxygenation," *J. Med. Toxicol.*, vol. 15, no. 3, pp. 178–183, Jul. 2019, doi: 10.1007/s13181-019-00707-0. [Online]. Available: https://doi.org/10.1007/s13181-019-00707-0. [Accessed: 12-May-2021]

[41] P. Shen, J.-F. Xu, Y.-Z. Gao, S.-L. Xia, S.-Y. Liu, and M. Zhang, "Establishment of a swine model of traumatic cardiac arrest induced by haemorrhage and ventricular fibrillation," *J. Int. Med. Res.*, vol. 48, no. 6, Jun. 2020, doi: 10.1177/0300060520931260. [Online]. Available: https://www.ncbi.nlm.nih.gov/pmc/articles/PMC7325463/. [Accessed: 12-May-2021]

[42] B. M. Deegan, E. R. Devine, M. C. Geraghty, E. Jones, G. ÓLaighin, and J. M. Serrador, "The relationship between cardiac output and dynamic cerebral autoregulation in humans," *J. Appl. Physiol.*, vol. 109, no. 5, pp. 1424–1431, Nov. 2010, doi: 10.1152/japplphysiol.01262.2009. [Online]. Available: https://www.ncbi.nlm.nih.gov/pmc/articles/PMC2980368/. [Accessed: 12-May-2021]

[43] S. P. Klein, V. De Sloovere, G. Meyfroidt, and B. Depreitere, "Autoregulation assessment by direct visualisation of pial arterial blood flow in the piglet brain," *Sci. Rep.*, vol. 9, no. 1, p. 13333, Sep. 2019, doi: 10.1038/s41598-019-50046-x. [Online]. Available: https://www.nature.com/articles/s41598-019-50046-x/tables/. [Accessed: 12-May-2021]

[44] M. Bachler, M. Hörtenhuber, M. Frank, S. Wassertheurer, and C. Mayer, "Simulation of Physiologic Ectopic Beats in Heartbeat Intervals to Validate Algorithms," *IFAC-Pap.*, vol. 48, no. 1, pp. 123–128, Jan. 2015, doi: 10.1016/j.ifacol.2015.05.105. [Online]. Available: https://www.sciencedirect.com/science/article/pii/S2405896315001068. [Accessed: 12-May-2021]

[45] T. Ronan, Z. Qi, and K. M. Naegle, "Avoiding common pitfalls when clustering biological data," *Sci. Signal.*, vol. 9, no. 432, pp. re6–re6, Jun. 2016, doi: 10.1126/scisignal.aad1932. [Online]. Available: https://stke.sciencemag.org/content/9/432/re6. [Accessed: 12-May-2021]

[46] F. Nielsen, "Hierarchical Clustering," 2016, pp. 195–211 [Online]. Available: https://www.researchgate.net/publication/314700681_Hierarchical_Clustering

[47] R. C. de Amorim, "Feature Relevance in Ward's Hierarchical Clustering Using the LpNorm," *J. Classif.*, vol. 32, no. 1, pp. 46–62, Apr. 2015, doi: 10.1007/s00357-015-9167-1. [Online]. Available: https://doi.org/10.1007/s00357-015-9167-1. [Accessed: 12-May-2021]

[48] N. Suthar, "A Technical Survey on DBSCAN Clustering Algorithm," vol. 4, no. 5, p. 7, 2013 [Online]. Available: https://www.ijser.org/researchpaper/A-Technical-Survey-on-DBSCAN-Clustering-Algorithm.pdf

[49] P. J. Rousseeuw, "Silhouettes: A graphical aid to the interpretation and validation of cluster analysis," *J. Comput. Appl. Math.*, vol. 20, pp. 53–65, Nov. 1987, doi: 10.1016/0377-0427(87)90125-7. [Online]. Available: https://www.sciencedirect.com/science/article/pii/0377042787901257. [Accessed: 12-May-2021]

[50] J. D'Errico, *John D'Errico (2021). Movingslope (https://www.mathworks.com/matlabcentral/fileexchange/16997-movingslope), MATLAB Central File Exchange. Retrieved March 15, 2021.* 2021 [Online]. Available: https://www.mathworks.com/matlabcentral/fileexchange/16997-movingslope

[51] M. Malik *et al.*, "Heart rate variability: Standards of measurement, physiological interpretation, and clinical use," *Eur. Heart J.*, vol. 17, no. 3, pp. 354–381, Mar. 1996, doi: 10.1093/oxfordjournals.eurheartj.a014868. [Online]. Available: https://doi.org/10.1093/oxfordjournals.eurheartj.a014868. [Accessed: 13-May-2021]

[52] S. Nurmaini *et al.*, "Electrocardiogram signal classification for automated delineation using bidirectional long short-term memory," *Inform. Med. Unlocked*, vol. 22, p. 100507, Jan. 2021, doi: 10.1016/j.imu.2020.100507. [Online]. Available: https://www.sciencedirect.com/science/article/pii/S2352914820306584. [Accessed: 16-May-2021]

[53] H. Abrishami, C. Han, X. Zhou, M. Campbell, and R. Czosek, "Supervised ECG Interval Segmentation Using LSTM Neural Network," p. 7 [Online]. Available: https://csce.ucmss.com/cr/books/2018/LFS/CSREA2018/BIC3264.pdf

Appendix A

Field	Data Structure	Size	Explanation
chanIndices	cell	1 x 1	Cell containing a double array with the indices of the channels. This array is [3,4,5]. This double array suggests that the signal segments are stored in these indices of **propValues**.
chanNames	cell	1 x 10	Cell array containing the names of the arteries
data	cell	1 x 12	Cell array for which cells 3 to 5 contain either an averge signal or pulse (raw) signal. Cell 1 and cell 2 are empty. Based on the available metadata, it is assumed that the respective artery from which the streams are obtained are shifted by two to the left in the cell array chanNames
rootIndex	double	1 x 1	No information available
groupIndices	double	1 x 1	No information available
groupNames	cell	1 x 1	Empty
propNames	cell	1 x 12	Nested cell array containing the explanation of properties of the measured data streams. Cell 1 contains string *name* cell 2 is empty. Cells 3 to cell 5 contain a 1 x 7 cell array with the following information: *wf_start_time, wf_start_offset, wf_increment, wf_samples, NI_ChannelNames, NI_UnitDescription, unit_string*.
propValues	cell	1 x 12	Nested cell array containing the data of the respective cells of **propNames**. Based on the size of the array, it is assumed that the data in each cell is the respective metadata of the signals in the cells in **data**
objectPathsOrig	cell	1 x 12	Cell array containing the paths of the channels. The paths are inconclusive, however, indicating which artery is connected to which channel. For example, cell 3 contains the following information: /'Untitled'/'carotid '
numberDataPointsRaw	cell	1 x 12	Double array containing the lengths of each signal segment in **data**. The first two entries are 0.
dataType	double	1 x 12	The base of the values in the signal streams in **data**. The signal segment are of base-10. Two first entries are 0, rest is 10.
dataTypeName	cell	1 x 12	The type of the signal streams in **data**. The signal segments are of type *double*. Two first cells contain string *void*, rest contain string *double*.

Appendix B
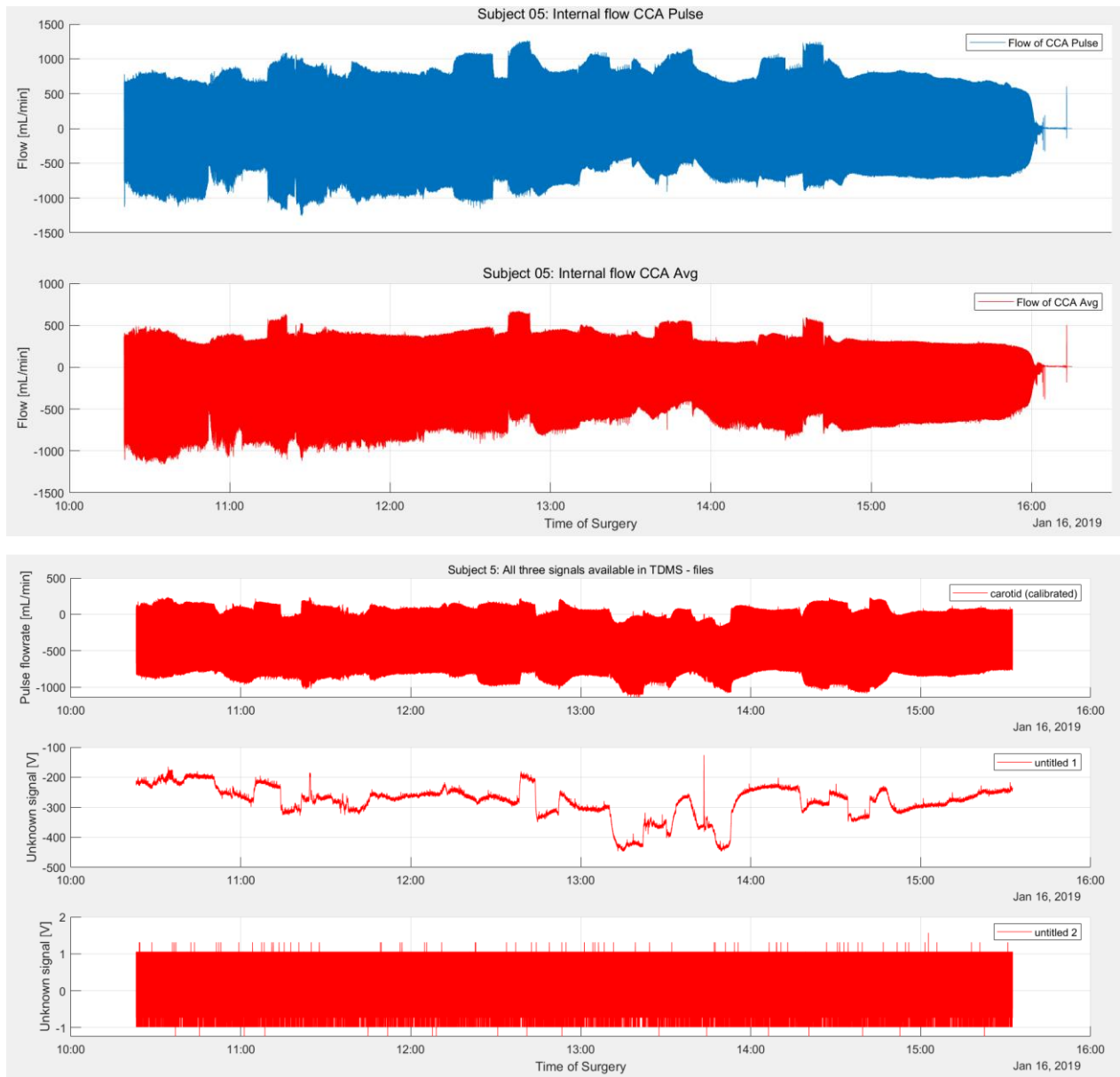
Appendix C

Subject 3: Distribution of the differences between the periodicities of successive landmarks
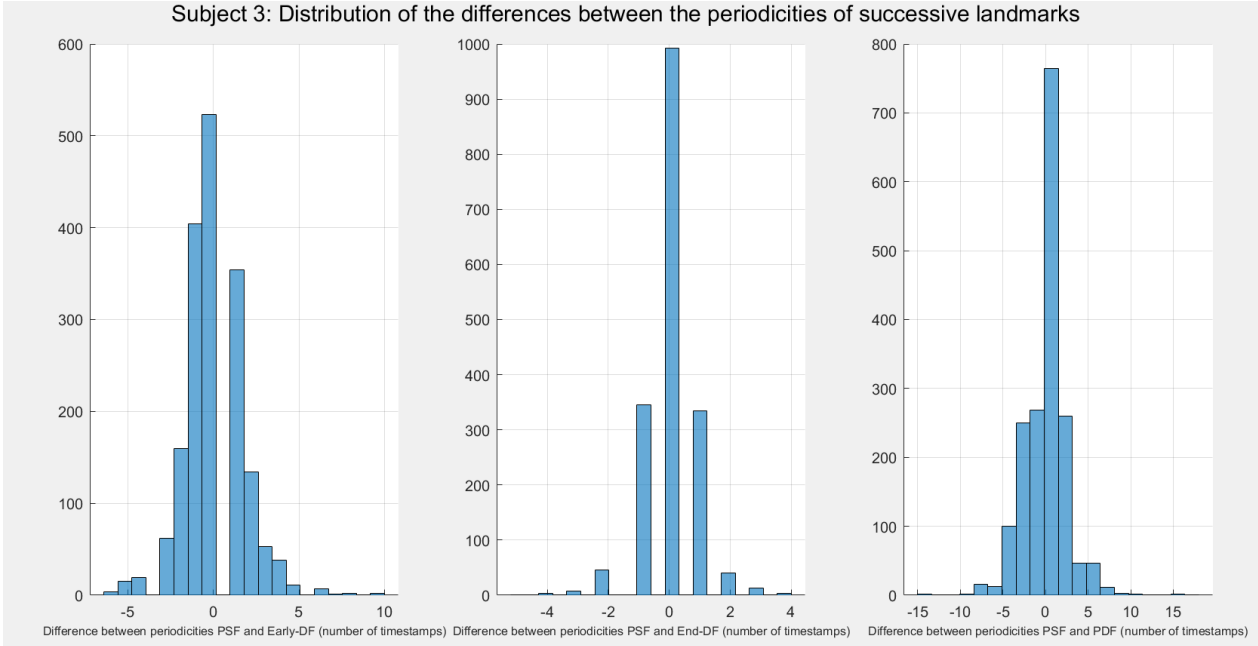
Subject 4: Distribution of the differences between the periodicities of successive landmarks
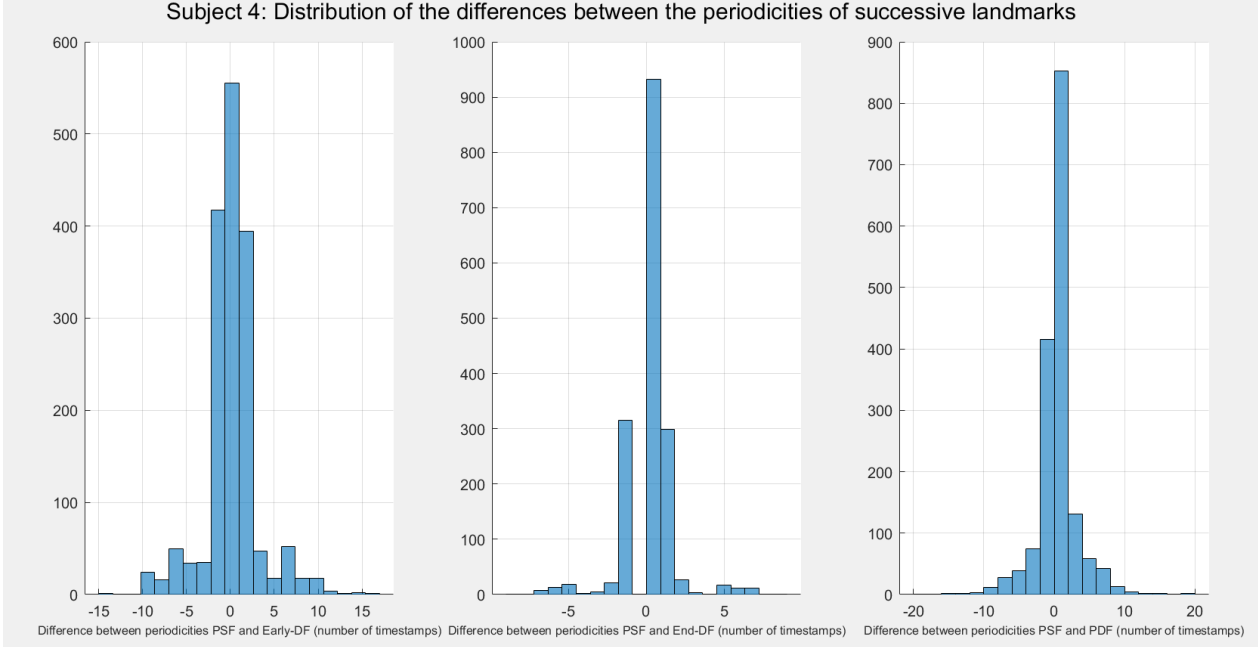
Subject 5: Distribution of the differences between the periodicities of successive landmarks
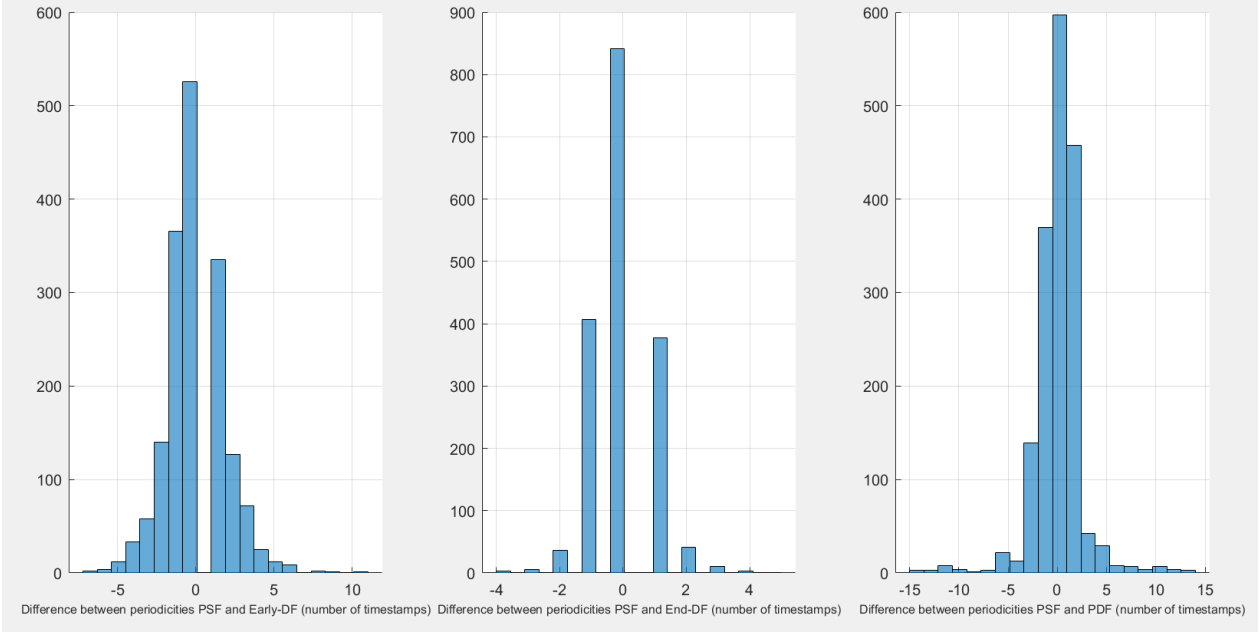
Subject 6: Distribution of the differences between the periodicities of successive landmarks
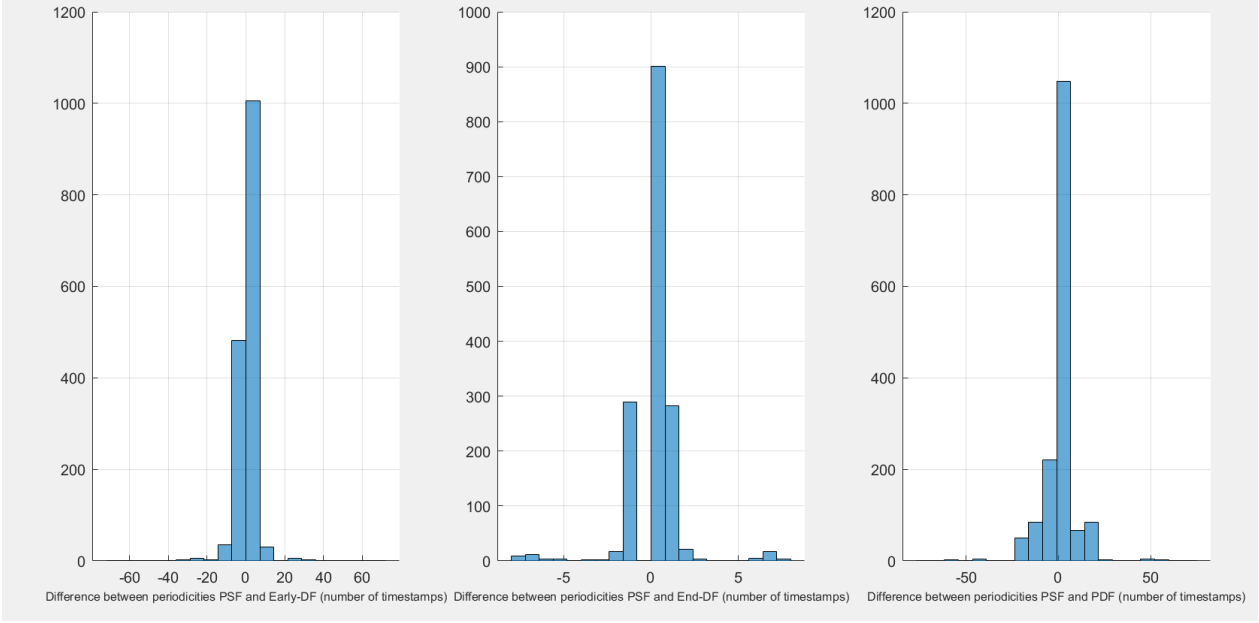
Subject 7: Distribution of the differences between the periodicities of successive landmarks
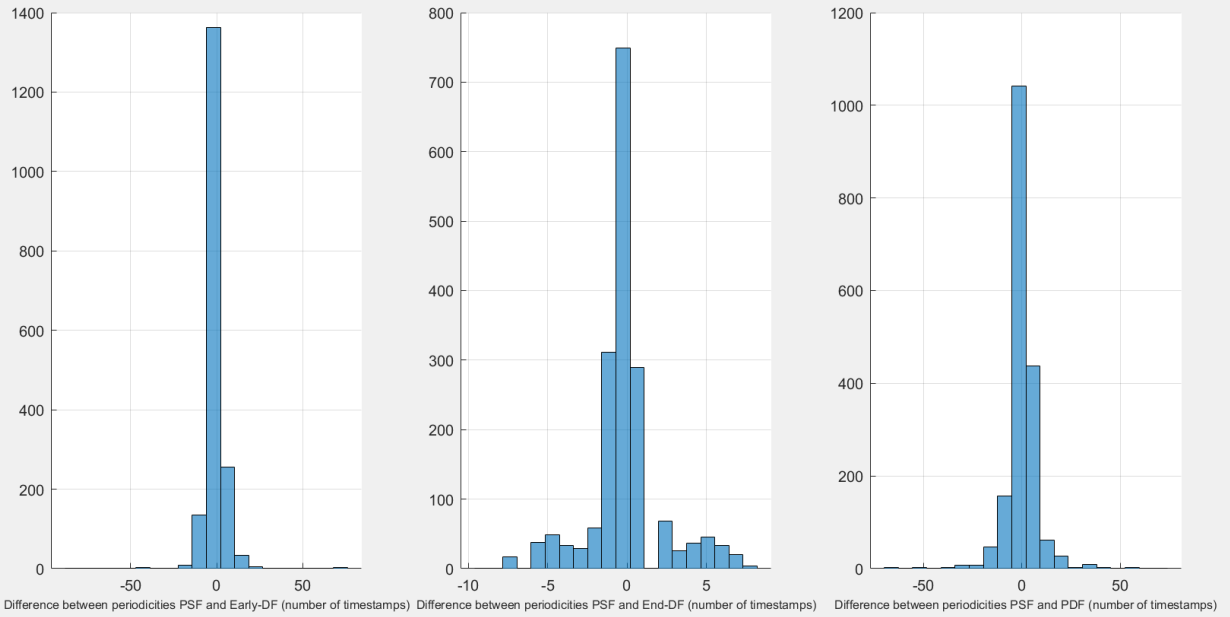
Subject 8: Distribution of the differences between the periodicities of successive landmarks
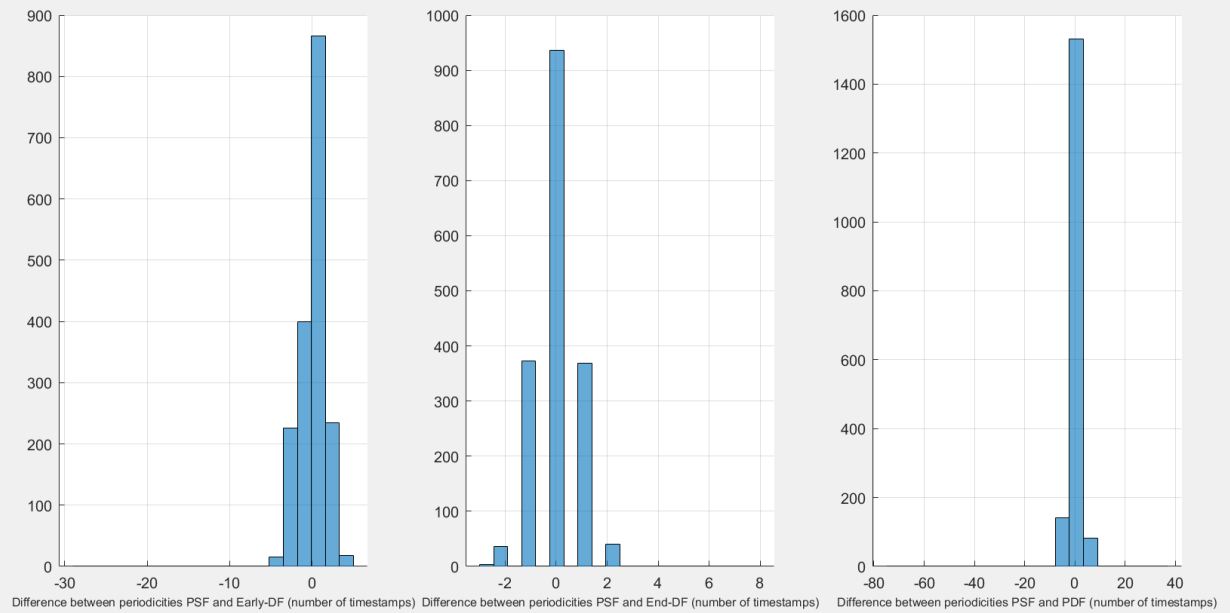
Subject 9: Distribution of the differences between the periodicities of successive landmarks
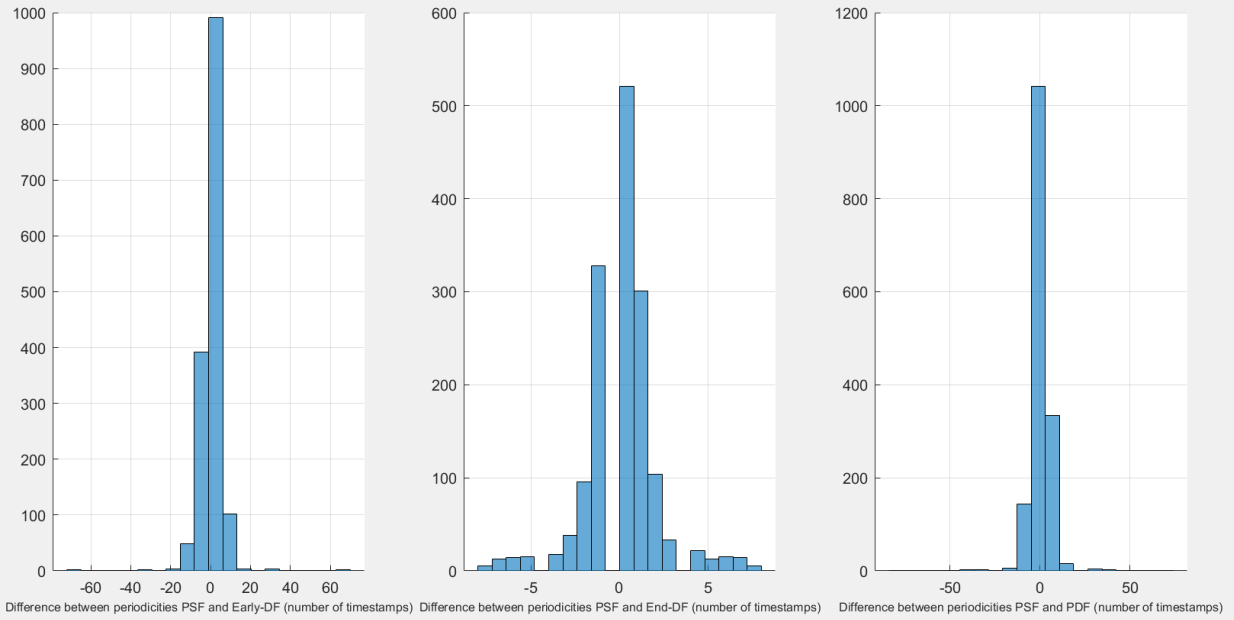
Subject 10: Distribution of the differences between the periodicities of successive landmarks
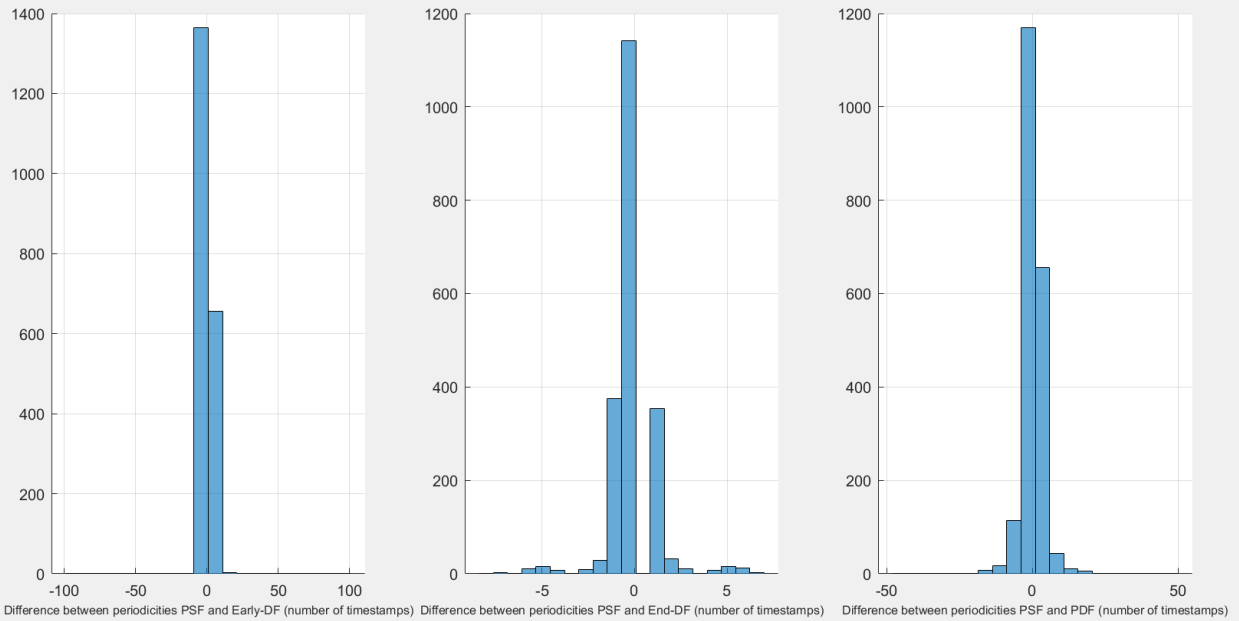
Subject 11: Distribution of the differences between the periodicities of successive landmarks
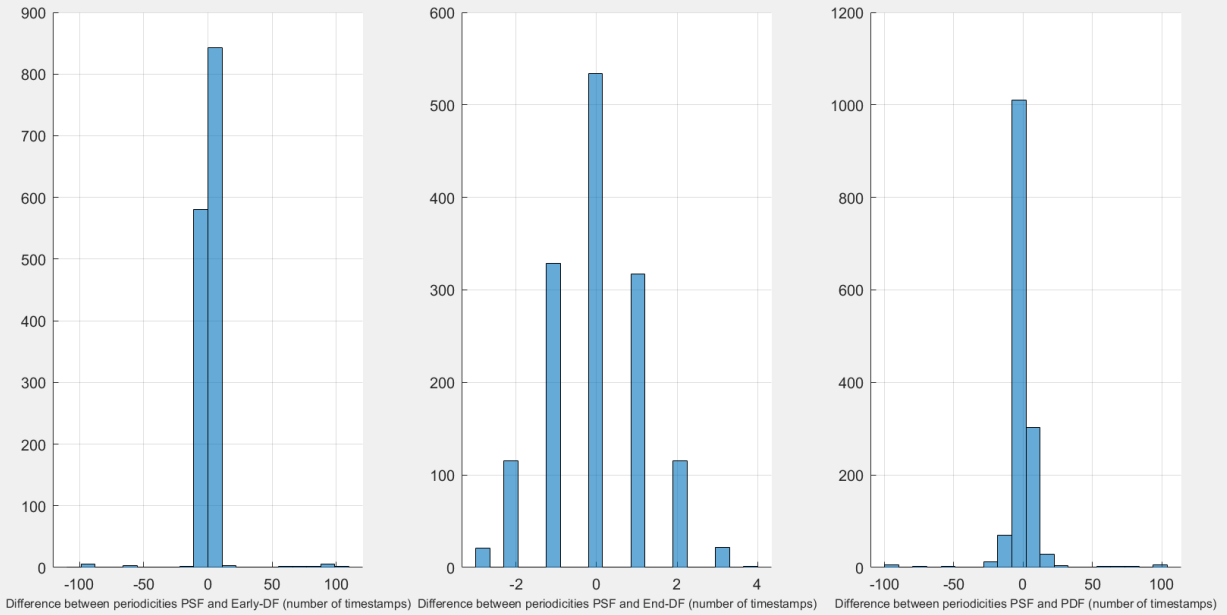
Subject 12: Distribution of the differences between the periodicities of successive landmarks
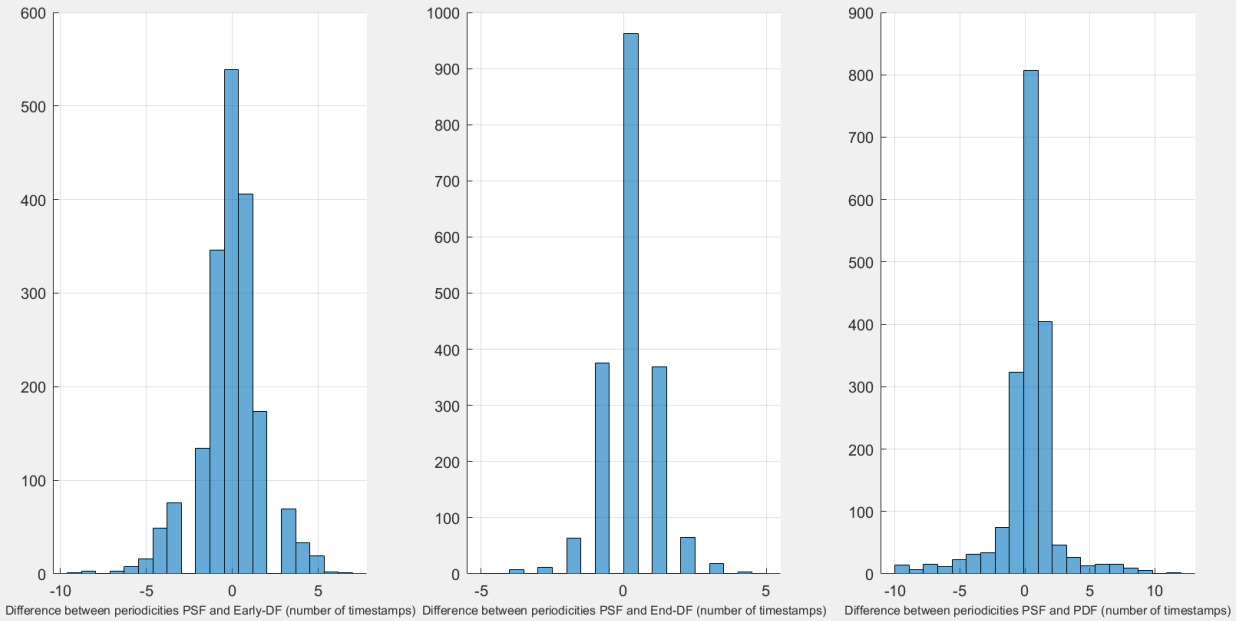
Subject 14: Distribution of the differences between the periodicities of successive landmarks